8-10-2005

Synthesis and Investigation of Nanomaterials by Homogeneous Nonaqueous Solution Phase Reactions

Zhihui Ban
University of New Orleans

SYNTHESIS AND INVESTIGATION OF NANOMATERIALS BY HOMOGENEOUS NONAQUEOUS SOLUTION PHASE REACTIONS

A Dissertation

Submitted to the Graduate Faculty of the
University of New Orleans
in partial fulfillment of the
requirements for the degree of

Doctor of Philosophy
in
The Department of Chemistry

by

Zhihui Ban

B.S. Zhejiang University, P. R. China, 1996
Ph. D. Dalian Institute of Chemical Physics, P. R. China, 2001
M.S. University of New Orleans, USA, 2004

August 2005

ACKNOWLEDGEMENTS

Many individuals have assisted me during graduate study, both at the Department of Chemistry and at the Advanced Materials Research Institute where I was graciously allowed to perform my dissertation research.

I would like to begin by thanking my major professor, Dr. Charles J. O'Connor for all of his guidance, assistance and support. I also thank my committee, Dr. John B. Wiley, Dr. Steven P. Nolan, Dr. Jiye Fang and Dr. Kevin Stokes, for their advice and encouragement.

I would like to thank Dr. Kevin Stokes and Dr. Yuri A. Barnakov for the Faraday rotation measurements and analysis, Dr. Vladimir O. Golub for the SQUID measurements and analysis.

I acknowledge the support from the Advanced Materials Research Institute through the Office of Naval Research Grant N00014-02-1-0729.

Special thanks to my wonderful wife, Yanjie, my parents and parents-in-law. Your love and support encourage me to go forward.

The dissertation is also for my 20-month-old daughter, Angelina. You are my angel and the best gift for our family.

TABLE OF CONTENTS

LIST OF TABLES

LIST OF FIGURES

ABSTRACT

The objective of this Ph.D. study is to explore an important and fertile research topic on the methods for synthesis of nanomaterials by homogeneous nonaqueous solution phase reaction. Research in this area focuses on synthesizing several kinds of nanomaterials in different environments and structure, including spherical nanoparticles, nanowires and core-shell structure composites

We first synthesized metallic nanomaterials by reductive chemical method in homogeneous solutions of polar aprotic solvent, such as ~10 nm Fe nanoparticles, ~6 nm Au nanoparticles, and ~100 nm Bi nanoparticles, these works are the preparation for the following studies.

Secondly, we synthesized bimetallic nanomaterials using the same method in the same solution, such as $Fe_{50}Co_{50}$ alloy and Bi doped with Mn. For FeCo alloy, after annealing at 500 °C, a pure phase of $Fe_{50}Co_{50}$ was obtained. And we first synthesized the nanowires of bismuth doped with manganese.

Thirdly, we synthesized core-shell structure nanocomposites, including either gold as the shell or polymer as the shell. Au-coated magnetic Fe nanoparticles have been successfully synthesized by partial replacement reaction in a polar aprotic solvent with about 11 nm core of Fe and about 2.5 nm shell of Au.

HRTEM images show clear core-shell structure with different crystal lattices from Fe and Au. Poly (vinyl pyrrolidone) (PVP) coated iron nanoparticles also have been successfully synthesized in a polar aprotic solvent, which shows the well-defined core-shell structures. In this approach, poly (vinyl pyrrolidone) (PVP) was employed as the polymer to directly coat on the metallic core (iron) nanoparticles.

In this work, a combination of TEM (transmission electron microscopy), EDS (energy disperse X-ray spectroscopy), XRD (X-ray powder diffractometry), ICP (inductively-coupled plasma spectrometer), TGA (thermogravimetric analysis), UV-visible absorption spectroscopy, IR (infrared) spectroscopy and SQUID magnetometry (superconducting quantum interference device) were employed to characterize the morphology, structure, composition and magnetic properties of the products.

In summary, this study successfully and systematically synthesized several kinds of nanocomposites in a system. The synthetic procedure is simple, economic and easily scaled-up for further applications. And many techniques were employed to characterize the products.

FOREWORD

"Until recently, there has been a gap in our ability to control the composition of matter on the nanometer scale. In our time, the size and complexity of the molecules we can design and make is increasing to encompass many tens, hundreds, even thousands of atoms. At the same time, the ability to pattern matter using lithographic and scanning probe manipulation techniques has also been extended down to the nanometer scale. This convergence of the top-down and bottom-up approaches at the nanometer scale marks the first time in history when it appears within reach to design a macroscopic functional material by controlling the composition of matter on every length scale from the atom up. Many important properties of materials are controlled or limited by behavior on the nanometer scale, and so there is great opportunity in this area."

---------- Paul Alivisatos "Welcome to Nano Letters," *Nano Letters*, 1 (1), 1-1, 2001.

CHAPTER 1 INTRODUCTION

1.1 PREFACE

Nowadays, materials have become an integral part of our life. In research, people like to classify the materials by their size, such as macro-scale, meso-scale, micro-scale, nano-scale, and atomic-scale, which are typically referred to length scales that are larger than 1 millimeter, between 0.1 and 1 millimeters, between 0.1 and 100 micrometers, between 0.1 and 100 nanometers, and less than 0.1 nanometer, respectively. The physical properties and behavior of isolated molecules at the atomic-scale and bulk materials at the macro-scale are well known. However, the properties of matter at the meso-, micro- and nano-scales cannot necessarily be predicted from those observed at larger or smaller scales. Instead, they exhibit important differences that cannot be explained by traditional models and theories. Some of these differences result from continuous modifications of characteristics with changing size. That is the *scale effect*.

Among these different length scale materials, research about nanomaterials, which are found in both biological systems and manmade structures, is one of the most attractive issues. Nature has been using nanomaterials for millions of years. Examples in which nanostructured elements play a vital role are magnetotactic bacteria[1], and molluscan teeth[2]. Another important example of nanomaterials in

nature is the storage of iron in a bioavailable form within the 8 nm protein cavity of ferritin.[3]

Scientific work on this subject can be traced back over 100 years. In 1861 the British chemist Thomas Graham coined the term colloid to describe a solution containing 1 to 100 nm diameter particles in suspension, which would be one of the earliest works in nanoscience.[4]

Since then, research on nanomaterials has been stimulated by their technological applications. The first technological uses of these materials were as catalysts[5,6] and pigments[7]. The large surface area to volume ratio increases the chemical activity. Because of this increased activity, there are significant cost advantages in fabricating catalysts from nanomaterials. Furthermore, technologically useful properties of nanomaterials are not limited to their structural, chemical, or mechanical behavior.

In recent years, the nanomaterials are experiencing a rapid development due to their existing and/or potential applications in a wide variety of technological areas such as catalysis, ceramics, electronics, solar cells[8], magnetic data storage[9], structural components, etc. To meet the technological demands in these areas, the size of the materials should be reduced to the nanometer scale. For example, the miniaturization of functional electronic devices demands the placement or assembly of nanometer scale components into well-defined structures. As the size reduces into the nanometer range, the materials exhibit peculiar and interesting

mechanical and physical properties, e.g. increased mechanical strength, enhanced diffusivity, higher specific heat and electrical resistivity compared to conventional coarse grained counterparts.[10]

Nanotechnology is opening a brand new and exciting world for human being.

1.2 NANOMATERIALS AND THEIR PROPERTIES AND APPLICATIONS

Roughly speaking, nanomaterials can be classified into nanocrystalline materials and nanoparticles. The former are polycrystalline bulk materials with grain sizes in the nanometer range (less than 100 nm), while the latter refers to ultrafine dispersive particles with diameters below 100 nm. Generally nanoparticles are considered as the building blocks of bulk nanocrystalline materials.

Depending on the dimensions nanomaterials can be further classified into (a) nanoparticles, (b) layered or lamellar structures, (c) filamentary structures, and (d) bulk nanostructured materials[11].

The unique properties of nanocrystalline materials are derived from their large number of grain boundaries compared to coarse-grained polycrystalline counterparts. Assuming, for simplicity, that grains have the shape of spheres or cubes, the volume fraction of nanocrystalline materials associated with the

boundaries, C can be calculated as:

$$C = 3\Delta / d$$

Where $\triangle$ is the average grain boundary thickness and d is the average grain diameter. Thus, the volume fraction of atoms in the grain boundaries can be as much as 49% for 5 nm grains and decrease to about 30% for 10 nm grains and 3% for 100 nm grains. In contrast, for coarse-grained materials with a grain size of >1 μ m, the volume fraction of atoms in the grain boundaries if negligibly small.

Thus the interface structure plays an important role in determining the physical and mechanical properties of nanocrystalline materials. Huang et al.[12] reported that nanocrystalline copper has a much higher resistivity and a larger temperature dependence of the resistivity than bulk copper. They attributed this effect to the grain boundary enhanced scattering of electrons. Nanocrystalline metals have been found to exhibit creep and superplasticity with high strain rates at lower temperatures than their micro-grained counterparts. High strain-rate superplasticity at lower temperatures is of practical interest because it can offer an efficiently near-net-shape forming technique to industrial sectors. Despite recent advances in the development of nanocrystalline materials, much work remains to be done to achieve a basic understanding of their deformation and fracture behavior. Nanocrystalline metals generally exhibit significantly higher yield strength and reduced tensile elongation relative to their microcrystalline counterparts.

Simply, the properties of nanomaterials mainly depend on four features, (1) grain size and size distribution, (2) chemical composition, (3) presence of interfaces (grain boundaries, free surface), and (4) interactions between the constituent domains[13]. Due to the large surface/interface to volume ratio in nanophase materials, a wide variety of size-related effects can be introduced by controlling the size of the particles[14]:

- The density of dislocation, interface to volume ratio and the grain size strongly influence the mechanical properties.
- Quantum confinement[15,16], i. e., quantization of the energy levels of the electrons due to confined grain size, has applications in semiconductors, optoelectronics, and non-linear optics. Nanoclusters, so-called quantum dots, for example can be developed to emit and absorb a specific wavelength of light by changing the particle diameters.
- The large amount of surface atoms increases the activity for catalytical applications.
- The magnetic properties of nano-sized particles depend on the large surface to volume ratio. Unlike bulk materials consisting usually of multiple magnetic domains, several small ferromagnetic particles can form only a single magnetic domain, giving rise to superparamagnetism. This behavior opens the possibility for applications in information storage. For superparamagnetic particles, the energy required to change

the direction of the magnetic moment of a particle is comparable to the ambient thermal energy. At this point, the rate at which the particles will randomly reverse direction becomes significant. This is particularly important in the field of data storage technology.

Research in nanomaterials is a multidisciplinary effort that involves interaction between researchers in the field of physics, chemistry, mechanics and materials science, or even biology and medicine. It has been stimulated by the interest for basic scientific investigations and their technological applications.

Nanomaterials and most of the applications derived from them are still in an early stage of technical development. There are several issues that remain to be addressed before nanomaterials will become potentially useful for industrial sectors. These issues include (1) developing economical and environmentally friendly technologies for the synthesis of high purity materials with large yield, (2) characterization of new structures and properties of nanophase materials, (3) fabrication of dense products from nanoparticles with full density and less contamination, and (4) retention of the ultrafine grain size in service in order to preserve the mechanical properties associated with the nanometer scale.

Nanodevices are one of the most interesting issues in nano-related field recently, which may be defined as structurally organized and functionally integrated chemical systems in the dimension of nanometers. The components may be photo-, electro-, iono-, magneto-, thermo-, mechano-, or chemoactive,

depending on whether they handle photons, electrons, or ions, respond to magnetic fields or to heat, undergo changes in mechanical properties, or perform a chemical reaction[17,18].

Areas of application that can be foreseen to benefit from the small size and organization of nanoscale objects are so broad and exciting. Here are some examples of application for nanotechnology:

- Giant Magnetoresistance in nanocrystalline materials
- Nanolayers with selective optical barriers > 90% of graphics
- Dispersions with optoelectronic properties, high reactivity
- Chemical and Bio-detectors
- Advanced drug delivery systems
- Chemical-Mechanical Polishing with Nanoparticle Slurries
- New Generation of Lasers
- Nanostructured Catalysts (in Chem. & Fuel Industry.)

In medicine, nanotechnology will mix with biotechnology well because they operate on similar scales. Since many things in biology are on the microscopic scale, having things on the nanoscale within the body will mean better distribution of medical drugs, new protein engineering techniques, and the possibility of nanorobots that could repair the human body from the inside out.

Electronics is currently the biggest focus in nanotechnology research. It's well known that modern semiconductor processes are approaching their fundamental limits. Demand for consumer electronics won't cease any time soon, so there is a definite need for new methods of miniaturization. The amazing thing about nanoelectronics is that they offer an entire order of magnitude increase in component density if we can ever truly build integrated devices out of quantum dots and nanowires.

1.3 METHODS FOR PRODUCING NANOMATERIALS

The interest in nanoscale objects is due to the exhibition of novel electronic, optical, magnetic, transport, photochemical, electrochemical, catalytic, mechanical, biological and medical properties and behaviors, depending on composition, size, and shape of the nanoproducts. In fact, many interesting phenomena at the nanoscale are caused by the tiny size of the organized structure and by interactions at their predominant and complex interfaces[19], which is different with the bulk materials. It is believed that when chemists are able to gain control over size and shape of the particles, further enhancement of material properties and device functions will surely be possible. Most of the discovered new materials and new physical or chemical properties are due to the change in both, composition or size.

As a result, the new applications and properties are rather a result of tailoring matter and subsequently arranging the components by means of chemical interactions, so, ideally, new properties can arise from a combination of inexpensive and environmentally harmless components[20]. But the chemist not only has to be able to synthesize perfect, i.e., monodispersed and shape-defined objects having nanometer dimensions, but they also could have to position these objects in appropriately organized arrays. This could be tackled either by using lithographic techniques[21] or templating methods (molecular and supramolecular assembly processes[22], or deposition inside the void spaces of nanoporous host materials[23]).

Before working with nanoparticles, it is first necessary to be able to produce them. At present, most of the nanochemistry is concerned with the development of novel methods for the synthesis and characterization of chemical systems within the size range of about 1 to 100 nm and their applications. Generally, there are two methods for producing nanomaterials. One method is to generate particles of the correct size from scratch using crystallization, direct generation or other similar techniques, which is often referred to as "bottom up." In the other method, referred to as "top down," larger particles are reduced through milling to achieve the desired nanoscale particles.

The current fabrication technology for nanoparticles is novel and versatile. Significant progress has been made over the last decade in understanding fundamental aspects of the synthesis of nanoparticles, nanorods, etc. Various

processing routes have been developed for the synthesis and commercial production of nanoparticles including vapor, liquid, solid state processing routes, and combined methods, such as the vapor–solid–liquid approach (Table 1-1)[24].

Table 1-1. Classification of available techniques to synthesize nanocrystalline particles and nanotubes

Route	***Processing***
Vapor	Physical vapor deposition, chemical vapor deposition, aerosol processing
Liquid	Sol-gel process, wet chemical synthesis
Solid	Mechanical alloying/milling, mechanochemical synthesis
Combined	Vapor-liquid-solid approach

Available techniques for the synthesis of nanoparticles via vapor routes range from physical vapor deposition (PVD) and chemical vapor deposition (CVD) to aerosol spraying. The liquid route involves sol–gel and wet chemical methods. The solid state route preparation takes place via mechanical milling and mechanochemical synthesis. Each method has its own advantages and disadvantages. Different synthesis routes would give us different internal structures of nanoproducts that would affect the properties of materials consolidated from

them. Due to their high specific surface areas, nanoparticles exhibit a high reactivity and strong tendency towards agglomeration. Moreover, rapid grain growth is likely to occur during processing at high temperatures. As unique properties of nanocrystaline materials derived from their fine grain size, it is of crucial importance to retain the microstructure at a nanometer scale during consolidation to form bulk materials. It is also noticed that pores are generated in bulk nanocrystalline materials consolidated from nanoparticles prepared by inert-gas condensation. Such nanopores can lead to a decrease in Young's modulus of consolidated nanocrystalline materials[25]. Electrodeposited samples are believed to be free from porosity, but they contain certain impurities and texture that may degrade their mechanical performances. Therefore, controlling these properties during synthesis and subsequent consolidation procedures are the largest challenges facing researchers.

Comprehensive understanding of the processing structure property relationships is essential in the development of novel nanomaterials with unique properties for structural engineering applications.

1.3.1 Vapor route

1.3.1.1 Physical vapor deposition

Physical vapor deposition (PVD) is a versatile synthesis method and capable of preparing thin film materials with structural control at the atomic or nanometer scale by careful monitoring the processing conditions. PVD involves the generation of vapor phase species either via evaporation, sputtering, laser ablation or ion beam. Inert gas condensation combined with thermal evaporation is commonly used to fabricate metallic and metal-oxide powders with a well defined and narrow size distribution[26,27,28]. This technique was originally introduced by Ganqvist and Buhrman[29] in 1976 and developed by Gleiter in 1981.

1.3.1.2 Chemical vapor deposition

Chemical vapor deposition (CVD) is a process where one or more gaseous adsorption species react or decompose on a hot surface to form stable solid products. More recently, Lai et al.[30] employed hot filament CVD to grow one dimensional SiC nanorods.

1.3.1.3 Spray conversion processing

This route involves the atomization of chemical precursors into aerosol droplets that are dispersed throughout a gas medium. The aerosols are then transported into a heated reactor where the solution is evaporated or combusted to form ultrafine particles or thin films. This technique is versatile and inexpensive because of the availability of various low cost chemical solutions and has been used to produce a variety of high purity and non-agglomerated metal oxide nanoparticles such as TiO_2, Al_2O_3, ZrO_2, V_2O_5 and Y_2O_3–ZrO_2[31,32].

1.3.2 Liquid route

1.3.2.1 Sol–gel process

Sol–gel processing[33] is particularly attractive because the chemical reactions can be tailored at the molecular level. Using molecular precursors to obtain an oxide or hydroxide network via hydrolysis and condensation reactions, sol–gel process provides new approaches and a better control in the preparation of nanomaterials. However, the alkoxides used are rather expensive, and the processing is tedious because it requires several sequential steps to form nanoparticles or nanocrystalline solids. The sol–gel processing method has been used for producing metal oxide and ceramic powders with high purity and high

homogeneity for many years. The sol–gel route offers a degree of control of composition and structure at the molecular level. The process involves the generation of a colloidal suspension ('sols') which are subsequently converted to viscous gels and solid materials. Ebelman produced the first silica gels in 1846 and Cossa synthesized alumina gels in 1870[34,35]. Since then, aerogels of zirconia, silazane, borate and other ceramics were synthesized using the sol–gel technique[36,37]. In the process, reactive metal precursors were initially hydrolyzed, followed by condensation and polymerization reactions. Metal alkoxides are metalorganic compounds having an organic ligand attached to a metal or metalloid atom. They are the result of direct or indirect reactions between a metal M and an alcohol ROH. Typical examples are methoxide (OMe; $MOCH_3$) and ethoxide (OEt; MOC_2H_5). During hydrolysis, the alkoxy groups (OR) are replaced by hydroxo ligands.

1.3.2.2 Wet chemical synthesis[38]

Solution-based processing routes used for the synthesis of nanoparticles include precipitation of solids from a supersaturated solution[39,40], homogeneous liquid phase chemical reduction[41,42,43], microemulsions[44], hydrothermal/solvothemal processing of nanoparticles and nanocomposites[45,46], and ultrasonic decomposition of chemical precursors[47,48,49]. These processes are

attractive due to their simplicity, versatility and availability of low cost precursors. Inorganic salt compounds used in the wet chemical synthesis routes are more versatile and economical than alkoxides employed in the sol–gel process. A typical example is the formation of nanocrytalline titania powders via hydrolysis of $TiCl_4$ at lower temperatures:

$$TiCl_4 + 2H_2O \Rightarrow TiO_2 + 4HCl$$

Salt reduction is one of the most commonly adopted methods to generate the metal colloid particles. The process involves the dissolution of metal salts in aqueous or non-aqueous environments followed by the reduction of metal cations to the zero-valent state. The nature of the metal salts determines the kind of reducing agent to be applied. To produce transition metal nanoparticles, group 6 metal chlorides such as $CrCl_3$, $MoCl_3$ and WCl_4 are reduced with $NaBEt_3$ in toluene solution at room temperature to form metal colloids of high yield.

Microemulsion synthetic methods can be used for synthesis of metals[50,51] or alloys[52] by reduction, and synthesis of metal oxides[53,54] or other inorganics[55,56].

In a sealed vessel (bomb, autoclave, etc.), solvents can be brought to temperatures well above their boiling points by the increase in autogenous pressures resulting from heating. Performing a chemical reaction under such conditions is referred to as *solvothermal processing* or, in the case of water as solvent, *hydrothermal processing*. More recently, Cheng et al.[57] developed a method for preparing nanoparticulate, phase-pure rutile and anatase from aqueous

$TiCl_4$ by a hydrothermal process. This method has become one of the important technique for preparation of nanomaterials.

Metal nanoparticles can also be generated via ultrasonic and thermal decomposition of metal salts or chemical precursors. Recently, ultrasonic waves have been employed to stimulate chemical reaction of inorganic salts. Sonication of argon-saturated aqueous solutions of NaAuCl and $PdCl_2$ results in the formation of noble metal AuPd alloy nanoparticles.

The *Rieke chemical synthesis technique*[58] produces highly reactive metal powders by reducing metal salts in ethereal or hydrocarbon solvents using alkali metals. This technique has been employed successfully to prepare elemental nanostructured materials including zinc, aluminum, manganese, magnesium, nickel, cobalt, and others. Our works are mainly based on this technique.

1.3.3 Solid route

1.3.3.1 Mechanical alloying/milling

The mechanical alloying/milling process is a solid state processing technique and was originally developed by Benjamin of the International Nickel Company for the production of oxide dispersion strengthened (ODS) superalloys[59]. In this process, high energy ball milling is used for synthesizing a variety of materials like

forming equilibrium and non-equilibrium phases. The mechanical energy transfer to the powder particles in these mills takes place by shear action or impact of the high velocity balls with the powder. During the process, raw powder particles with a size of several microns experience severe plastic deformation, i.e. undergo a repetitive cold welding and fracturing mechanism[60]. Vibratory mill, planetary mill, uniball mill and attritor mill are commonly used to perform mechanical alloying/milling. Due to mechanical limitations, these methods cannot produce very small particles. However, the advantage of this method is its relative simplicity, low cost, and the possibility to scale it up to tonnage quantities.

1.3.3.2 Mechanochemical synthesis

This process involves mechanical activation of solid state displacement reactions in ball mill. Thus, mechanical energy is used to induce chemical reactions. The chemical precursors typically consist of mixtures of oxides, chlorides and/or metals that react either during milling or during subsequent heat treatment to form a composite powder consisting of the dispersion of ultrafine particles within a soluble salt matrix. The ultrafine particle is then recovered by selective removal of the matrix phase through washing with an appropriate solvent. Mechanochemical synthesis is generally based on the following displacement reaction:

$$AxC + yB \rightarrow xA + ByC$$

where A_xC and B are precursors, A is the desired product and B_yC is a by-product of the reaction. This process has been used successfully to prepare nanoparticles of a number of materials, including transition metals[61,62], oxide ceramics[63], and oxide semiconductors[64].

1.4 LITERATURE

[1] Blakemore, R. P.; Frankel, R. B. And Kalmijn, A. J. *Nature* **1980**, *286*, 384.

[2] Lowen, H. A. *Science* **1962**, *137*, 279.

[3] Wade, V. J.; Devi, S.; Arosio, P.; Treffry, A.; Harrison, P. M. and Mann, S. *J. Mol. Biol.* **1991**, *221*, 1443.

[4] Edelstein, A. S.; Cammarata, R. C. (ed) *Nanomaterials: synthesis, properties, and applications*, **1996,** Institute of Physics Publishing.

[5] Ponec, V. *Catal. Rev. Sci. Eng.* **1975**, *11*, 41.

[6] Sinfelt, J. H. *Bimetallic catalysts*, **1983,** New York Wiley.

[7] Martens, C. R. (ed) **1968** *Technology of Paints, Varnishes and Lacquers (New York: Reinhold)* P 335.

[8] Interrante, L. B.; Hampden-Smith, M. *J. Chemistry of Advanced Materials, An Overview* **1998**, WILEY-VCH.

[9] Ozin, G. A., *Adv. Mater*. **1992**, *4*, 612.

[10] Gleiter, H. *Prog. Matter. Sci*. **1989**, *33*, 223.

[11] Suryanarayana, C.; Koch, C. C. *Non-Equilibrium Processing of Materials* **1999**, Pergamon Materials Series.

[12] Huang, Y. K.; Menovsky, A. A.; de Boer, F. R. *Nanostruct. Mater.* **1993**, *2*, 505.

[13] Gonsalve, K. E.; Rangarajan, S. P.; Wang, J. *Handbook of Nanostrutured Materials and Nanotechnology, Volume 1, Synthesis and Process*, **2000**, Academic Press.

[14] Wang, Z. L., *Characterization of Nanophase Materials* **2000**, WILEY-VCH

[15] Alivisatos A. P. *Science* **1996**, 271, 933.

[16] Li, J.; Wang, L. W. *Chem. Mater*. **2004**, *16*, 4012.

[17] Lehn, J. M. *Angew. Chem. Int. Ed. Engl.* **1988**, *27*, 89.

[18] Lehn, J. M. *Angew. Chem. Int. Ed. Engl*. **1990**, *29*, 1304.

[19] Smalley, R. E. *Nanotechnology – A revolution in the Making – Vision for R&D in the Next Decade* **1999**, Interagency Working Group on Nanoscience, Engineering and Technology.

[20] Antonietti, M.; Coltner, C. *Angew. Chem. Int. Ed. Engl*. **1997**, *36*, 911.

[21] Wallraff, G. M.; Hinsberg, W. D. *Chem. Rev*. **1999**, *99*, 1801.

[22] Goltner, C. G.; Antonietti, M. *Adv. Mater*. **1997**, *9*, 431.

[23] Hulteen, J. C.; Martin, C. R. *J. Mater. Chem.* **1997**, *7*, 1075.

[24] Tjong, S. C.; Chen, H. *Materials Science and Engineering R.* **2004**, *45*, 1.

[25] Sanders, P. G.; barker, J. G.; Weertman, J. R. *J. Mater. Res*. **1996**, *11*, 311.

[26] Montejano-Carrizales, J. M.; Aguilera-granja, F.; Moran-Lopez, J. L. *Nanostruct. Mater.* **1997**, *8,* 269.

[27] Diaz, G.; Jose-Yacaman, M. *Mater. Chem. Phys.* **1995**, *41*, 240.

[28] Okuda, S.; Kobiyama, M.; Inami, T.; Takamura, S. *Scr. Metall*. **2001**, *44*, 2009.

[29] Granqvist, C. G.; Buhrman, R. A. *J. Appl. Phys.* **1976**, *47*, 2200.

[30] Lai, H. L.; Wong, N. B.; Zhou, X. T.; Peng, H. Y.; Au, F. C.; Wang, N.; Bello, I.; Lee, C. S.; Lee, S. T.; Duan, X. F. *Appl. Phys. Lett*. **2000**, *76*, 294.

[31] Karthikeyan, J.; berndt, C. C.; Tikkanen, J.; Wang, J. Y.; King, A. H.; Herman, H. *Nanostruct.l Mater*. **1997**, *8*, 61.

[32] Singhal, A.; Skandan, G.; Glumac, N.; Kear, B. H. *Scr. Mater.* **2001**, *44*, 2203.

[33] Livage, L.; Henry, M.; Sanchez, C. *Prog. Solid State Chem*. **1988**, *18*, 259.

[34] Ebelman, M. *Ann. Chim. Phys.* **1846**, *16*, 129.

[35] Cossa, A. *II Nuevo Cimento* **1870,** *3*, 228.

[36] Stock, A.; Somieski, K. *Ber. Chem. Ges.* **1921**, *54*, 740.

[37] Tohge, N.; Moore, G. S.; Mackenzie, J. D. *J. Non-cryst. Solids* **1984**, *63*, 95.

[38] Cushing, B. L.; Kolesnichenko, V. L.; O'Connor, C. J. *Chem. Rev.* **2004**, *104*, 3893.

[39] Hoffmann, H.; Bowen, P.; Jongen, N.; Lemaire, J. *Sci. Mater*. **2001**, *44*, 2197.

[40] Li, Y.; Fan, Y.; Chen, Y. *J. Mater. Chem*. **2002**, *12*, 1387.

[41] Deng, D.; Hampden-Smith, M. J. *Chem. Mater*. **1993**, *5*, 681.

[42] Lima, Jr. E.; Drago, V.; Bolsoni, R.; Fichtner, P. F. *Solid State Commun.* **2003,** *125*, 265.

[43] Huang, C. Y.; Chiang, H. J.; Huang, J. C.; Sheen, S. R. *Nanostruct. Mater.* **1998,** *8*, 1393.

[44] Winsor, P. A. *Chem. Rev.* **1968**, 1.

[45] Yu, S. H. *J. Ceram. Soc. Jpn*. **2001**, *109*, S65.

[46] Rajamathi, M.; Seshadri, R. *Curr. Opin. Solid State Mater. Sci*. **2002**, *6,* 337.

[47] Oshima, R.; Yamamoto, T.; Mizukoshi, Y.; Nagata, Y.; Maeda, Y. *Nanostruct. Mater*. **1999**, *12*, 111.

[48] Suslick, K. S.; Choe, S. B.; Cichowlas, A. A.; Grinstaff, M. W. *Nature* **1991**, *353,* 414.

[49] Gonsalves, K. E.; Rangarajan, S. P.; Garcia-Ruitz, A.; Law, C. C. *J. Mater. Sci. Lett*. **1996**, *15*, 1261.

[50] Lisiecki, I.; Pileni, M. P. *J. Am. Chem. Soc*. **1993**, *115*, 3887.

[51] Lisiecki, I.; Pileni, M. P. *J. Phys. Chem*. **1995**, *99*, 5077.

[52] Carpenter, E. E.; Sims, J. A.; Wienmann, J. A.; Zhou, W. L.; O'Connor, C. J. *J. Appl. Phys*. **2000**, *87*, 5615.

[53] O'Connor, C. J.; Seip, C. T.; Carpenter, E. E.; Li, S.; John, V. T. *Nanostruct. Mater*. **1999**, *12*, 65.

[54] Zhang, Z. J.; Wang, Z. L.; Chakoumakos, B. C.; Yin, J. S. *J. Am. Chem. Soc*. **1998**, *120,* 1800.

[55] Binnig, G.; Rohrer, H.; Gerber, C.; Welbel, G. *Appl. Phys. Lett*. **1982**, *40*, 178.

[56] Hiral, T.; Tsubaki, Y.; Sato, H.; Komasawa,. I. *J. Chem. Eng. Jpn.* **1995**, *28*, 468.

[57] Cheng, H.; Ma, J.; Zhao, Z.; Qi, L. *Chem. Mater*. **1995**, *7*, 663.

[58] Rieke, R. D. *Crit. Rev. Surf. Chem*. **1991** *1*, 131.

[59] Benjamin, J. S. *Metall. Trans*. **1970**, *1,* 2943.

[60] Koch, C. C. *Nanostruct. Mater.* **1993**, *2*, 109.

[61] Ding, J.; Suzuki, T.; McCormick, P. G.; Street, R. *J. Phys. D* **1996**, *29*, 2365.

[62] Baburaj, E.; Hubert, K.; Froes, F. *J. Alloys Compd.* **1997**, *257*, 146.

[63] Ding, J.; Miao, W. F.; McCormick, P. G.; Street, R. *Appl. Phys. Lett*. **1995**, *67*, 3804.

[64] Cukrov, L. M.; Tsuzuki, T.; McCormick, P. G. *Scr. Mater*. **2001**, *44*, 1787.

CHAPTER 2 SCOPE AND OBJECTIVES

The objective of this study is to explore an important and fertile research topic on the methods for synthesis of nanomaterials by homogeneous nonaqueous solution phase reactions. Research in this work focuses on synthesizing several kinds of nanomaterials in different environments and structure, including spherical nanoparticles, nanowires and core-shell structure composites

The underlying objective here is to efficiently synthesize different kinds of metallic nanocomposites and core-shell structure magnetic nanocomposites in one system, which potentially can be applied in biosensors and drug target or drug delivery. This investigation will allow us to get many kinds of nanomaterials in the simple system, which is economic and easily scale-up.

First, this dissertation focuses on systematically synthesizing different nanomaterials in one simple system, such as metallic, bimetallic, and core-shell structure including gold coated materials and polymer coated materials, especially for magnetic materials.

Second, this dissertation focuses on employing several methods to characterize and identify the products, such as iron coated with gold, which has some trouble for using XRD to identify due to the overlap of their patterns.

Furthermore, most of the research in this dissertation is the preparation for future application. Functionalizing the gold or polymer on the core shell magnetic nanoparticles and applying them in bio- or medical- related system is another project following this work.

CHAPTER 3 EXPERIMENTAL SECTION

3.1 SYNTHESIS TECHNIQUES

3.1.1 General techniques

Air- and moisture sensitive substances were handled under inert atmosphere, either working with Schlenk techniques or within dry boxes. Argon was used as inert gas, additionally cleaned by purification columns (HYDROSORB, OXISORB®-Glas) to remove residues of oxygen and nitrogen. The vacuum line was connected to a vacuum pump (Edwards) with a maximum vacuum of $5 \sim 10^{-3}$ mbar.

3.1.2 Chemicals

All chemicals and solvents were used as received without additional purification. All kinds of metal chlorides (99%) were purchased from Alfa Aesar. 1-methyl-2-pyrrolidinone and tetrahydronaphthalene (anhydrous, 99.5%) and naphthalene (99%) were purchased from Aldrich, sodium metal (99%) was purchased from Fisher.

3.1.2 Reaction setups

The idea of this synthesis strategy is to reduce metal cations by Na using naphthalene as an electron carrier in homogeneous solutions with polar aprotic solvent. Using this method, we have systematically investigated three types of nanomaterials.

MCl_x + xNa(naphthalide) → M---$(L)_n$ + xNaCl

(M: metal (Fe, Co, Ni, Mn, Bi, ……))

One type of nanomaterial is metal nanoparticles, the process is the following:

MCl_x + xNa(naphthalide) —nL→ M ------- (L)n

The metal precursors are usually metallic chlorides, which are easily dissolved in the system solvent. And after reducing process, NaCl could be precipitated and separated from the system easily.

The second type is metal alloy nanoparticles, the process is described as follows:

M_A^{n+} + M_B^{n+} + R —nL→ AB alloy —(L)n

The two metallic precursors are dissolved in same solvent separately and mixed together. Then reduced and annealed.

The third one is metallic core-shell structure nanoparticles, the process is described as follows,

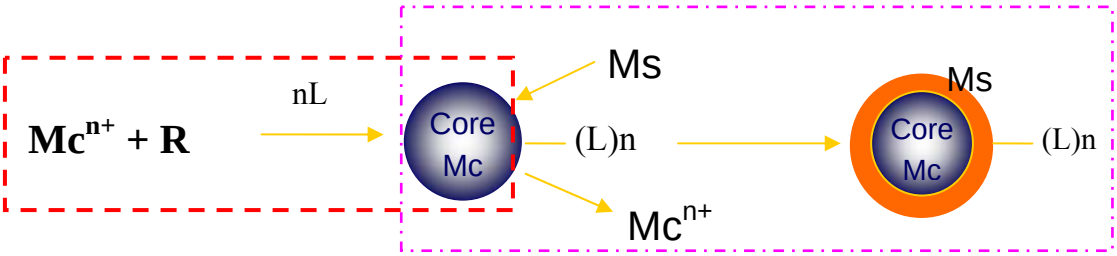

Here, L is capping agent, R is the reducing agent, Mc is the core metal, and Ms is the shell metal. First, the core metallic precursor was reduced by Na to form nanoparticles at certain size that depends on the annealing temperature. After that the solution of the shell metallic precursor was added to the prepared core nanoparticle solution very slowly to let the metal on the surface of the core nanoparticles reduce the shell cations and finally form metallic core-shell structure nanoproducts.

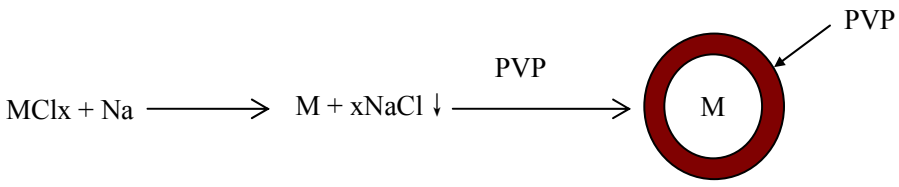

Another core-shell structure nonmaterial, which would be discussed in the dissertation, is polymer coated nanomaterial. Poly (vinyl pyrrolidone) was employed as the coating material and directly covered on the surface of the metallic core nanoparticles as shown above.

3.2 ANALYSIS AND CHARACTERIZATION

3.2.1 X-ray Powder Diffraction[1]

The X-ray powder diffraction (XRD) diagrams of all samples (except iron) were collected in transmission mode on a Phillips-X'PERT Diffractometer (Cu, *Ka*= 1.54056 Å) source with a graphite monochrometer. The data collection and analysis were carried out using the software supplied with the diffractometer. Particle's size can be calculated by the Scherrer equation: $Dc=K\lambda/\beta cos\theta$. Where *Dc* accounts for the average crystal size (here the diameter of the nanoparticles), K = 0.89 is the Scherrer coefficient, λ denoting the X-ray wavelength is equal to *Ka* (shown above). β is the full width at half-maximum (FWHM) and θ is the diffraction angle.

3.2.2 Transmission Electron Microscopy (TEM)[2]

Transmission electronic microscopy (TEM) is widely used to observe the morphology of the nanoproducts and to check their uniformity. By using TEM, a large variety of materials such as ceramics, minerals, metals, alloys, semiconductors, glass and polymers can be observed. The main requirements for the samples are: they must not outgas due to the high vacuum ambient of work, and they have to be appropriately thinned to be observed. In our work, TEM investigations were performed on a JEOL 2010 microscope. For the investigation of the longitudinal shape and structure, the nano-material was deposited onto a perforated carbon foil supported on a copper grid.

3.2.3 Energy Dispersive Spectroscopy (EDS)

Elemental analysis was carried out using an EDAX attachment on a JEOL 2010 TEM with the electron beam focused to two nanometers. EDS is a method of X-ray analysis, which discriminates by energy levels the characteristic X-rays emitted from a sample. The EDS system uses a solid-state detector, which receives counts of all X-rays at once, and divides the energy spectrum of X-rays into different ranges. A collection of X-ray energies from 0 to 40 KeV, can be collected and displayed on a computer screen. Peaks will show up on the spectrum,

corresponding to energies of elements present in the sample. The area included within a peak is roughly proportional to the amount of the corresponding element in the sample, although the detector efficiency decreases with increasing energy. The EDS system can be used for quantitative analysis by counting the X-rays received in the channels that correspond with a peak of interest. EDS is a quick way to find out what is in a sample.

3.2.4 Chemical analysis

3.2.4.1 Fourier Transform Infra Red (FT-IR)[3]

A FT-IR spectrometer (Thermo Nicolet NEXUS 670 FT-IR) was employed to characterize the surface properties of the nanoproducts, especially for polymer coated nanocomposites. FT-IR is most useful for identifying chemicals that are either organic or inorganic. It can be utilized to quantitate some components of an unknown mixture. It can be applied to the analysis of solids, liquids, and gasses. The term Fourier Transform Infrared Spectroscopy (FT-IR) refers to a fairly recent development in the manner in which the data is collected and converted from an interference pattern to a spectrum. Today's FT-IR instruments are computerized which makes them faster and more sensitive than the older dispersive instruments.

3.2.4.2 UV-visible spectroscopy[4]

UV-vis spectroscopy probes the electronic transitions of molecules as they absorb light in the UV and visible regions of the electromagnetic spectrum. Any species with an extended system of alternating double and single bonds will absorb UV light, and anything with color absorbs visible light, making UV-vis spectroscopy applicable to a wide range of samples. Since gold has plasmon property, UV-Visible was employed to measure some gold related information.

3.2.4.3 Inductively Coupled Plasma (ICP)[5]

ICP analysis was performed with CCD Simultaneous ICP- optical emission spectrometry (OES) spectrometer to analyze the composition in the nanoproducts. In the ICP-OES, plasma is used as an energy source, producing heat of 5500° - 8000°K and up to 10000°K in some regions, enough to ionize and excite most analyte atoms. Upon the electron's decay to its ground state, light is emitted and detected. Because the excited ion only emits light of certain wavelengths, spectral lines dependent on the element are produced. These lines can then be used to qualitatively determine the components of the sample. A calibration curve of spectra intensity and concentration can be used to quantitatively determine the concentration of analyte in the sample.

3.2.4.4 ThermoGravimetric Analysis (TGA)[6]

Thermal Analyst 2000 Thermogravimetric Analyzer was employed. Thermogravimetry is one of the oldest thermal analytical procedures and has been used extensively in the study of polymeric systems. The technique involves monitoring the weight loss of the sample in a chosen atmosphere (usually nitrogen or air) as a function of temperature. The usefulness of TGA for analyzing complex systems such as rubber vulcanites was greatly enhanced by the introduction of the ability to record simultaneously the first derivative of the weight loss. This is sometimes referred to as derivative thermogravimetric analysis (DTA). The method can not only give us the composition ratio in the nanoproducts, but also give us the information of the composition.

3.2.5 Magnetic measurement[7]

Magnetic measurements were performed on a SQUID magnetometer (MPMS 5S, Quantum Design). A SQUID detector is a state-of-the-art superconducting susceptometer with a Josephson junction element. It is capable of amplifying very small changes in a magnetic field into a large electrical signal. It can therefore measure a magnetic susceptibility as small as 10^{-10} emu over a wide temperature range (near 0 K to 400 K).

The magnetic measurements include magnetic susceptibility and magnetization. Magnetic susceptibility can be measured as a function of temperature in the presence of a static magnetic field (*DC-M/H*), an alternating magnetic field (*AC-dM/dH*) or both. Typically, samples were characterized utilizing *DC* susceptibility and magnetization as a function of field measurements.

A *DC* measurement can be done with two different methods. Either the sample is cooled in the presence of a magnetic field or in the absence; e. g., *FC* (field cooling) and *ZFC* (zero field cooling). In a field cooled experiment the sample is loaded at room temperature and cooled in the presence of a magnetic field. This causes the spins of the sample to align with the external field. In a zero field cooled experiment the sample is loaded at room temperature and cooled in the absence of a field. This allows the spins to align randomly. In typical bulk samples the external measuring field is not sufficient to overcome the natural ordering of the samples, therefore, the *FC* and *ZFC* susceptibility curves look similar. In spin glass and superparamagnetic materials, however, there is marked difference in the two curves.

Field cooled (*FC*) and zero field cooled (*ZFC*) magnetization experiments at low field are very useful for elucidating superparamagnetic properties. They are simple and point out the irreversible properties below a certain temperature, roughly the mean blocking temperature T_B related to the characteristic time of the experiment. However, quantitative features can be obtained only with a precise

analysis of the phenomenon. This detailed analysis depends on the experimental process and on the sample parameters, such as, the volume distributions, the particle arrangement, the interaction effects, and so on. Much information can be derived form such an analysis concerning mainly the barrier energy distribution and the related volume distributions. The particle magnetic state, the effect of the interparticle interactions form dynamic as well as static points of view can be derived.

3.3 LITERATURE

[1] Jenkins, R.; Snyder, R. L. *Introduction to X-ray powder Diffractometry*, **1996**, John Wiley &Sons, Inc..

[2] Williams, D. B.; Carter, C. B. *Transmission Electron Microscopy: A Textbook for Materials Science*, **1996**, Plenum US.

[3] Ferraro, J. R.; Basile, L. J. *Fourier Transform Infrared Spectroscopy: Applications to Chemical Systems (vol. 1)*, **1978**, Academic Press.

[4] Misra, P.; Dubinskii, M. A. *Ultraviolet Spectroscopy and UV Lasers,* **2002**, Marcel Dekker.

[5] Nolte, J. *ICP Emission Spectrometry: A Practical Guide,* **2003**, Wiley-VCH.

[6] Keattch, C. J. *An Introduction to Thermogravimetry*, **1969**, Heyden, in

co-operation with Sadtler Research Laboratories, Philadelphia.

[7] O'Connor, C. J.; Tang, J.; Zhang, J. H. *Nanosize Magnetic Particles, MagnetoScience: Molecules to Materials,* ed. by J. S. Miller and M. Drillon, **2001**, Wiley-VCH, New York.

CHAPTER 4 SYNTHESIS OF METALLIC NANOMATERIALS

4.1 INTRODUCTION

Although metallic nanoparticles have found applications for centuries in paints and pigments, only recently are they of importance due to their potential applications in emerging areas of nanoscience and technology[1,2], especially in optical probes[3, 4], nanoscale ferromagnets[5, 6], catalysts for organic reactions[7], electrical devices[8], biological labels[9], and biological sensors[10]. Size, shape, and surface morphology[11] play pivotal roles in controlling the physical, chemical, optical, and electronic properties of these nanoscopic materials. Preparation of nanoparticles generally involves the reduction of metal ions in solutions or in high temperature gaseous environments. The high surface energy of these particles makes them extremely reactive, and most systems undergo aggregation without protection or passivation of their surfaces. Some of the commonly used methods for surface passivation include protection by self-assembled monolayers, the most popular being thiol-functionalized organics[12]; encapsulation in the H_2O pools of reverse microemulsions[13]; and dispersion in polymeric matrixes[14].

4.2 SYNTHESIS OF METALLIC NANOPARTICLES IN POLAR SOLVENT AND THEIR CHARACTERIZATION

4.2.1 Introduction

Metallic nanoparticles can be prepared by adding liquid reducing agents to the aqueous solutions of respective salts at adjusted pH[15]. Nanoscale ferromagnetic particles can be obtained by the reduction of metal salts with aqueous sodium or potassium borohydride[16, 17].

Metallic nanoparticles can also be synthesized using organic and organometallic reagents. Metal colloids, which can be used in applications requiring dispersed particles, for example, ferrofluids, have been made by the thermolysis of transition metal carbonyls in an inert atmosphere. Crystalline iron colloids with particle size between 5 and 20 nm have been produced by thermolysis of $Fe(CO)_5$ in polymer solutions[18]. However, the surface of these nanoscale particles oxidized when they were exposed to the room atmosphere. In general, the post-synthesis handling of nanoparticles requires special attention. Thermal decomposition of $Fe(CO)_5$ in an organic surfactant liquid also produced ferrofluids of amorphous iron particles with an 8.5 nm median diameter[19]. It was suggested that carbon atom impurities stabilized the amorphous structure of the particles. The colloidal stability of this ferrofluid was achieved by the long-chain surfactant molecules that prevented the close approach of particles because of

entropic repulsion, thus preventing agglomeration. In this chapter, metallic iron, bismuth and gold nanoparticles would be prepared in polar solvent by reductive chemical method.

4.2.2 Metallic iron

4.2.2.1 Synthesis

The reduction reactions were conducted in polar aprotic solvents. In a typical synthesis, 2 mmol of $FeCl_3$ were dissolved in NMPO (1-methyl-2-pyrrolidinone) to form a yellow solution (# A). 6 mmol of Na were dissolved in NMPO with 6 mmol of naphthalene to form a dark green solution (# B). The solution # A was added into solution # B quickly with intensive stirring at room temperature. The color of mixture changed to dark brown immediately. The mixture was further stirred for two hours and then centrifuged to remove the sodium chloride. Then 4 drops of capping agent, 4-benzylpyridine, was added into the solution followed by heating and refluxing at 165°C for three hours. A black mixture was obtained and cooled to room temperature. The product that was obtained was added tetrahydronaphthalene and then centrifuged yielding a black paste and then added tetrahydronanphthalene to be washed and centrifuged for several times. All the above synthesis operations were performed in an argon atmosphere glove box. The sample was dried in

vacuum. Powder was subjected to characterization by transmission electron microscopy (TEM), energy disperse X-ray spectroscopy (EDS), superconducting quantum interference device (SQUID) (after sealed with paraffin).

4.2.2.2 Characterization

Figure 4-1 is the TEM results and Figure 4-2 is the SQUID result of hysteresis loop at room temperature. The result of TEM shows that the mean size of the nanoparticles is about 10 nm, and from the high resolution picture, the lattice fringes of the nanoparticles is clearly visible. The result of SQUID hysteresis loop at 300 K shows that the magnetic saturation is around 280 emu/g, which is very close to pure iron. And it is well known that for any kind of magnetic iron oxide, the magnetic saturation is lower than 100 emu/g.

Figure 4-1. TEM image for 10 nm iron nanoparticles synthesized at 165 °C.

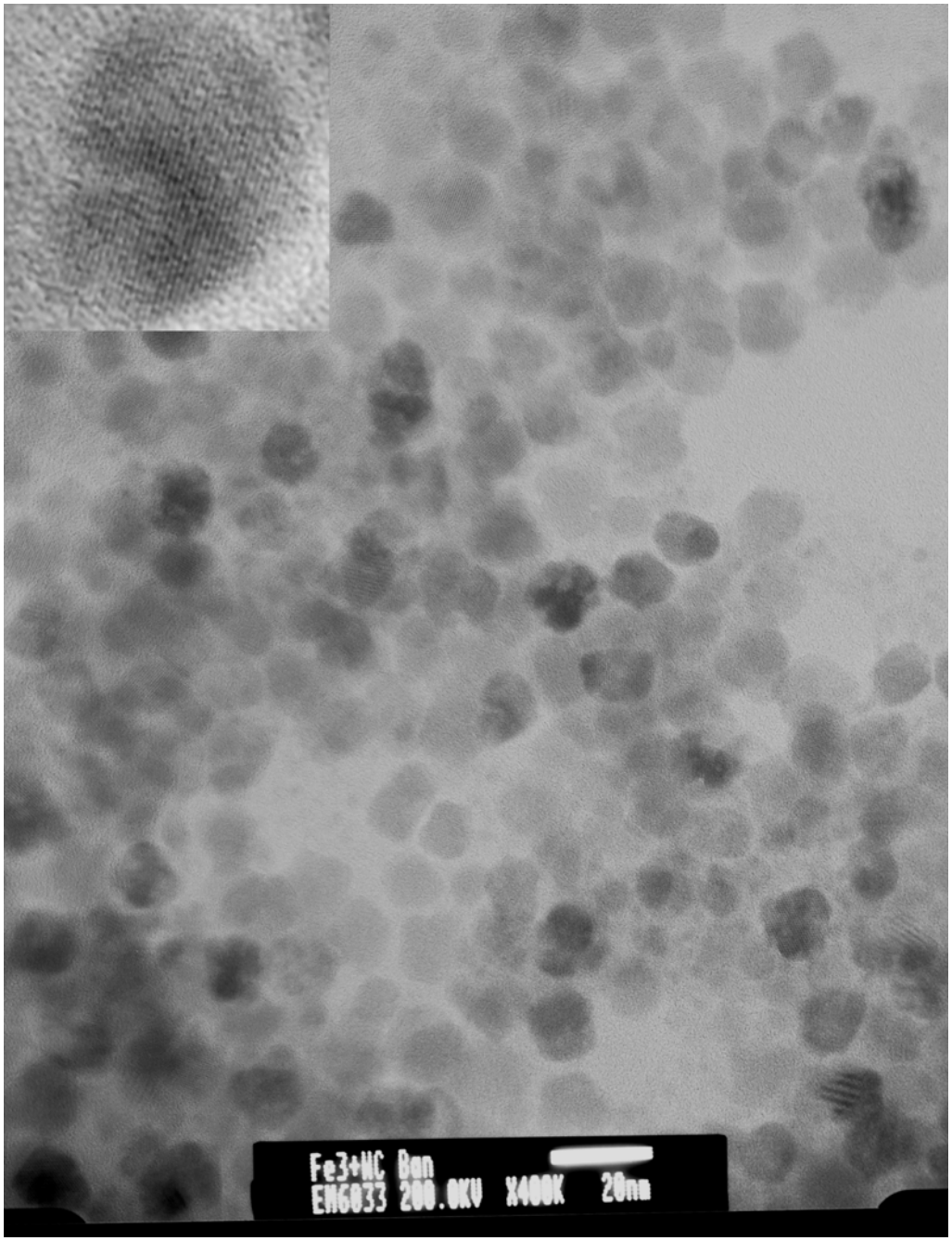

Figure 4-2. Magnetic hysteresis loop at 300 K for 10 nm iron nanoparticles synthesized at 165 °C (this sample was sealed with paraffin to protect from oxidation). The saturation magnetization is around 280 emu/g.

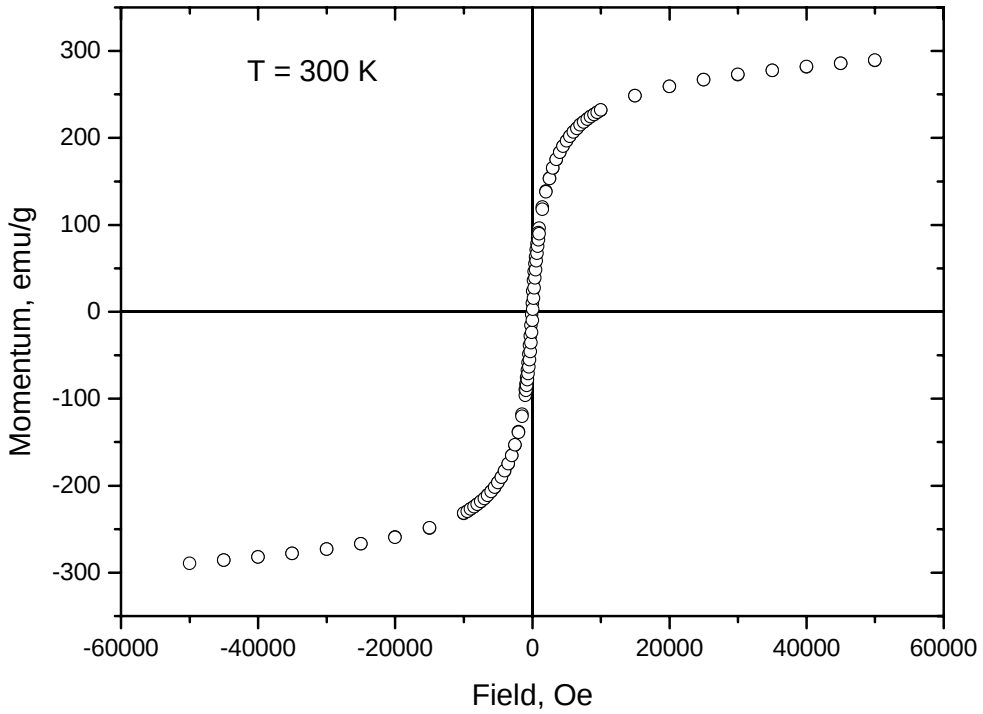

4.2.3 Metallic bismuth

4.2.3.1 Synthesis

The reduction reactions were conducted in polar aprotic solvents. In a typical synthesis, 2 mmol of $BiCl_3$ were dissolved in NMPO (1-methyl-2-pyrrolidinone) to form a white solution (# A). 6 mmol of Na were dissolved in NMPO with 6 mmol of naphthalene to form a dark green solution (# B). A 0.7 mmol of dehydrated $HAuCl_4$ was dissolved in NMPO (# C). The solution # A was added into solution # B quickly with intensive stirring at room temperature. The color of mixture changed to dark immediately. The mixture was further stirred for two hours and then centrifuged to remove the sodium chloride. Then 4 drops of capping agent, 4-benzylpyridine, was added into the solution followed by heating and refluxing at 190°C for three hours. A black mixture was obtained and cooled to room temperature. The product that was obtained was added to tetrahydronaphthalene and then centrifuged yielding a black paste and then added tetrahydronanphthalene to be washed and centrifuged for several times. All the above synthesis operations were performed in an argon atmosphere glove box. The sample was dried in vacuum and characterized by transmission electron microscopy (TEM), energy dispersive X-ray spectroscopy (EDS).

4.2.3.2 Characterization

Figure 4-3 is the TEM image for the as-synthesized Bi nanoparticles. For the image we can see the mean size of the spherical Bi nanoparticle is around 100 nm. The Bi nanoparticles are in good shape, and monolayer dispersed.

Figure 4-4 is the EDS analysis result for the Bi nanoparticles. EDS shows the presence of copper, carbon, and bismuth. The copper and carbon are from the TEM grid, and the bismuth is from the sample.

Figure 4-3. TEM image for ~100 nm Bi nanoparticles synthesized at 190 °C.

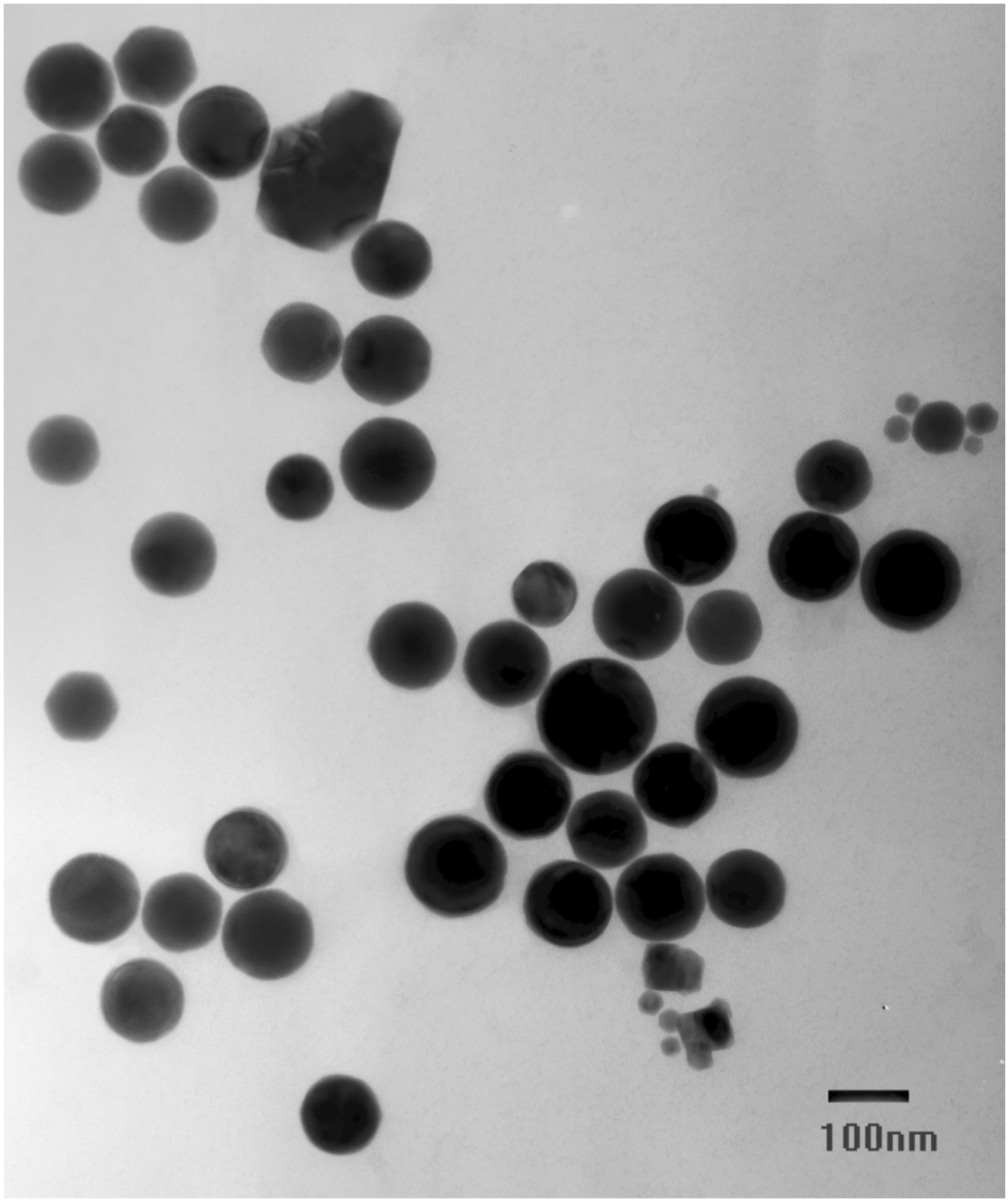

Figure 4-4 EDS analysis result for ~100 nm Bi nanoparticles

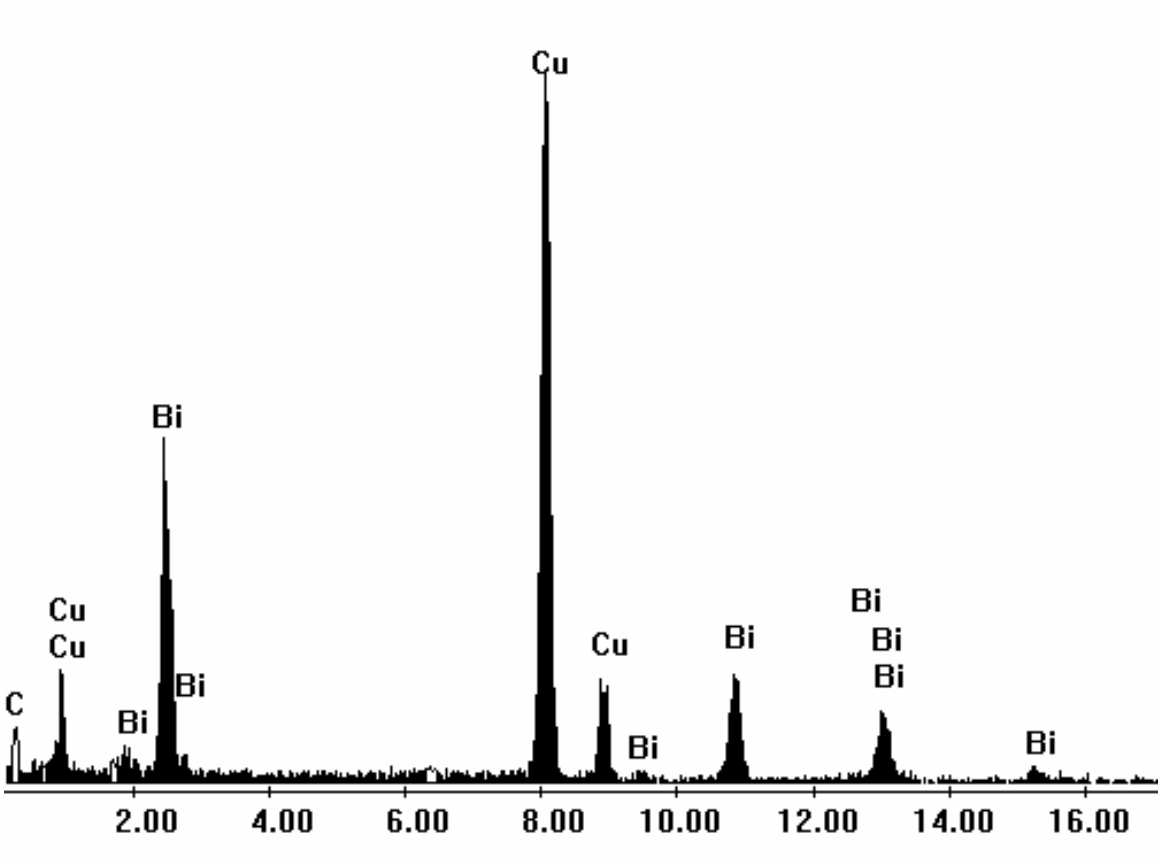

4.2.4 Metallic gold

Since the development of simple solution-phase methods for the synthesis and stabilization of gold nanoparticles[20], research in this field has undergone a rapid expansion. Applications of gold nanoparticles now include biological markers[21], DNA sensors[22], molecular recognition systems[23], and nanoscale electronics[24]. The use of polymer systems interacting with colloidal metal nanoparticles has been explored as a means of particle size control, stabilization, and organization[25], but stabilization has typically been through pendant groups attached to the polymer backbone (e.g., 2-pyrrolidone, cyano, thiol, or pyridine groups). The only reported stabilization of metal nanoparticles by a polymer backbone involved chemical vapor deposition rather than chemistry in solution[26].

4.2.4.1 Synthesis

The reduction reactions were conducted in polar aprotic solvents. In a typical synthesis, 2 mmol of $HAuCl_4$ were dissolved in NMPO (1-methyl-2-pyrrolidinone) to form a yellow solution (# A). 6 mmol of Na were dissolved in NMPO with 6 mmol of naphthalene to form a dark green solution (# B). The solution # A was added into solution # B quickly with intensive stirring at room temperature. The color of mixture changed to dark brown immediately. The mixture was further

stirred for two hours and then centrifuged to remove the sodium chloride. Then 4 drops of capping agent, 4-benzylpyridine, was added into the solution followed by heating and refluxing at 120°C for three hours. A black mixture was obtained and cooled to room temperature. The product that was obtained was added to tetrahydronaphthalene and then centrifuged yielding a black paste and then added tetrahydronanphthalene to be washed and centrifuged for several times. All the above synthesis operations were performed in an argon atmosphere glove box. The sample was dried in vacuum and subjected to characterization by transmission electron microscopy (TEM), UV-visible absorption spectroscopy.

4.2.4.2 Characterization

Figure 4-5 shows the typical TEM image of gold nanoparticles. From the image, we can see the particles are well monodispersed, and the mean size is 5.87 nm with STDEV 0.323 nm. The histogram of the size distribution is shown in Figure 4-6 for monodispersed gold nanoparticles (Figure 4-5).

Figure 4-5. TEM image for ~6 nm Au nanoparticles synthesized at 120 °C.

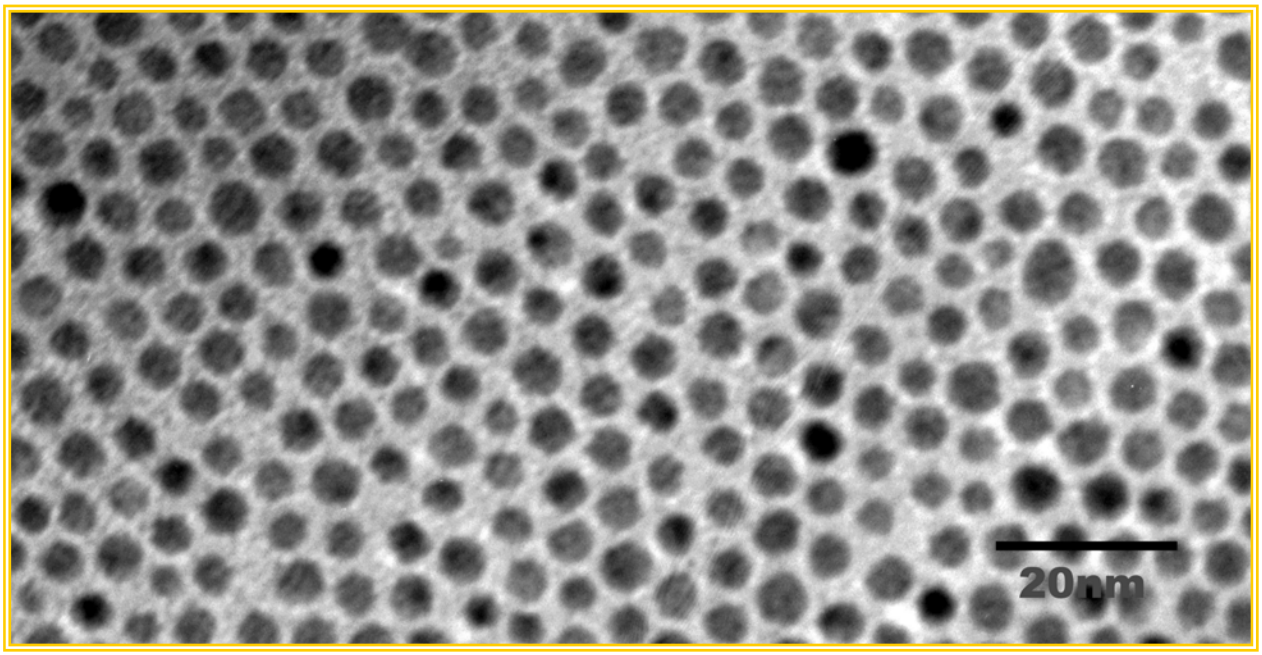

Figure 4-6. Size histogram of spherical Au nanoparticles synthesize at 120 °C. The particles have an average size of 5.87 nm and a standard deviation of 0.323 nm.

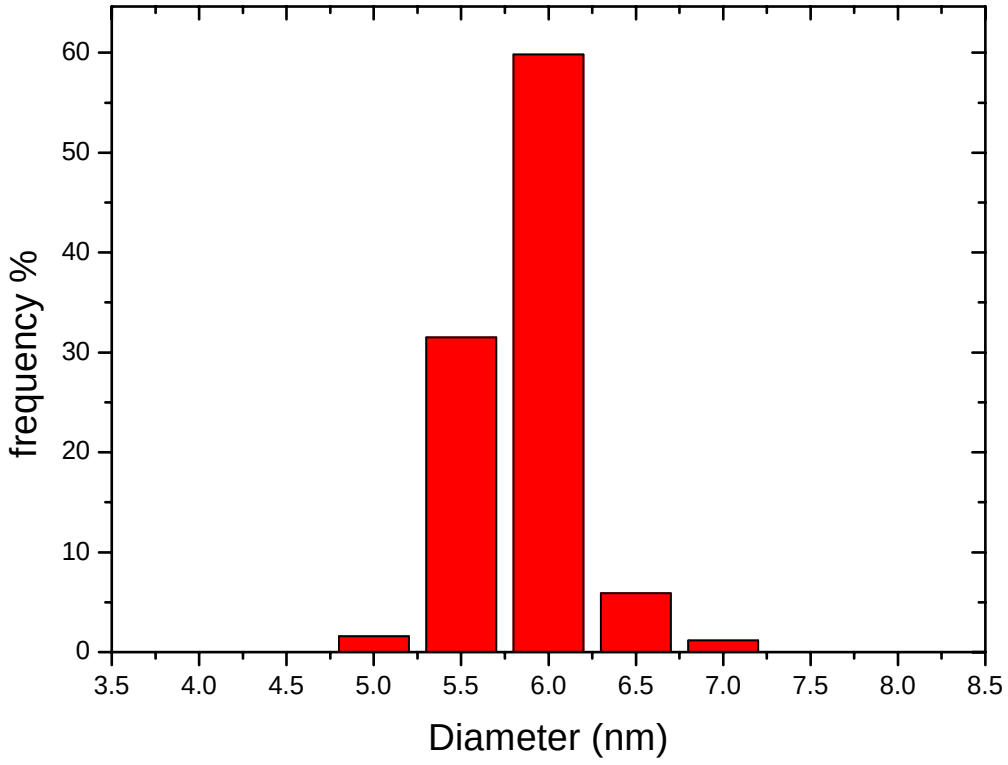

It is known that pure Au nanoparticles exhibit an absorption peak due to excitation of surface plasmon (SP), i.e. collective oscillations of Drude-like conduction electrons and d-band electrons that are optically excited into the conduction band. The peak position is normally within the range of 515-530 nm and its value depends on the particle's size, shape, environment, and dielectric properties. Figure 4-7 shows optical absorption spectra of the Au samples. The spectrum shows the SP peak at 520 nm which corresponds to isolated and randomly oriented spherical Au nanoparticles.

Figure 4-7. UV-vis spectrum (optical density (OD) versus wavelength) of ~6 nm monodispersed gold nanoparticles, the peak position is around 520 nm.

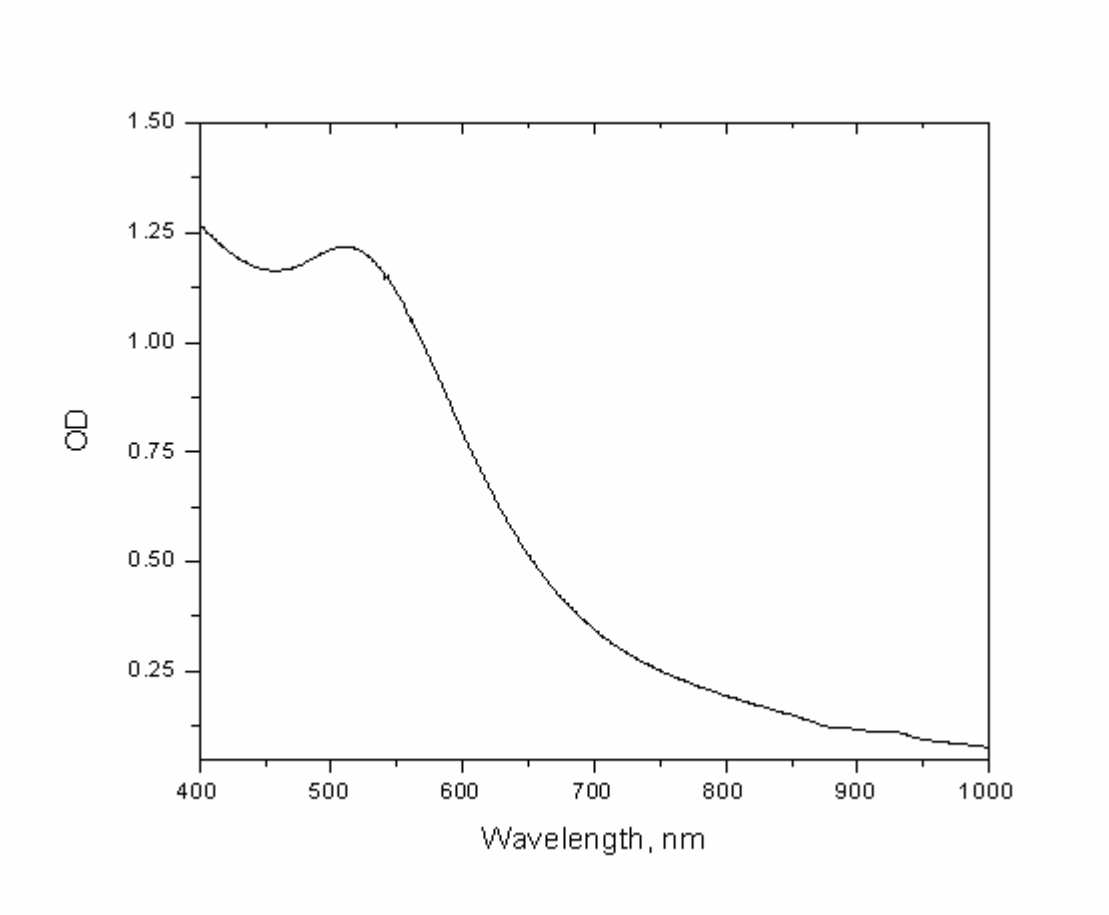

4.3 DISCUSSION AND SUMMARY

In this chapter, three different size nanoparticles were prepared by reductive chemical method, including ~10 nm Fe nanoparticles, ~100 nm Bi nanoparticles and ~6 nm Au nanoparticles. The composition and crystal structures of the products were demonstrated by XRD, TEM, SQUID and UV-visible methods. In this synthesis method, metal cations were reduced by Na using naphthalene as an electron carrier in 1-methyl-2-pyrrolidinone solvent. Since metallic Na is one of the most strongest reducing agents, all the reductive processes could happen at room temperature, no more heating was needed except in the annealing process for the growth of nanoparticles. And most metal cations can be reduced by Na. Another benefit that can be reached by using this system is that the by-product, NaCl, can be easily removed from the reaction system just by centrifuging. 1-methyl-2-pyrrolidinoe is the best solvent for many chemicals except NaCl, which would be the precipitate. It was known that the size, structure, and composition distribution of the nanoproducts depended on the preparation conditions. In the above studies, the concentration of the precursors and reducing agent, and the amount of capping agent were readily optimized after many experiments. The annealing temperature and annealing time would be changed for different nanoproducts since the different conditions for forming different crystal structures. Different annealing temperature usually could form different size of nanoproducts.

Higher temperature would form the bigger size, and at same time, the risk of aggregation also would increase with the increasing of annealing temperature. The above temperatures that we employed for those three nanoparticles were selected from different temperatures to present the typical morphology for them. And at another aspect, even for different compounds, we still could see that the size of the nanoproducts would increase with the increasing of the annealing temperature. Another important factor that would affect the size and morphology of the nanoproducts is the capping agent. We did not do too much research in that field since that is not the purpose in this study. And the capping agent, 4-benzylpyridine, we employed here, works very well. We only changed it to poly vinyl pyrrolidone when we prepared polymer coated core-shell structure nanoproduct, which would be discussed in Chapter 7.

In summary, the study presented in this chapter serve as the basis for further research, such as preparation of bimetallic nanoproducts and core-shell structure nanocompounds in the same systems. These studies will be presented in subsequent chapters.

4.3 LITERATURE

[1] Li, L.; Hu, J.; Alivisatos, A. P. *Nano Lett.* **2001**, *1*, 349.

[2] Zheng, J.; Stevenson, M. S.; Hikida, R. S.; Patten, P. G. V. *J. Phys. Chem. B* **2002**, *106*, 1252.

[3] Taton, T. A.; Lu, G.; Mirkin, C. A. *J. Am. Chem. Soc.* **2001**, *123*, 5164.

[4] Maier, S. A.; Kik, P. G.; Atwater, H. A.; Meltzer, S.; Harel, E.; Koel, B. E.; Requicha, A. A. G. *Nat. Mater.* **2003**, *2*, 229.

[5] Black, C. T.; Murray, C. B.; Sandstrom, R. L.; Sun, S. *Science* **2000**, *290*, 1131.

[6] Sun, S.; Murray, C. B.; Weller, D.; Folks, L.; Moser, A. *Science* **2000**, *287*, 1989.

[7] Le Bars, J.; Specht, U.; Bradley, J. S.; Blackmond, D. G. *Langmuir* **1999**, *15*, 7621.

[8] Fissan H.; Kennedy M. K.; Krinke T. J.; Kruis F. E. *J. Nanopart. Res.* **2003**, *5*, 299.

[9] Jin, R.; Cao, Y.; Mirkin, C. A.; Kelly, K. L.; Schatz, G. C.; Zheng, J. G. *Science* **2001**, *294*, 1901.

[10] a) Yu, L.; Banerjee, I. A.; Matsui, H. *J. Am. Chem. Soc.* **2003**, *125*, 14837. (b) Bruchez, M. Jr.; Moronne, M.; Gin, P.; Weiss, S.; Alivisatos, A. P. *Science* **1998**, *281*, 2013. (c) Storhoff, J. J.; Elghanian, R.; Mucic, R. C.; Mirkin, C. A.; Letsinger, R. L. *J. Am. Chem. Soc.* **1998**, *120*, 1959.

[11] (a) El-Sayed, M. A. *Acc. Chem. Res.* **2001**, *34*, 257. (b) Li, J.; Wang, L. W. *Nano*

Lett. **2003**, *3*, 1357.

[12] Brust, M.; Kiely, C. J. *Colloids and Surfaces A* **2002**, *202*, 175.

[13] Petit, C.; Lixon, P.; Pileni, M. *J. Phys. Chem. B* **1993**, *97*, 12974.

[14] Suslick, K. S.; Fang, M.; Hyeon, T. *J. Am. Chem. Soc.* **1996**, *118*, 11960.

[15] Yang K. C.; Rowan B. D., **1984**, *Metals Handbook* 9th edn, vol 7 (Metals Park, OH: ASM) *p148*.

[16] van Wonterghem, J.; Morup, S.; Koch, C. J. W.; Charles, S. W.; Wells, S. *Nature*, **1996,** *322*, 622.

[17] Inoue, A.; Saida, J.; Masumoto, T. *Metall. Trans. A.* **1988,** *19*, 2315.

[18] Griffiths, C. H.; O'Horo, M. P.; Smith, T. W. *J. Appl. Phys*., **1979**, *50*, 7108.

[19] van Wonterghem, J.; Morup, S.; Charles, S.; Wells, S. V. *J. Phys. Rev. Lett.*, **1985**, *55*, 410.

[20] (a) Brust, M.; Walker, M.; Bethell, D.; Schiffrin, D. J.; Whyman, R. *J. Chem. Soc., Chem. Commun.* **1994**, 801, (b) Brust, M.; Fink, J.; Bethell, D.; Schiffrin, D. J.; Kiely, C. *J. Chem. Soc., Chem. Commun.* **1995**, 1655. (c) Green, M.; O'Brien, P. *Chem. Commun.* **2000**, 183.

[21] Slot, J. W.; Geuze, H. J. *J. Cell. Biol.* **1981**, *90*, 533.

[22] (a) Elghanian, R.; Storhoff, J. J.; Mucic, R. C.; Letsinger, R. L.; Mirkin, C. A. *Science* **1997**, *277*, 1078. (b) Storhoff, J. J.; Elghanian, R.; Mucic, R. C.; Mirkin, C. A.; Letsinger, R. L. *J. Am. Chem. Soc.* **1998**, *120*, 1959.

[23] (a) Liu, J.; Xu, R.; Kaifer, A. E. *Langmuir* **1998**, *14*, 7337. (b) Labande, A.; Astruc, D. *Chem. Commun.* **2000**, 1007.

[24] (a) Andres, R. P.; Bielefeld, J. D.; Henderson, J. I.; Janes, D. B.; Kolagunta, V. R.; Kubiak, C. P.; Mahoney, W. J.; Osifchin, R. G.; *Science* **1996**, *273*, 1690. (b) Sato, T.; Ahmed, H.; Brown, D.; Johnson, B. F. G. *J. Appl. Phys.* **1997**, *82*, 696.

[25] Esumi, K. Hosoya, T.; Suzuki, A.; Torigoe, K.; *Langmuir* **2000**, *16*, 2978.

[26] (a) Akamatsu, K.; Deki, S. *J. Mater. Chem.* **1997**, *7,* 1773. (b) Sayo, K.; Deki, S.; Hayashi, S. *J. Mater. Chem.* **1999**, *9*, 937.

CHAPTER 5 SYNTHESIS OF BIMETALLIC NANOMATERIALS

5.1 INTRODUCTION

In the past decade, considerable efforts have been devoted to bimetallic nanoparticles owing to their different catalytic properties,[1,2,3] surface plasma band energy,[4,5] optical and electrochemical properties,[5,6] and magnetic properties[7,8] relative to the individual metals. A number of methods have been used to prepare the bimetallic nanoparticles, including alcohol reduction,[1,9,10] citrate reduction,[5,11] polyol processes,[12] borohydride reduction,[13] solvent extraction reduction,[4,14,15] sonochemical methods,[16] photolytic reduction,[17,18] radiolytic reduction,[19,20] laser ablation,[21,22] and metal evaporation-condensation.[23] The particle size was usually controlled via protective agents such as soluble polymers and organic ligands, or via the adsorption of anions on particle surface. It was shown that the size, structure, and composition distribution of the resultant particles depended on the preparation conditions.

The enhanced performance of bimetallic nanoparticles compared with the single metal ones is noteworthy.[7,8] For example, recently, alloy based colossal magneto-resistive (CMR) attracts many researchers. And many kinds of alloy nanomaterials have been synthesized. Here, we study the synthesis of MnBi and

FeCo alloys, and for MnBi compound, a new phase with interesting magnetic behavior has been found.

5.2 SYNTHESIS OF FeCo ALLOY

There has been an increasing demand in the design of motors and generators for use in electric vehicles and other applications operating at high temperature. The key issue of designing those motors and generators is to develop new soft magnetic material with excellent magnetic and mechanical properties at high temperatures. The Fe-Co alloys exhibit high saturation magnetization Ms and high Curie temperatures Tc (Tc = 900℃) that make them potential candidates for the high temperature applications. It is well known that Fe and Co form bcc solid solution (Co_xFe_{100-x}) over an extensive range.

In this chapter, $Fe_{50}Co_{50}$ alloy was synthesized in our synthesis system and the obtained sample was characterized.

All syntheses have been performed in a nitrogen atmosphere glove box. The reduction reactions of starting metal cations were performed at room temperature in homogeneous solutions of polar aprotic solvent. In a typical synthesis, 1 mmol of $FeCl_3$ and 1 mmol of $CoCl_2$ were dissolved in 6 ml of 1-methyl-2-pyrrolidinone (NMPO) to form solutions respectively. 5 mmol of Na was dissolved in a solution of 6 ml of NMPO with 5 mmol of naphthalene. After stirring overnight, the

solutions were centrifuged. Solutions of both metal chlorides were mixed with each other and then the solution of Na naphthalide was added into the resulting liquid quickly (over a matter of seconds) while stirring vigorous. The color immediately changed to dark brownish. The mixture was stirred for two hours at room temperature and then centrifuged to remove sodium chloride. The solution was heated at 140^{o}C for 1 hour. The resulting black cloudy suspensions after cooling were diluted with tetralin and a drop of solution was taken for TEM analysis. And after dried by vacuum, the residue was further annealed at 500 ^{o}C for 30 mins then used to prepare the samples for XRD and SQUID

Figure 5-1 shows the XRD pattern for the annealed sample, all the reflections correspond to pure phase of $Fe_{50}Co_{50}$, which indicates pure $Fe_{50}Co_{50}$ alloy was obtained. Figure 5-2 shows the TEM images of the different samples (left image: as-synthesized sample, 140 ^{o}C; right image: sample after annealed at 500 ^{o}C) and the EDS result for the sample after annealed at 500 ^{o}C. The TEM images show that before annealed, the particle size is around 5 nm, and after annealed at 500 ^{o}C, the particle size was increased to 20~50 nm. The good thing is that even annealed at 500 ^{o}C, the obtained samples are still in nanoscale. The EDS result shows that the atom ratio between Fe and Co is almost 1:1, which is identical with the XRD result. Figure 5-3 shows the hysteresis loop at 5 K and 300 K for the sample after annealed at 500 ^{o}C. The sample is ferromagnetic at room temperature, the coercivity is around 350 KOe and the saturation magnetization is above 160 emu/g.

By consider the impurity inside (e.g. organic surfactant), the value should correspond to FeCo alloy exactly.

Figure 5-1. XRD pattern for FeCo alloy sample after annealed at 500 ^{o}C, all the reflections correspond to $Fe_{50}Co_{50}$ phase.

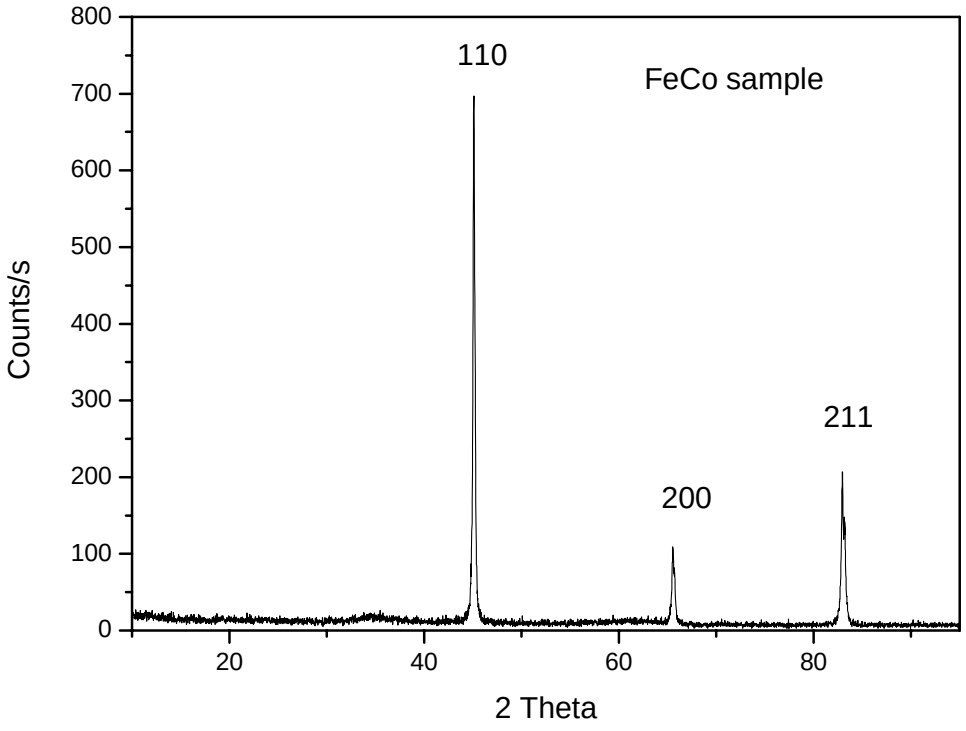

Figure 5-2. TEM images of the different samples (left image: as-synthesized sample, 140 ^{o}C; right image: sample after annealed at 500 ^{o}C) and the EDS result for the sample after annealed at 500 ^{o}C.

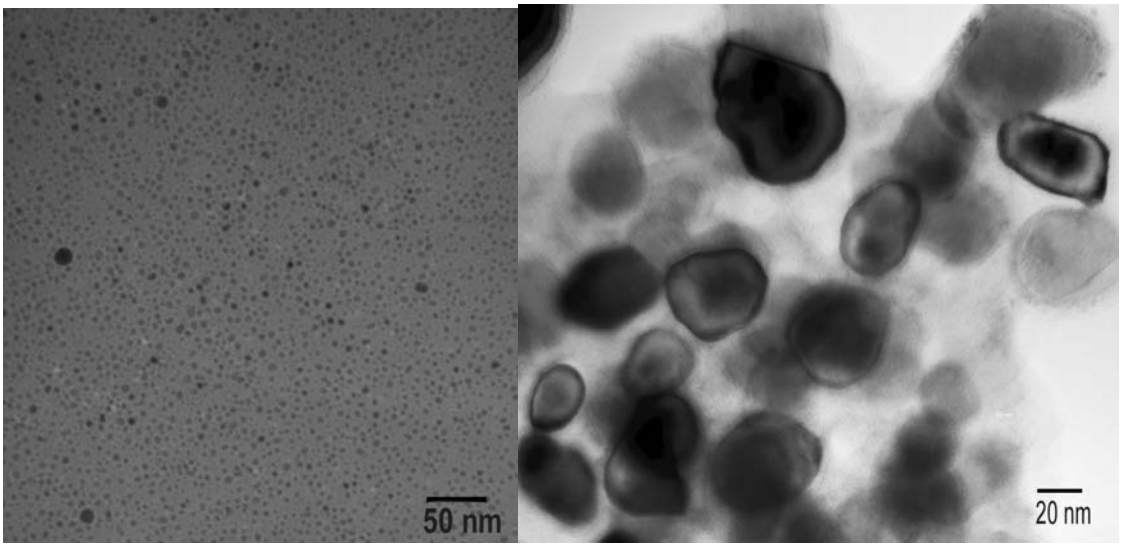

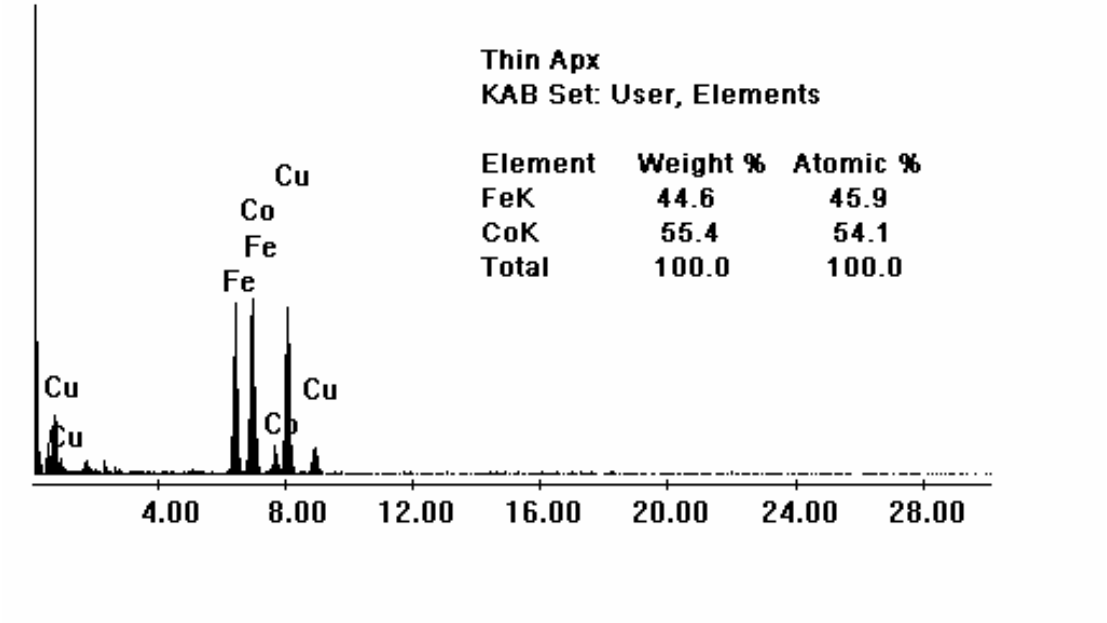

Figure 5-3. Magnetic hysteresis loop at 5 K and 300 K for the sample after annealed at 500 ^{o}C. The sample is ferromagnetic at room temperature, the coercivity is around 350 KOe and the saturation magnetization is above 160 emu/g.

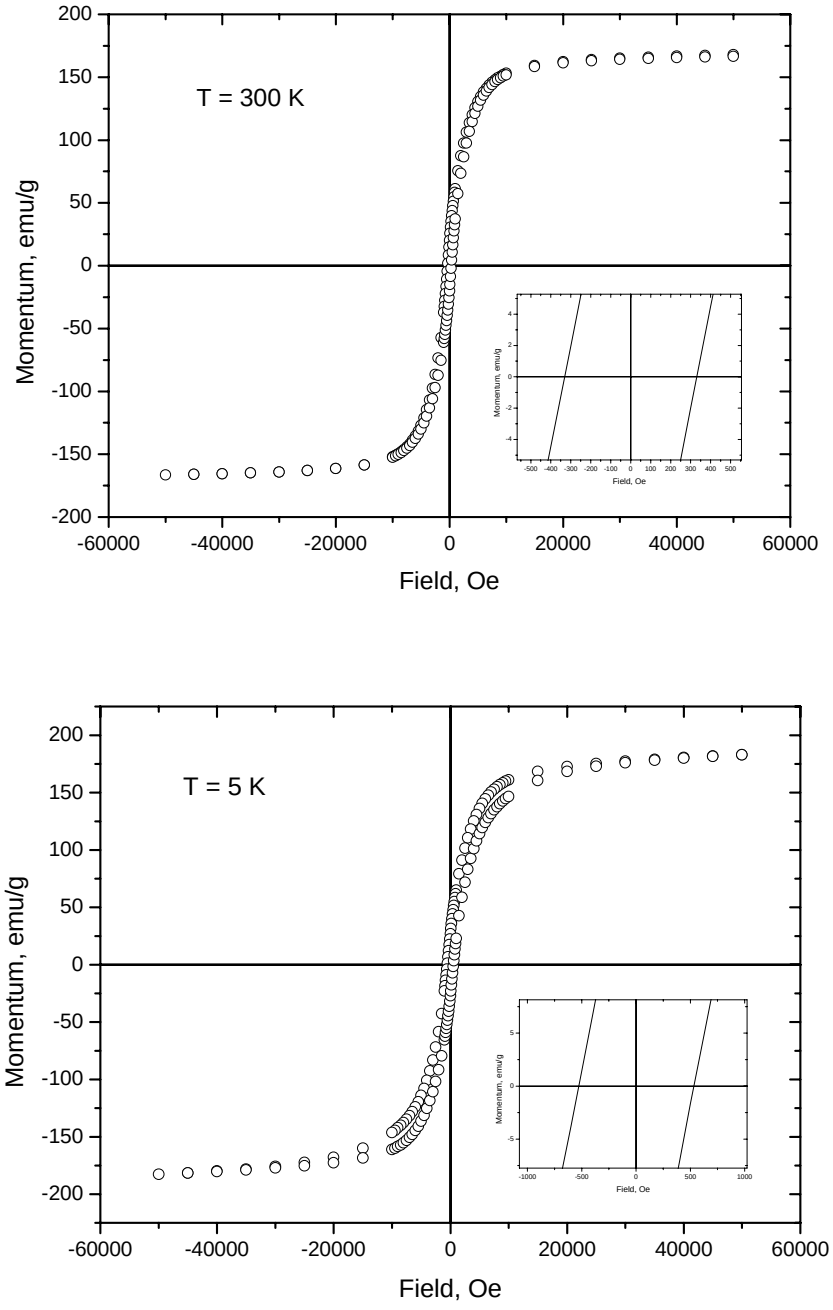

5.3 SYNTHESIS OF MnBi NANOWIRES

5.3.1 Introduction

One-dimensional (1D) nanometer-scale crystalline wires have attracted considerable recent scientific interest due to their unusual properties and potential applications in fabricating nanoscale electronic, photonic, electrochemical, electro-mechanical, and sensing devices[24]. The preparation of 1D nanostructures can be focused on the manner in which atoms or other building blocks are rationally assembled into a structure with nanometer cross section but much larger lengths[25]. Templates or catalysts have been widely used to grow 1D nanostructures[26,27,28,29]; for example templates are used to confine the growth of wires, while catalysts may act as the energetically favorable sites for the growth of reactant moleculars[24(a),30]. Recent studies have shown that the 1D nanostructure might be prepared under properly controlled conditions, even without the presence of catalysts or templates. This implies that the formation of the 1D nanostructure is thermodynamically preferable for many substances under certain conditions[31,32]. Many investigations of the growth process of nanowires have been carried out and several mechanisms were proposed.[33,34,35,36,37] Xia and Sun recently demonstrated a solution-phase method that generated silver nanowires by reducing silver nitrate with ethylene glycol in the presence of poly (vinyl pyrrolidone) (PVP).[38],[39],[40] In this report we used a method of homogeneous non-aqueous solution-phase reaction

in polar aprotic solvents to synthesize the bismuth doped with manganese 1D nanostructure without the use of catalysts or templates. Based on the existence of intermediate products, a mechanism of the formation of the nanowire is proposed. Related doped nanowires have been shown to be promising thermoelectric materials with enhanced efficiency.

5.3.2 Experimental

All chemicals and solvents were used as received without additional purification. Manganese chloride (99%) and bismuth chloride (99%) were purchased from Alfa Aesar. 1-methyl-2-pyrrolidinone and tetrahydronaphthalene (anhydrous, 99.5%) and naphthalene (99%) were purchased from Aldrich, sodium metal (99%) was purchased from Fisher.

All syntheses have been performed in a nitrogen atmosphere glove box. The reduction reactions of starting metal cations were performed at room temperature in homogeneous solutions of polar aprotic solvent. In a typical synthesis, 1 mmol of $MnCl_2$ and 1 mmol of $BiCl_3$ were dissolved in 6 ml of 1-methyl-2-pyrrolidinone (NMPO) to form solutions respectively. 5 mmol of Na was dissolved in a solution of 6 ml of NMPO with 5 mmol of naphthalene. After stirring overnight, the solutions were centrifuged. Solutions of both metal chlorides were mixed with

each other and then the solution of Na naphthalide was added into the resulting liquid quickly (over a matter of seconds) while stirring vigorous. The color immediately changed to dark brownish. The mixture was stirred for two hours at room temperature and then centrifuged to remove sodium chloride. The resulting liquid did not exhibit the light scattering properties.

The solution was split into 3 equal portions. Portions (a), (b) and (c) were heated (~130^{o}C, ~190^{o}C, ~205^{o}C, respectively) for 1 hour. The resulting black cloudy suspensions after cooling were diluted with tetralin and a drop of each solution was taken for TEM analysis. Portion (c) was washed with tetralin and then evaporated in vacuum; the residue was used to prepare the samples for XRD and SQUID.

Transmission electron micrographs and EDX spectra were obtained on the JEOL 2010 microscope; X-ray diffractograms were obtained on Philips X'pert-MPD X-ray powder diffractometer; ICP analysis was performed with CCD Simultaneous ICP-OES spectrometer, magnetic measurements were performed on MPMS-5S SQUID Susceptometer.

5.3.3 Results and discussion

The nanostructure of the products was examined with transmission electron microscopy. As shown in Figures 5-4, 5-5 and 5-6, all samples dispersed on the

TEM grids show nanowire morphology. Figure 5-4 shows the sample that was annealed at a temperature of 130 ^{o}C; in lower resolution (Figure 5-4 a), the structure appears to be a simple nanowire, but in higher resolution (Figure 5-4 b), we can see that the nanowires are actually the chains of self-assembled particles. The driving force for this assembling comes probably from the intrinsic anisotropy of inter-nanoparticle interactions.[33]

Figure 5-4. TEM images of the MnBi sample with annealing temperature at 130 ^{o}C. Figure a is at lower resolution, which shows the simple nanowire morphology; Figure b is at higher resolution, which shows the nanowires are actually the chains of self-assembled particles.

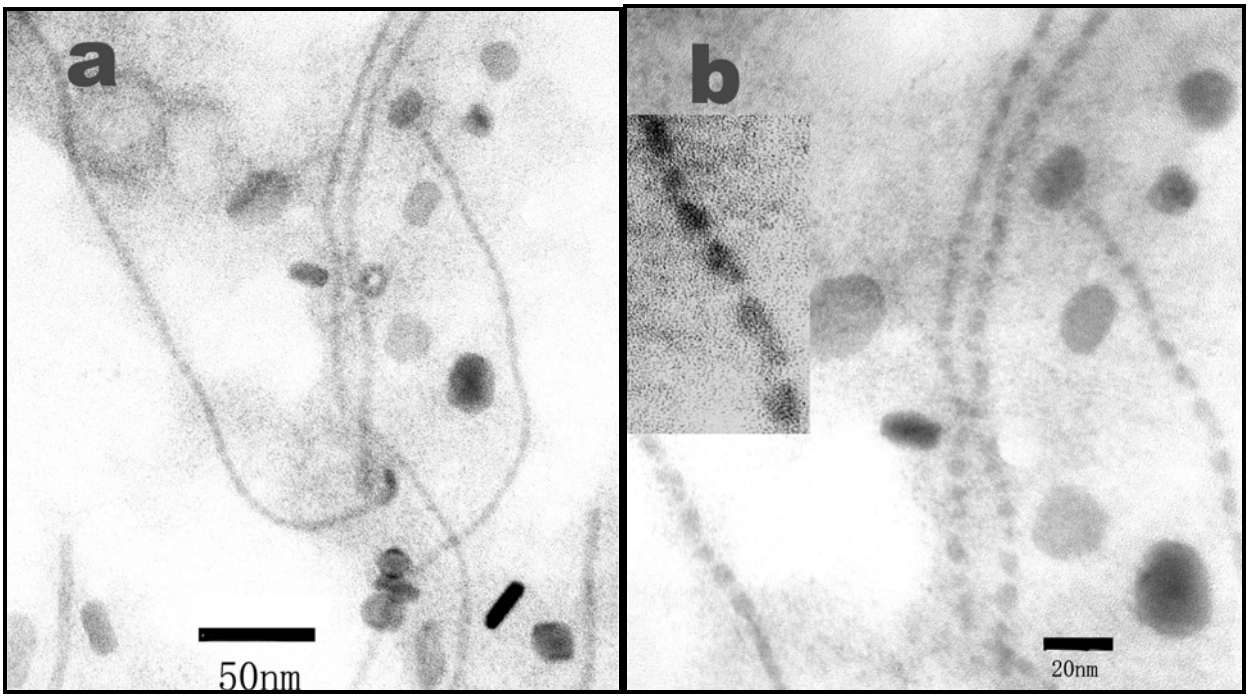

When the annealing temperature increased to 190 ^{o}C, as shown in Figure 5-5, we see some details of the formation of the nanowires. Some particles form the core ("bone") of the nanowire and some particles form the surface structure of the nanowire. An interesting phenomenon is that the surface particles of the nanowire maintain the same wire width to make the nanowire look very uniform. From A and B in Figure 5-5 (b), we see both of the core and surface particles are crystalline. This "shell" can not be an oxide since this structure is not obtained after further reaction at elevated temperatures. As shown below, the XRD pattern also suggests there is no oxidation.

Figure 5-5. TEM images of the MnBi sample with annealing temperature at 190 ^{o}C. A and B in Figure b show the crystalline structure of "bones" and shell particles.

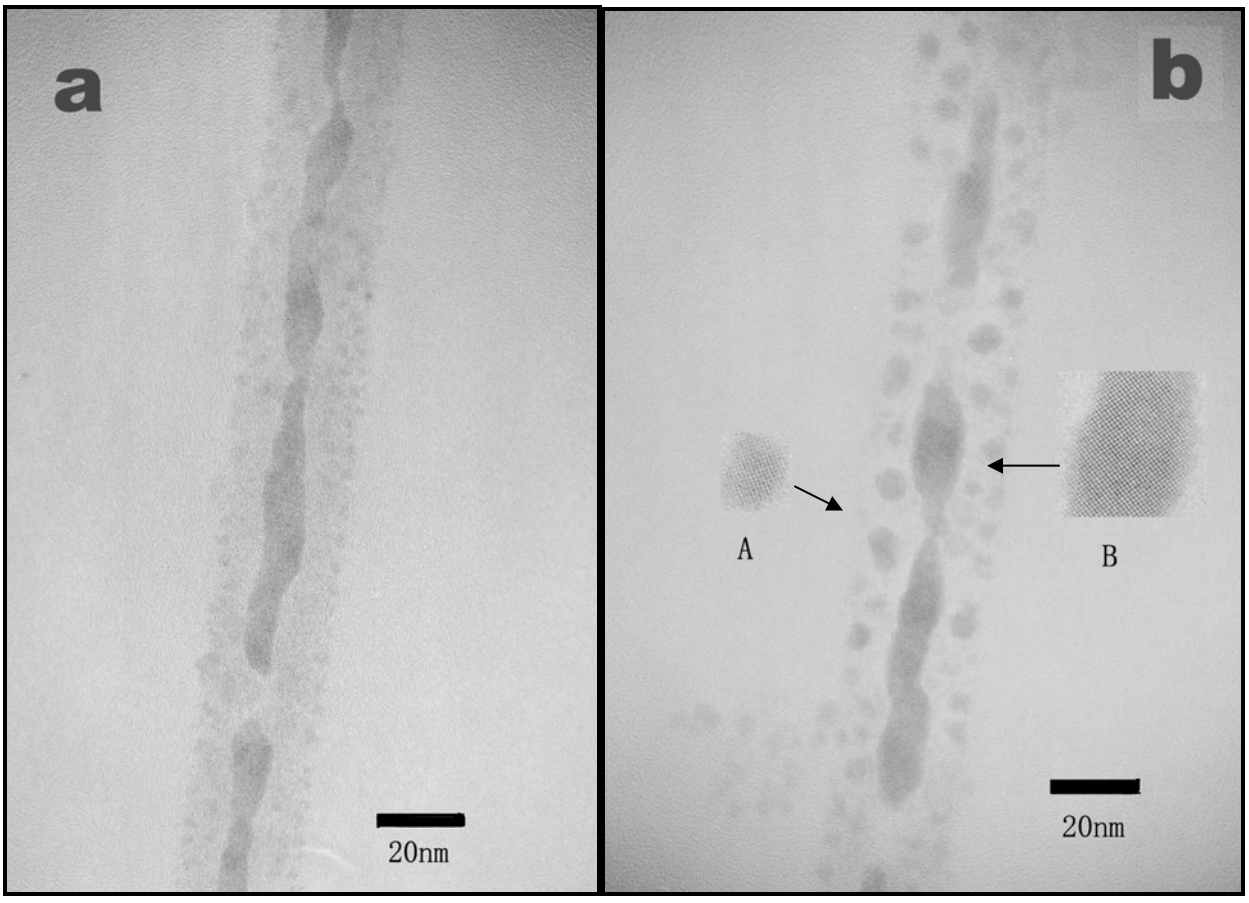

Figure 5-6 is the TEM image of a single nanowire sample that was annealed at 205 ^{o}C. This nanowire is dense, long and uniform in diameter (10 nm) throughout the entire length (several micro-meters) of the nanowire. The "bone" and shell particles (as shown in Figure2) have grown together very well through the Ostwald ripening process;[41] the edge is very clear and the tail part has a sharp crystal structure (as shown in the small image in Figure 5-6). The Energy Dispersive X-ray Spectra (EDS) obtained from the sample after annealing at 205 ^{o}C (sample in Figure 5-6) is given in Figure 5-7. This result shows the molar ratio between Mn and Bi for the nanowire is 1:9. From ICP (Inductively-Coupled Plasma) spectrometer analysis, the same ratio between bismuth and manganese was obtained (Bi: 45.960 ppm, SD=0.05380; Mn: 5.1914 ppm, SD=0.08567).

Figure 5-6. TEM and HRTEM images of the $Mn_{0.1}Bi_{0.9}$ single nanowire with annealing temperature at 205 ^{o}C, and diffraction pattern for the single nanowire. The nanowire grows in <11-20> direction.

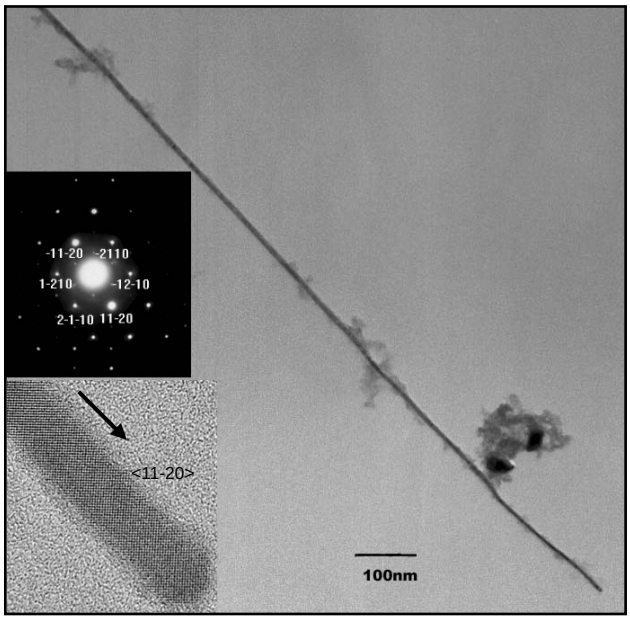

Figure 5-7. EDX spectrum of the MnBi single nanowire (shown in Figure 5-6), the molar ratio between Mn and Bi for the nanowire is 1:9.

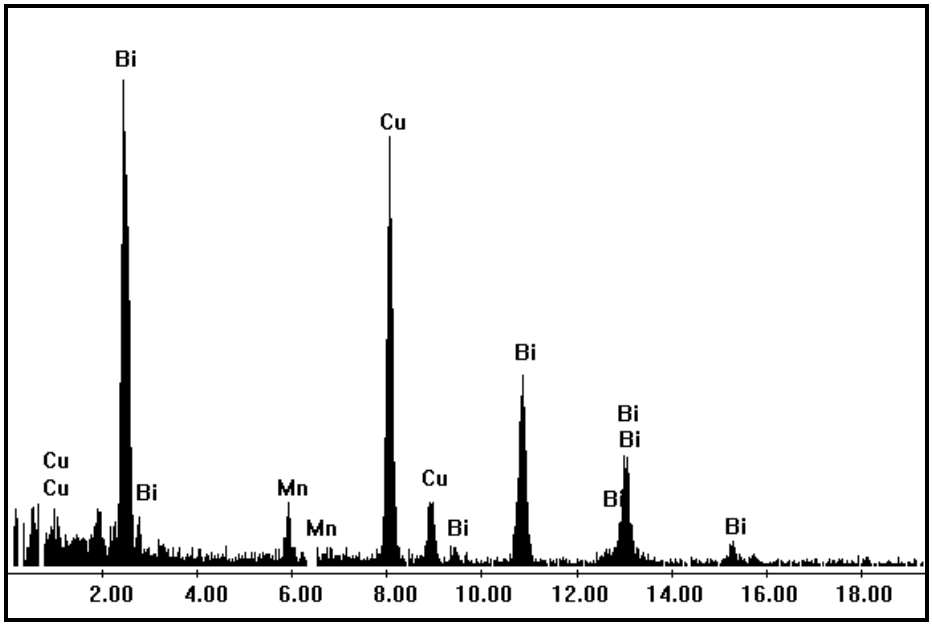

After examining many nanowires and many areas of each single nanowire, the typical electron diffraction pattern for the single nanowire is shown in Figure 3. In the HRTEM image as shown in Figure 5-6, the lattice spacing of the nanowire is 0.24 nm corresponding to the (11-20) diffraction in the electron diffraction pattern. The HRTEM image and electron diffraction pattern demonstrate that the bismuth doped with manganese nanowires grow along the <11-20> direction.

The XRD technique was used to study the phase of the as-prepared nanowires. The XRD pattern, as shown in Figure 5-8, is for sample (c) mixed with standard Si powder for reference. This pattern can be indexed to the rhombohedral phase with lattice constant a=4.544(1) Å, c=11.838(1) Å. We found that there is a difference in the lattice constants between the manganese doped sample and pure bismuth. For pure bismuth, a=4.546 Å, c=11.86 Å (JCPDF, 5-519). The difference in parameter c is due to the manganese doping in a bismuth unit cell, resulting in the decrease of parameter c. This result corresponds to the molar ratio between manganese and bismuth (1:9). Since the sample is a powder and the nanowires are disordered, we can not find any preferred orientation of the nanowires from the XRD pattern.

Figure 5-8. XRD patterns for the MnBi sample with the annealing temperature at 205 ^{o}C, and standard Si powder as the reference.

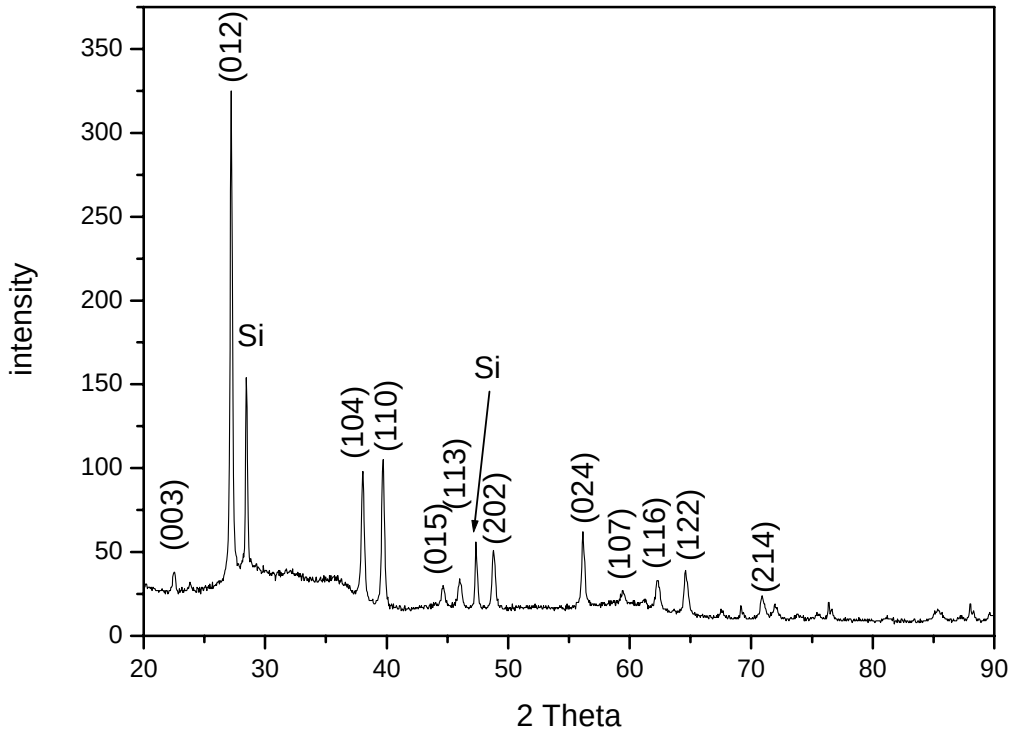

Magnetic properties of the nanowires were investigated using quantum design MPMS-5S SQUID magnetometer. The as-prepared nanowire is paramagnetic at room temperature (see Figure 5-9b). However around 40 K a sharp increase in magnetic susceptibility was observed which is associated with a paramagnetic to ferromagnetic transition (Figure 5-9c). The hysteresis loop at 5 K is presented in Figure 5-9a. The nanowire has high coercivity (~8 kOe) and low magnetization (~10 emu/g). These magnetic properties point to the formation of some metastable phase due to the incorporation of manganese into bismuth matrix. And from the phase diagram[42] as shown in Figure 5-10, we can see that this metastable phase may form with the molar ratio of 1:9 between Mn and Bi. Annealing of the sample at 600 ^{o}C leads to the decomposition of this phase into the mixture of MnBi alloy and Bi, which usually takes place for the manganese-bismuth alloy with excess bismuth prepared by conventional techniques. Small amounts of MnBi alloy leads to the appearance of the hysteresis loop at room temperature in sample c after annealing at 600^{o}C (Figure 5-9d). We have also measured the FC and ZFC cures for the sample annealed at 600 ^{o}C, which suggests there the presence of some ferromagnetic materials (MnBi alloy).

Figure 5-9. SQUID results for the MnBi sample after annealed at 205 ^{o}C, (a) hysteresis loop at 5K, ferromagnetic behavior; (b) hysteresis loop at 300K, paramagnetic behavior; (c) FC-ZFC curve for original product, magnetic field is 100Oe, a transition from paramagnetic to ferromagnetic happened around 40 k; (d) hysteresis loop at 300K for the MnBi sample after further annealed at 600 ^{o}C, protected by argon. The small figure inside shows the separation of the hysteresis loop.

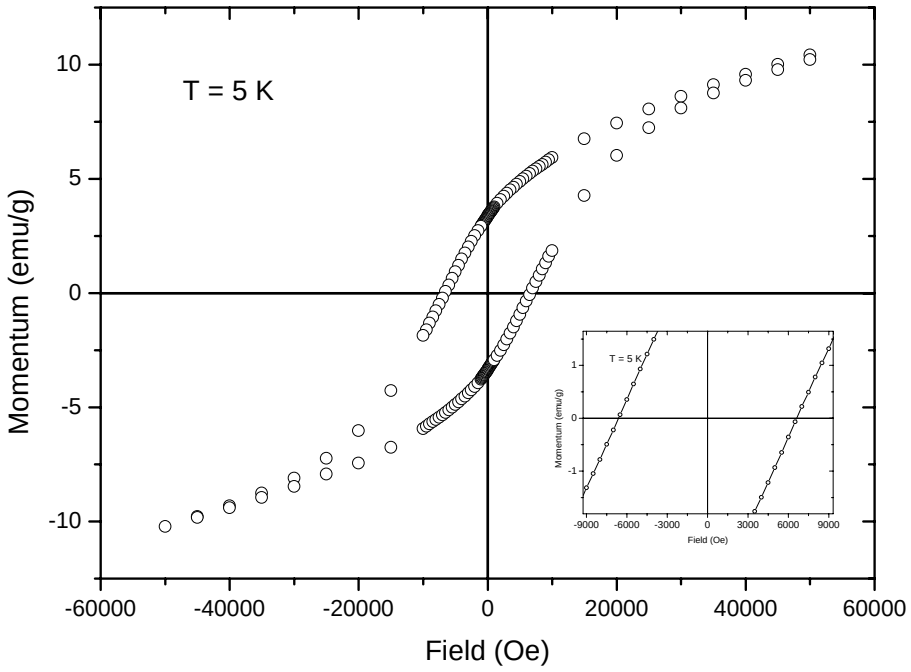
T = 5 K
Momentum (emu/g)
Field (Oe)
10
5
0
-5
-10
-60000
-40000
-20000
0
20000
40000
60000
T = 5 K
Momentum (emu/g)
Field (Oe)
1
0
-1
-9000
-6000
-3000
0
3000
6000
9000

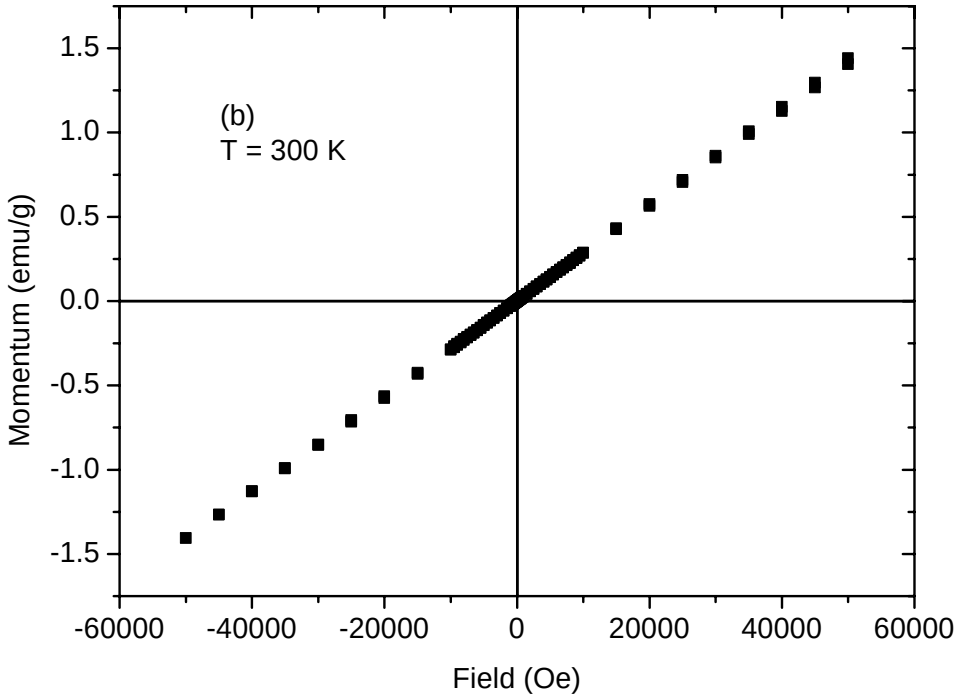
(b)
T = 300 K
Momentum (emu/g)
Field (Oe)
1.5
1.0
0.5
0.0
-0.5
-1.0
-1.5
-60000
-40000
-20000
0
20000
40000
60000

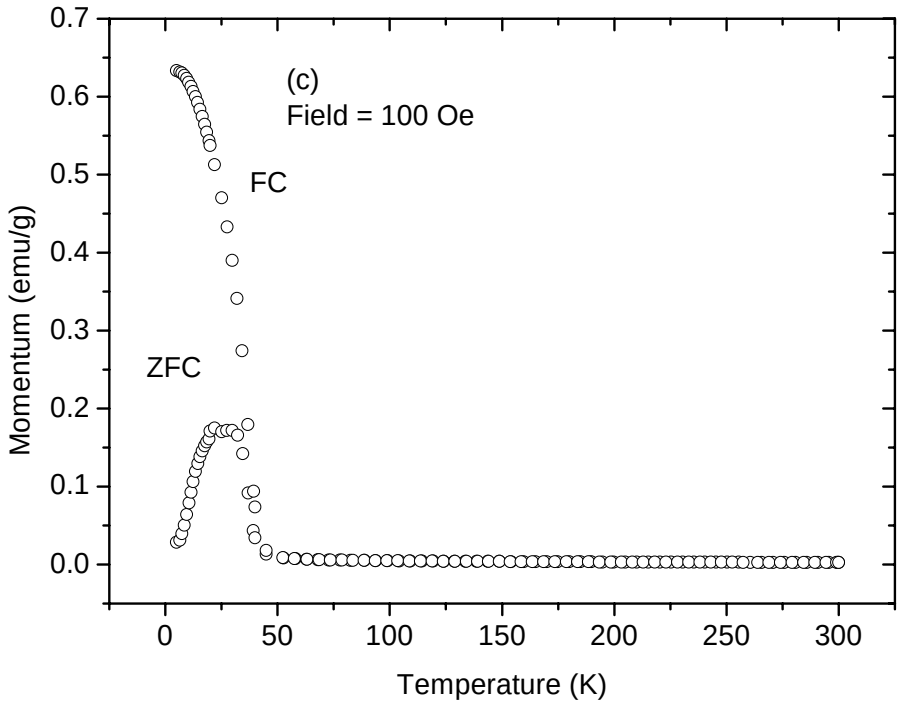
(c)
Field = 100 Oe
FC
ZFC
Momentum (emu/g)
Temperature (K)
0.7
0.6
0.5
0.4
0.3
0.2
0.1
0.0
0
50
100
150
200
250
300

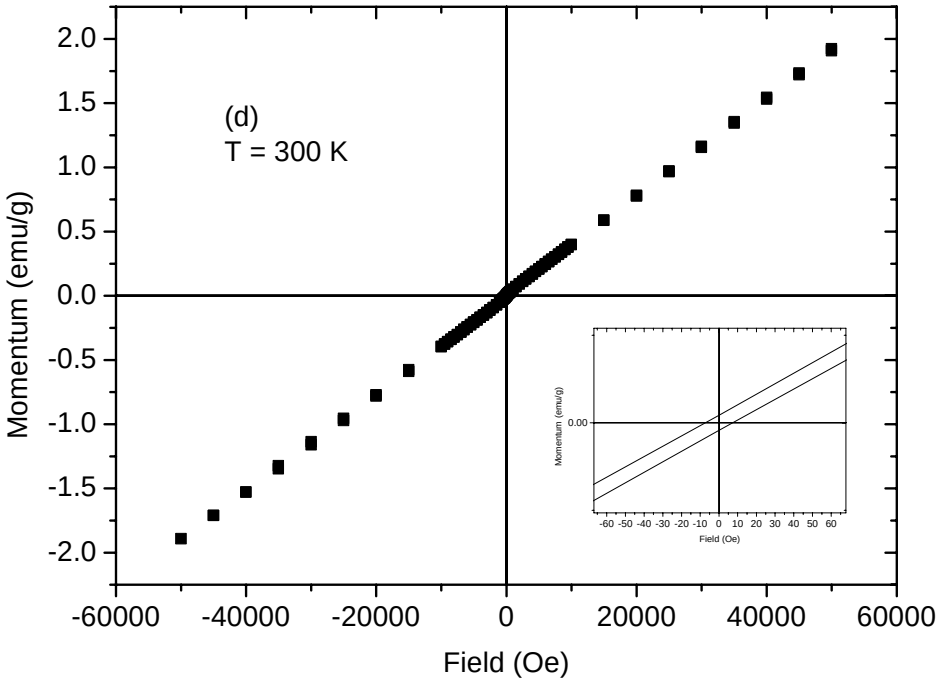
(d)
T = 300 K
Momentum (emu/g)
Field (Oe)
2.0
1.5
1.0
0.5
0.0
-0.5
-1.0
-1.5
-2.0
-60000
-40000
-20000
0
20000
40000
60000
0.00
-60 -50 -40 -30 -20 -10 0 10 20 30 40 50 60

Figure 5-10. Bi-Mn phase diagram. (Ref. 42)

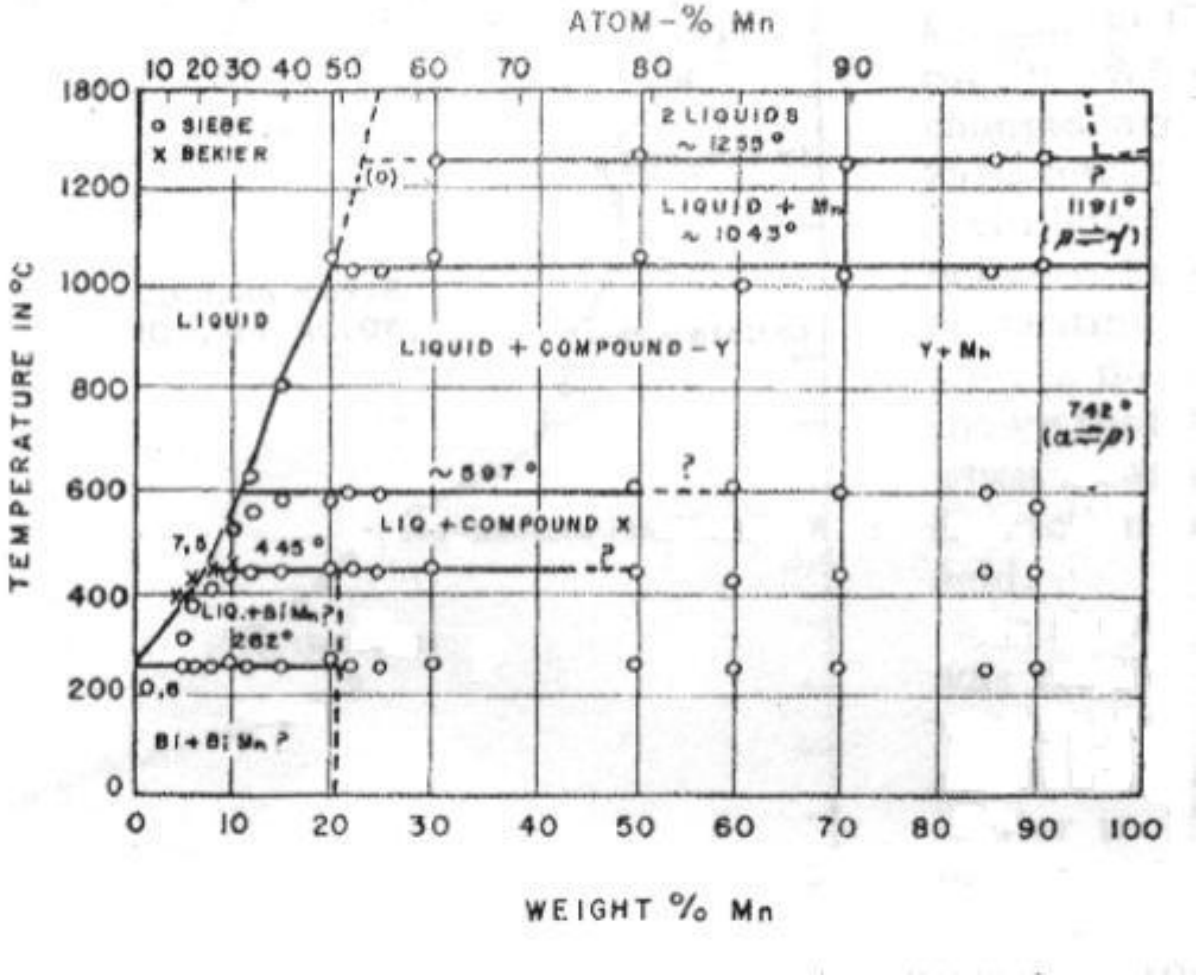

The formation of the nanowires from a colloidal system is a very complicated process. Based on the above results, the proposed mechanism of the process is shown in Figure 5-11, which is a simple 4 stage model. The process begins with rapid nucleation and formation of small particles followed by their self-assembling in chains (A) due to the intrinsic anisotropy of inter-nanoparticle interactions; then those particles come together with increasing temperature to form nanorods (we call it X-axial growth: along the nanowire growth direction) (B), these nanorods connect as nanowires. At the same time, other smaller particles are attracted to the wires (we call it Y-axial growth: perpendicular to the nanowire growth direction) (C) and make the wires thicker (D) through the Ostwald ripening process.

Figure 5-11. Schematic illustration of growth mechanism for the nanowire including four stages (A) particles self-assembling; (B) X-axial growth (along the nanowire growth direction); (C) Y-axial growth (perpendicular to the nanowire growth direction); (D) form the well growth nanowire. (B) and (C) processes can happen at same time, and (B) has the priority.

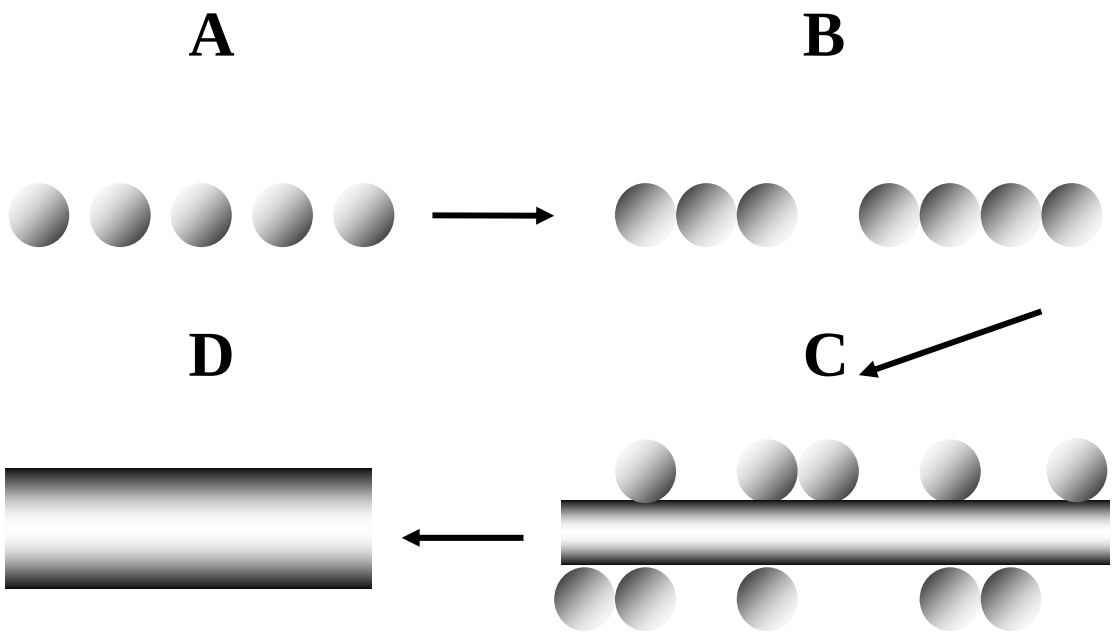

5.4 CONCLUSIONS

Bimetallic nanomaterials were synthesized in this system, such as $Fe_{50}Co_{50}$ alloy and Bi doped with Mn. For FeCo alloy, after annealing at 500 °C, a pure phase of $Fe_{50}Co_{50}$ was obtained. Highly uniform, high aspect ratio single crystal bismuth doped with manganese nanowires were also successfully prepared by using simple homogeneous non-aqueous solution reactions. Based on the intermediates obtained at different temperature, a mechanism of the nanowire growth process was proposed. This low-temperature synthetic route does not require elaborate equipment and proceeds without the participation of catalysts or templates, and thus offer great opportunity for scale-up preparation of 1D nanostructure materials. This kind of uniform bismuth doped with manganese nanowire could have potential applications in thermoelectric and magnetic devices.

5.5 LITERATURE

[1] Toshima, N.; Yonezawa, T.; Kushihashi, K. *J. Chem. Soc., Faraday Trans.* **1993**, *89*, 2537.

[2] Harada, M.; Asakura, K.; Ueki, Y.; Toshima, N. *J. Phys. Chem.* **1993**, *97*, 5103.

[3] Wang, Y.; Toshima, N. *J. Phys. Chem. B* **1997**, *101*, 5301.

[4] Han, S. W.; Kim, Y.; Kim, K. *J. Colloid Interface Sci.* **1998**, *208*, 272.

[5] Link, S.; Wang, S. Z. L.; El-Sayed, M. A. *J. Phys. Chem. B* **1999**, *103*, 3529.

[6] Chen, D. H.; Chen, C. J. *J. Mater. Chem*. **2002**, *12*, 1557.

[7] Bian, B.; Hirotsu, Y.; Sato, K.; Ohkubo, T.; Makino, A. *J. Electron Microsc.* **1999**, *48*, 753.

[8] Sun, S.; Murry, C. B.; Weller, D.; Folk, L.; Moser, A. *Science* **2000**, *287*, 1989.

[9] Toshima, N.; Wang, Y. *Langmuir* **1994**, *10*, 4574.

[10] Yonezawa, T.; Toshima, N. *J. Chem. Soc. Faraday Trans.* **1995**, *91*, 4111.

[11] Freeman, R. G.; Hommer, M. B.; grabar, K. C.; Jackson, M. A.; Natan, M. J. *J. Phys. Chem.* **1996**, *100*, 718.

[12] Silvert, P. Y.; Vijayakrishnan, V.; Vibert, P.; Herrera-Urbina, R.; Elhsissen, K. T. *Nanostruct. Mater.* **1996**, *7*, 611.

[13] Liz-Marzan, L. M.; Philipse, A. P. *J. Phys. Chem*. **1995**, *99*, 15120.

[14] Esumi, K.; Shiratori, M.; Ishizuka, H.; Tano, T.; Torigoe, K.; Meguro, K. *Langmuir*, **1991**, *7*, 457.

[15] Brust, M.; Walker, M.; Bethell, D.; Schiffrin, D. J.; Whyman, R. *J. Chem. Soc. Chem. Commun.* **1994**, 801.

[16] Mizukoshi, Y.; Okitsu, K.; Maeda, Y.; Yamamoto, T. A.; Oshima, R.; Nagata, Y. *J. Phys. Chem. B* **1997**, *101*, 7033.

[17] Remita, S.; Mostafavi, M.; Delcourt, M. O. *Radiat. Phys. Chem*. **1996**, *47*, 275.

[18] Sato, T.; Kuroda, S.; Takami, A.; Yonezawa, Y.; Hada, H. *Appl. Organomet.*

Chem. **1991**, **5**, 261.

[19] Mulvaney, P.; Giersig, M.; Henglein, A. *J. Phys. Chem*. **1993**, *97*, 7061.

[20] Treguer, M.; de Cointet, C.; Remita, H.; Khatouri, J.; Mostafavi, M.; Amblard, J.; Belloni, J.; de Keyzer, R. *J. Phys. Chem. B* **1998**, *102*, 4310.

[21] Hodak, J. H.; Henglein, A.; Giersig, M.; Hartland, G. V. *J. Phys. Chem. B* **2000**, *104*, 11708.

[22] Chen. Y. H.; Yeh, C. S. *Chem. Commun*. **2000**, 371.

[23] Papavassiliou, G. C. *J. Phys. F: Met. Phys.* **1976**, *6*, L103.

[24] (a) Morales, A. M.; Liber, C. M. *Science* **1998**, *279*, 208. (b) Kelly, D.; Wegrowe, J.; Truong, T.; Hoffer, X.; Ansermet, J. *Phy. Rev. B* **2003**, *68*, 13. (c) Saito, S. *Science* **1997**, *278*, 77. (d) Bockrath, M.; Cobden, D. H.; McEuen, P. L.; Chopra, N. G.; Zettl, A.; Thess, A.; Smalley, R. R. *Science* **1997**, *275*, 1992. (e) Zhang, Z.; Blom, D. A.; Gai, Z.; Thompson, J. R.; Shen, J.; Dai, S. *J. Am. Chem. Soc.* **2003**, *125*, 7528. (f) Collins, P. G.; Zettl, A.; Bando, H.; Thess, A.; Smalley, R. E. *Science* **1997**, *278*, 100. (g) Zhu, Y.; Bando, Y.; Xue, D.; Xu, F.; Golberg, D. *J. Am. Chem. Soc*. **2003**, *125*, 14226. (h) Suenaga, L.; Colliex, C.; Demoncy, N.; Loiseau, A.; Pascard, H.; Willaime, F. *Science* **1997**, *278*, 653.

[25] Hu, J.; Odom, T. W.; Lieber, C. M. *Acc.Chem. Res.* **1999**, *32*, 435.

[26] Spange, S. *Angew. Chem., Int. Ed.* **2003**, *42*, 4430.

[27] Tian, B.; Che, S.; Liu, Z.; Liu, X.; Fan, W.; Tatsumi, T.; Terasaki, O.; Zhao, D.

Chem. Comm. **2003**, *21*, 2726.

[28] Wang, Y.; Herricks, T.; Xia, Y. *Nano Lett*. **2003**, *3*, 1163.

[29] Hofmann, S.; Ducati, C.; Neill, R. J.; Piscanec, S.; Ferrari, A. C.; Geng, J.; Dunin-Borkowski, R. E.; Robertson, J. J. *App. Phy*. **2003**, *94*, 6005.

[30] Duan, X. F.; Huang, Y.; Cui, Y.; Wang, J. F.; Lieber, C. M. *Nature* **2001**, *409*, 66.

[31] Wang, X.; Li, Y. *J. Am. Chem. Soc.* **2002**, *124*, 2880.

[32] Caswell, K. K.; Bender, C. M.; Murphy, C. J. *Nano Lett.* **2003**, *3*, 667.

[33] Tang, Z.; Kotov, N.A.; Giersig, M. *Science* **2002**, *297*, 237.

[34] Tian, M.; Wang, J.; Kurtz, J.; Mallouk, T. E.; Chan, M. H. W. *Nano Lett*. **2003**, *3*, 919.

[35] Stach, E. A.; Pauzauskie, P. J.; Kuykendall, T.; Goldberger, J.; He, R.; Yang, P. *Nano Lett*. **2003**, *3*, 867.

[36] Wu, Y.; Fan, R.; Yang, P. *Nano Lett*. **2002**, *2*, 83.

[37] Yan, Y.; Liu, P.; Romero, M. J.; Al-Jassim, M. M. *J. App. Phy.* **2003**, *93*, 4807.

[38] Sun, Y.; Gates, B.; Mayers, B.; Xia, Y. *Nano Lett*. **2002**, *2*, 165.

[39] Sun, Y.; Xia, Y. *Adv. Mater*. **2002**, *14*, 833.

[40] Sun, Y.; Yin, Y.; Mayers, B.; Herricks, Y.; Xia, Y. *Chem. Mater*. **2002**, *14*, 4736.

[41] Poosen, A. R.; Carter, W. C. *Physica A* **1998**, *261*, 232.

[42] Seybolt, A. U.; Hansen, H.; Roberts, B. W.; Yurcisin. P. *J. Metals*, **1956**, *8*, 606.

CHAPTER 6 SYNTHESIS OF METALLIC CORE-SHELL STRUCTURE NANOMATERIALS

6.1 INTRODUCTION

Currently, magnetic nanoparticles are playing an important role in the wide range of sophisticated bio-medical applications, such as targeted drug delivery, biochemical sensing, and ultra-sensitive disease detection. The decrease of particle size leads to increase of its reactivity and their magnetic properties are dominated by superparamagnetism and surface effects[1]. Several works report a possibility to passivate a surface of magnetic nanoparticles (γ - Fe_2O_3, Co, Fe, etc.) by another inert shell (SiO_2, gold, silver, polymer, etc.)[2-9]. A diamagnetic layer could potentially reduce magnetic properties of the magnetic core of nanoparticle. Despite this, gold has become a favored coating material because of its specific surface functionality for subsequent treatment with chemical or bio-medical agents [10-11]. Meanwhile, it protects the magnetic core against oxidation, without drastic reduction of the magnetic properties. It is expected that iron nanoparticles can be passivated to avoid oxidation by gold coating and not modify the magnetic properties (such as coercivity or blocking temperature). The reverse micelle

method for synthesis of Fe@Au nanoparticles has been previously developed by our group[12].

Core-shell structure nanomaterials have many potential applications in biosciences and other fields, which are due to the surface properties of materials (e.g. functionality, absorption ability, catalysis) while the bulk materials will still keep some of the important properties of the core materials (e.g. magnetism).

Techniques to overcoat nanoparticles with an inorganic shell are remarkably general with only a few modest constraints[13]: (a) The existing nanoparticle seeds must withstand the conditions under which the second phase is deposited, (b) the surface energies of the two phases must be sufficiently similar so that the barrier for heterogeneous nucleation of the second phase is lower than that for homogeneous nucleation, and (c) the seed nanoparticle and the overcoat material must not readily interdiffuse under the deposition conditions. Typically seed nanoparticles are prepared and isolated by one of the standard procedures, size-selected, and then redispersed in a fresh solution of solvent and stabilizers. The solution is then heated while precursors for the inorganic shell are gradually added to allow the material to heterogeneously nucleate on the seed nanoparticles. If the rate of precursor addition does not exceed the rate of deposition on the seeds, the precursor concentration never reaches the threshold for homogeneous nucleation of a second inorganic phase.

Here, several kinds of core-shell structure materials were prepared, and some preliminary results were obtained by using non-aqueous solution phase reactions. In this work, we will present another simple method for the synthesis of gold-coated iron nanoparticles by partial replacement reaction. The idea of the method is to use reducing agents (Na, K, Li) to reduce ML_n (M = Fe, Co, Ni; L = Cl, Br; n = 2, 3) to form the metallic core nanoparticles[14], and then use the surface of metallic core particles to reduce Au^{3+} to form gold coated metallic nanoparticles, as shown in scheme 1. Xia et al.[15] have used a similar concept with galvanic replacement reactions for generating metal nanostructures with hollow interiors.

6.2 IRON@GOLD CORE-SHELL STRUCTURE NANOCOMPOSITES

6.2.1 Synthesis

The reduction reactions were conducted in polar aprotic solvents. In a typical synthesis, 2 mmol of $FeCl_3$ were dissolved in NMPO (1-methyl-2-pyrrolidinone) to form a yellow solution (# A). 6 mmol of Na were dissolved in NMPO with 6 mmol of naphthalene to form a dark green solution (# B). A 0.7 mmol of dehydrated $HAuCl_4$ was dissolved in NMPO (# C). The solution # A was added into solution # B quickly with intensive stirring at room temperature. The color of mixture

changed to dark brown immediately. The mixture was further stirred for two hours and then centrifuged to remove the sodium chloride. Then a small amount of capping agent, 4-benzylpyridine, was added into the solution followed by heating and refluxing at 165°C for three hours. A black mixture was obtained and cooled to 60°C, and then solution # C was added slowly then heated with stirring to 125^{o}C for 4 hours. The product that was obtained was added to tetrahydronaphthalene and then centrifuged yielding a black paste which is the product. All the above synthesis operations were performed in an argon atmosphere glove box. The sample was dried in vacuum and washed with EtOH, 8% HCl solution, water and EtOH several times until a colorless suspension was made. A further purification stage included a magnetic separation by magnetic field H = 5 kOe in order to get separate Fe@Au from pure gold nanoparticles. The magnetically separated powder was dried in the air and subjected to characterization by transmission electron microscopy (TEM), energy disperse X-ray spectroscopy (EDS), superconducting quantum interference device (SQUID), X-ray diffraction (XRD), thermograviometric analysis (TGA), UV-visible absorption spectroscopy and faraday rotation.

Scheme 6-1. The reaction route to synthesize metallic core-shell nanoparticles.

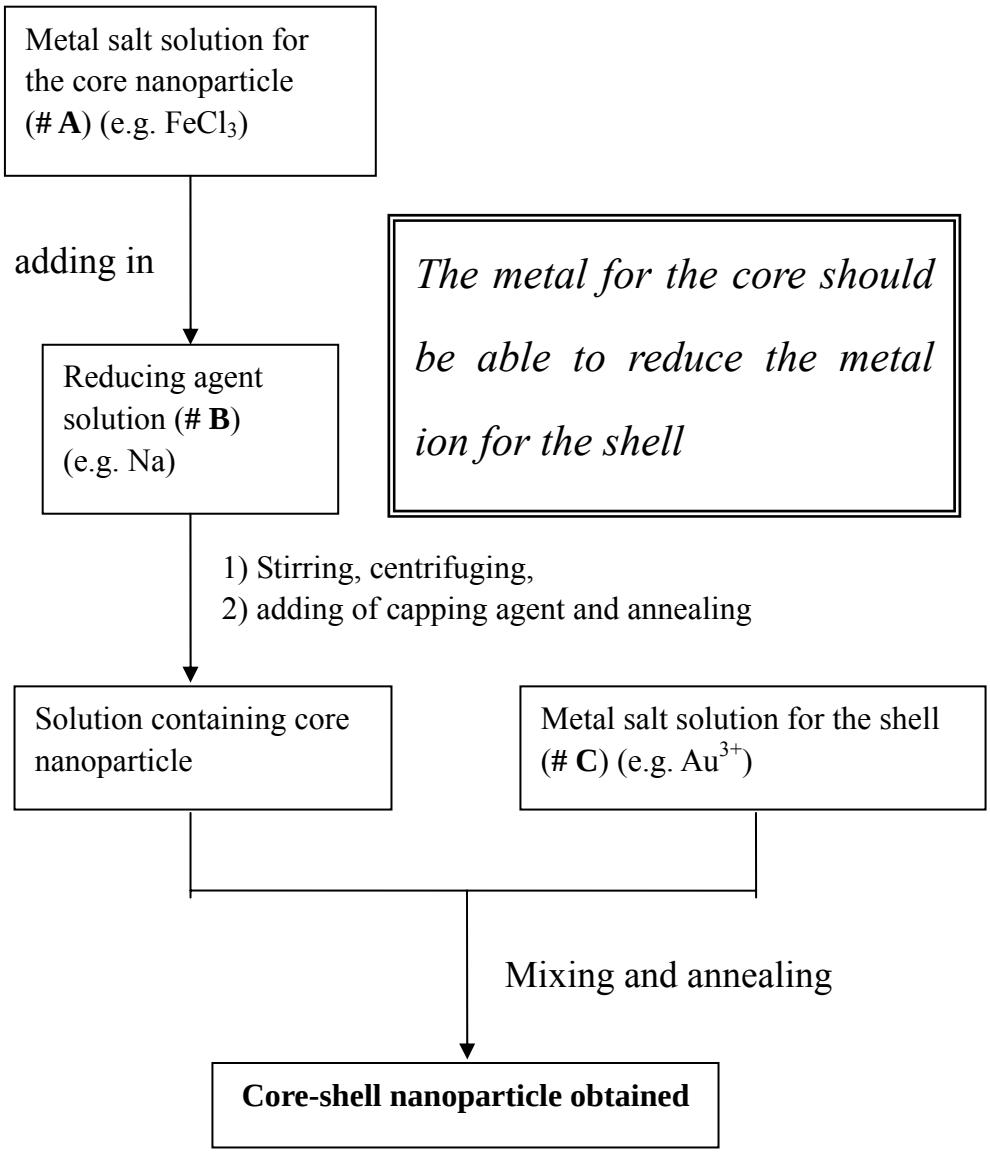

6.2.2 Characterization

6.2.2.1 TEM characterization

Figure 6-1(a, b, c) show three typical TEM images of gold coated iron nanoparticles. The dark contrast in the central part of the particles shows cores with a size of about 11 nm. The light contrast on the periphery of the particles shows the shells with a thickness of about 2.5 nm. The average diameter of the core-shell particle is 16 nm with ~15 % size deviation. The composition of the nanoparticles was estimated by EDS (Figure 6-1d). EDS shows the presence of copper, gold, and iron. The copper is from the TEM grid, and the gold and iron are from the sample. This result indicates that the molar ratio between Fe and Au is 1.4 : 1. The detailed core-shell structure (Fe@Au) of a single particle is observed in the high resolution TEM image in Figure 6-2. There are four representative HRTEM images. The crystalline Au shells are running directly from the surface of iron particle and have a different orientation from particle to particle. The lattice fringes of the shell are clearly shown with the spacing of ~2.4 Å and ~2.0 Å. This corresponds to the {111} and {200} lattice planes for gold, respectively. HRTEM images of our core-shell particles also show crystal lattices of the iron core with interplanar distances ~2.0 Å and ~1.4 Å. This corresponds to the {110} and {200} lattice planes of iron, respectively.

Figure 6-1. (a) (b) (c) TEM micrograph of iron coated with gold nanoparticle, about 16 nm with ~15% size deviation (11 nm core and 2.5 nm shell). (d) EDS result of Fe@Au particle, the molar ratio Fe:Au = 57.2:42.8

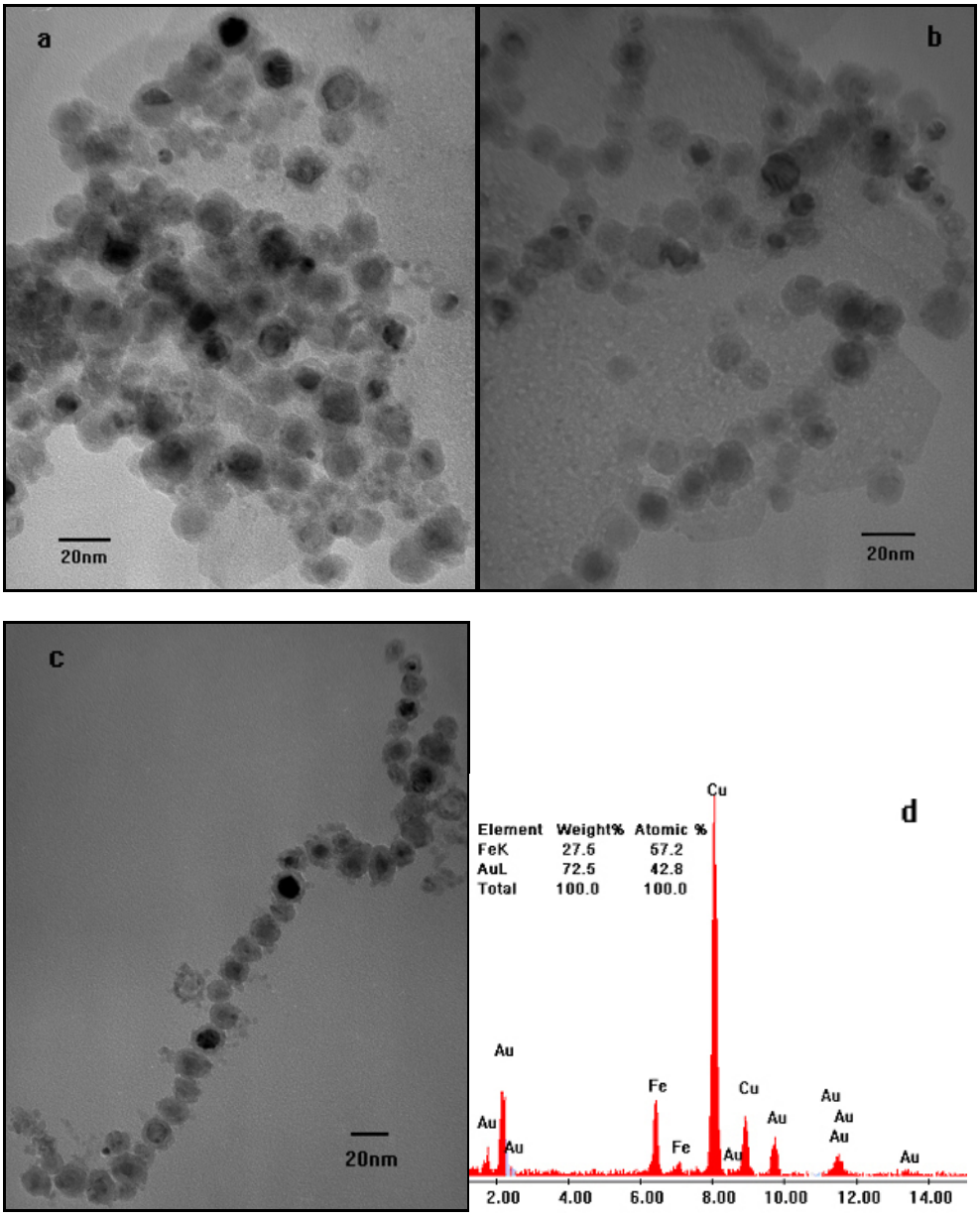

Figure 6-2. High-resolution TEM images of Fe@Au nanoparticles showing the fringes of (111) and (200) crystal planes of gold shells and (110), (200) crystal planes of iron cores.

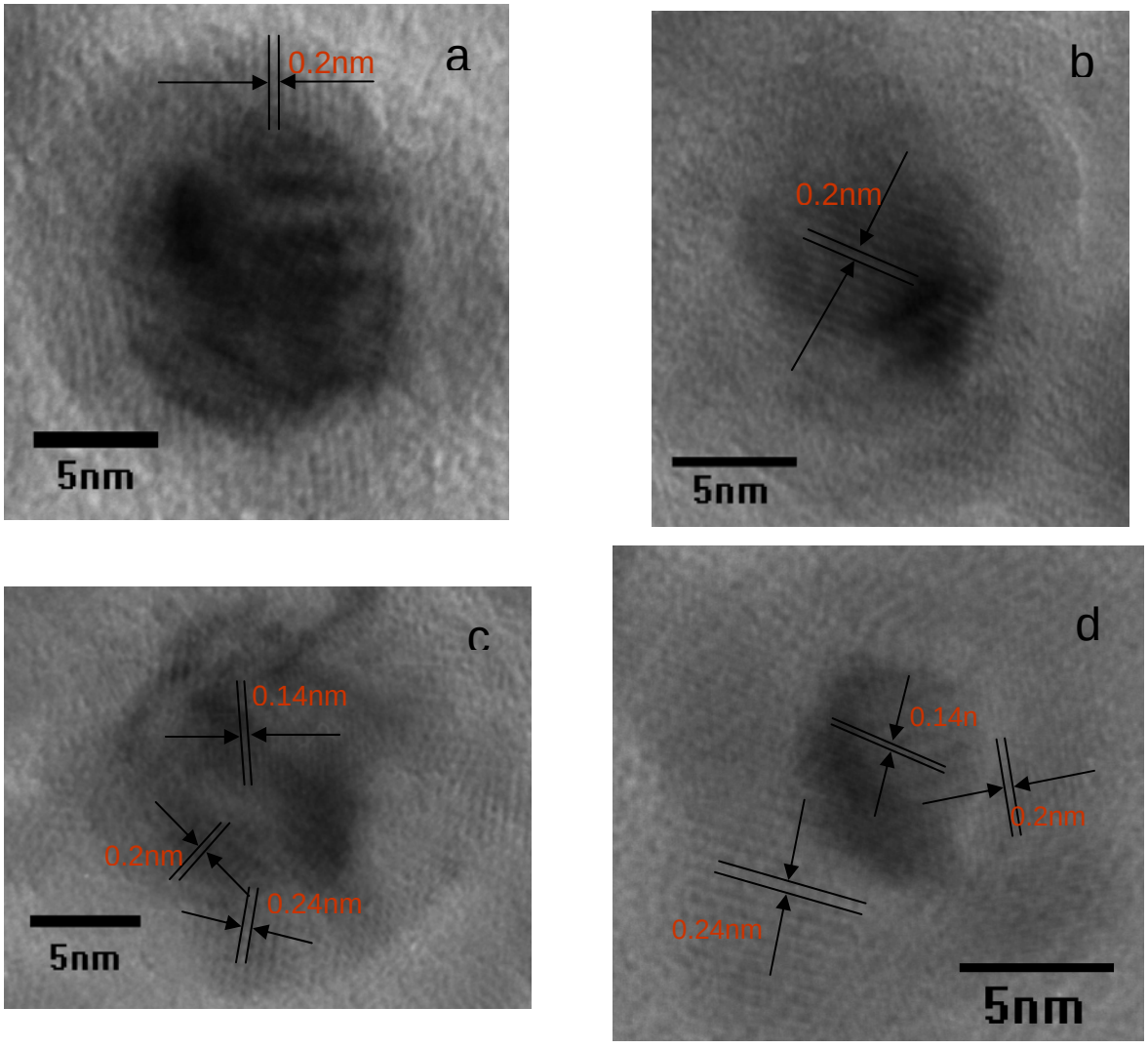

6.2.2.2 TGA characterization

The characterization of the core-shell structure of the sample can be studied by TGA measurements in different atmospheres (see Figure 6-3). The TGA curves of the obtained sample in air (a) and 8% H_2 in argon (b) atmospheres are shown in Figure 6-3. From Figure 6-3a, one can only see the weight loss that is due to the decomposition of organic ligands in the sample. A similar TGA curve was obtained in hydrogen atmosphere (Figure 6-3b). There is also only weight loss. However, one can notice that, in the case of air atmosphere, the weight loss is a little bit smaller than it is in hydrogen. This difference is probably due to the fact that some iron nanoparticles in the as-synthesized sample were coated with both gold and organic ligands instead of being completely coated with only gold. During the measurement of TGA in air atmosphere, the organics were decomposed, and the inside iron was oxidized (i.e., weight gain), which makes the absolute value of weight loss in air atmosphere be diminished.

Figure 6-3. TGA of Fe@Au (a) in air, weight loss ~4.8%; (b) in 8% hydrogen in argon, weight loss ~5.8%.

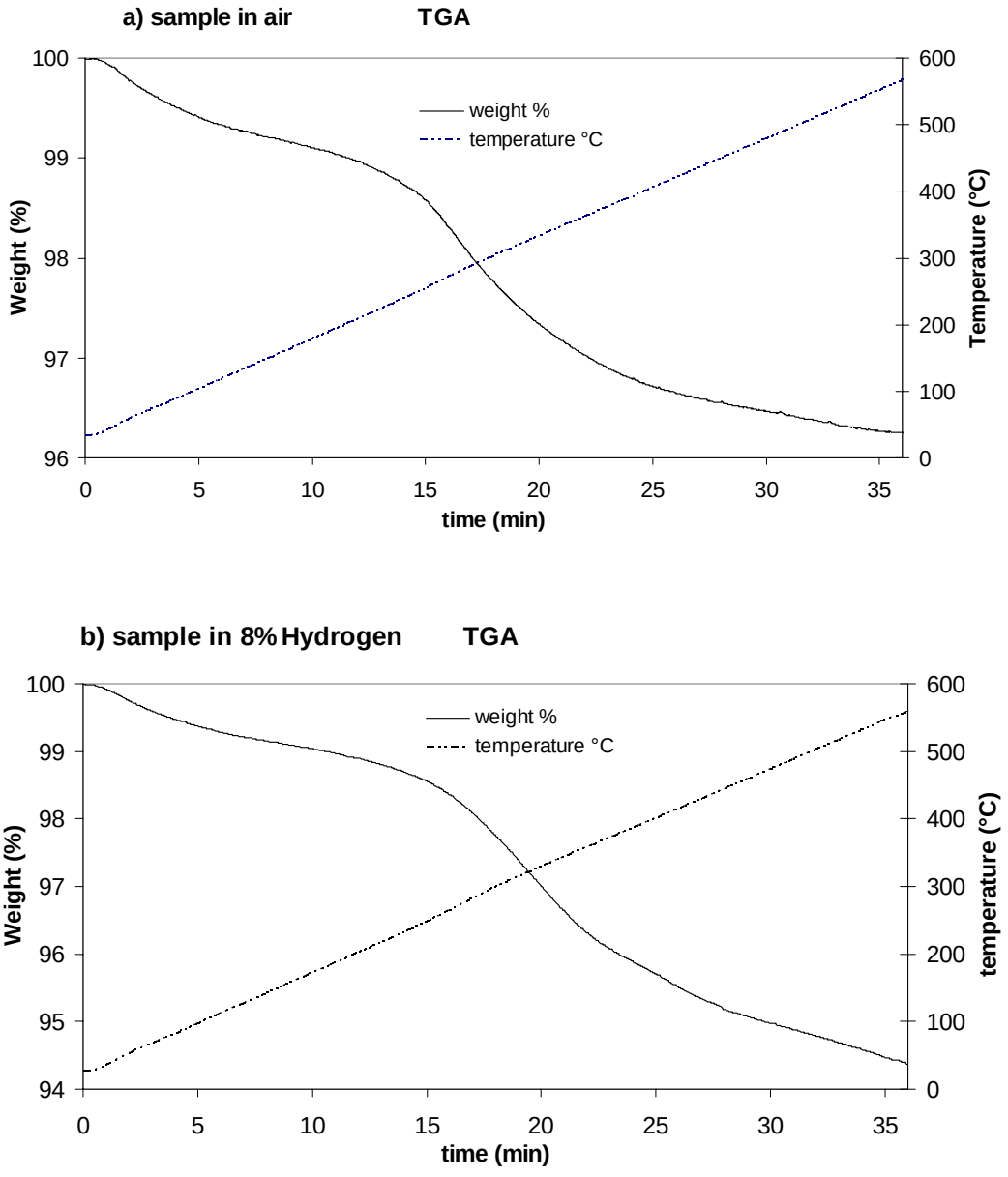

6.2.2.3 X-ray diffraction characterization

The X-ray diffraction (XRD) pattern of Fe@Au nanoparticles is in Figure 6-4. All the reflections correspond to FCC bulk gold (JCPDS 4-784). The pattern of α-iron (JCPDS 6-696) is hidden under the pattern of gold due to the overlap of their diffraction peaks at $2\theta = 44.8°$, 65.3°, and 82.5°. As shown above (Figure 6-1d), EDS data indicates the presence of both iron and gold. The diffraction pattern also does not show the presence of any known iron oxides. This again confirms that the iron nanoparticles are successfully coated and passivated by the gold shell.

Figure 6-4. XRD pattern of iron coated with gold, all the reflections correspond to FCC gold and α-iron.

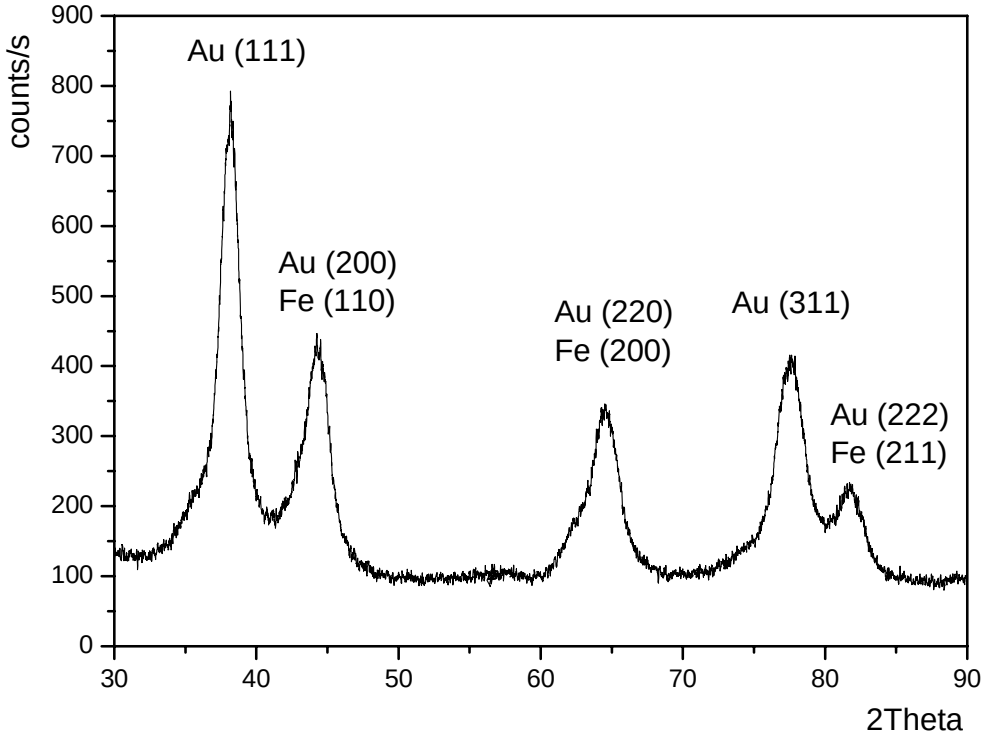

6.2.2.4 Magnetic characterization

The Fe@Au core-shell nanoparticles are ferromagnetic at room temperature. Figure 5 shows the hysteresis loop, measured at room temperature. The core-shell particles have coercivity (H_c) of 25 Oe (see the small figure in Figure 6-5). The magnetic saturation is 45 emu/g. By calculation of composition from EDS and TGA data, one can estimate the value of the magnetic saturation, which is equal to 170 emu/gFe. Bulk iron has a large magnetic saturation of 216 emu/g. However, magnetic saturation of iron powders is 60-70% of that of pure iron, which is 130-151 emu/g [16]. The value that is obtained is a little higher than the value reported for iron powder. This might correspond to better crystallinity of the Fe core, as well as well passivation of its core by the gold shell. It should be mentioned that iron oxides (Fe_3O_4, γ-Fe_2O_3) are superparamagnetic in this size range, and can have a maximum magnetic saturation about 100 emu/g.

Figure 6-5. Magnetic hysteresis loop at room temperature for Fe@Au core-shell nanoparticles after being washed with 8% hydrochloric acid. The saturation magnetization is 45 emu/g, which translates into 170 emu/gFe. Inset shows a small coercivity ~20 Oe at room temperature.

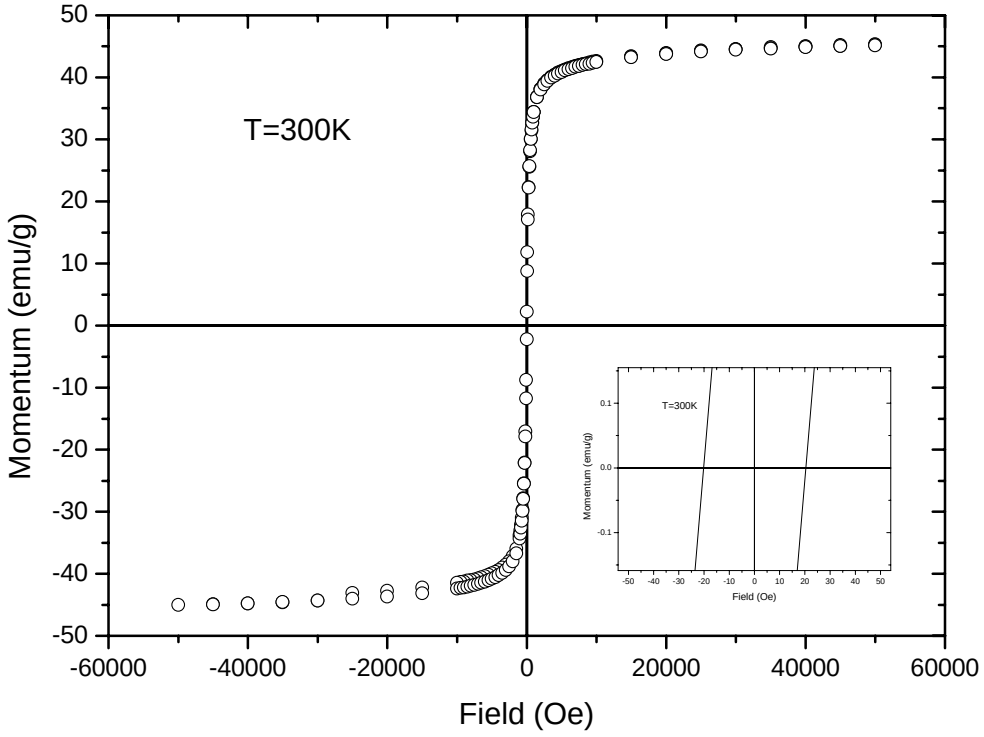

6.2.2.5 Optical absorption characterization

It is known that pure Au nanoparticles exhibit an absorption peak due to excitation of surface plasmon (SP), i.e. collective oscillations of Drude-like conduction electrons and d-band electrons that are optically excited into the conduction band. The peak position is normally within the range of 515-530 nm and its value depends on the particle's size, shape, environment, and dielectric properties. Figure 6-6 shows optical absorption spectra of three samples: a –Au colloids synthesized by a two phase reaction with thiols as capping ligands, b – Fe@Au liquid phase after removal of magnetic particles (i.e., Fe@Au) from the sample, c – Fe@Au core-shell nanocompounds.

The spectrum (a) shows the SP peak at 520 nm which corresponds to isolated and randomly oriented spherical Au nanoparticles. The spectrum (b) has its SP peak at 577nm. The TEM image of this sample reveals that the majority of the sample is highly agglomerated Au nanoparticles with a size about 10 nm. A. Lazarides et al.[17] pointed out that aggregation of Au particles induces a broadening and red-shift of SP peak due to a collective interaction of the electrons of the interconnected particles.

The interesting behavior of SP is observed for the core-shell nanocomposites (figure 6-6c), where Au is a shell. The reported results of the similar geometries of binary nanocomposites, like dielectric SiO_2@Au[18], semiconductor Au_2S@Au[19] and

half-metal Fe_2O_3@Au[9] demonstrate that these core-shell nanoparticles have tunable plasmon resonance that depends on the ratio of the core radius to the total radius. Similarly, as in the case of Au connected particles, there is a red-shift of SP peak position with a decrease of the shell thickness and a blue-shift with an increase of the shell thickness. This effect is explained in terms of the domination of Drude-like electrons that participate in the collective plasmon resonance based on Mie scattering theory and quasi-statistic calculations. The SP peak position for our core-shell nanoparticles is centered at 680 nm. This position is relatively well matched with that reported from the calculated dependence $r_1/r_2 = f$ (SP peak position) for dielectric and semiconductor cores, where $r_1 = 5.5$ nm is the core radius, and $r_2 = 8$ nm is the total particle radius ($r_1/r_2 = 5.5/8 = 0.69$). The small deviation from exact matched value $r_1/r_2 = 0.75$[19], due to ferromagnetic origin of the core, which affects the dielectric properties of plasmon's environment and size deviation of shell's thickness. However, experimentally, based on our HRTEM observation with some relevant data discussed above, we would assign this SP peak as plasmon resonance in our Fe@Au core-shell nanomaterials.

Figure 6-6. UV-vis spectra (optical density (OD) versus wavelength) of (a) separated Au nanoparticles ~6 nm; (b) aggregated Au nanoparticles ~10 nm; (c) Fe@Au core-shell nanoparticles, ~11 nm core and 2.5 nm shell.

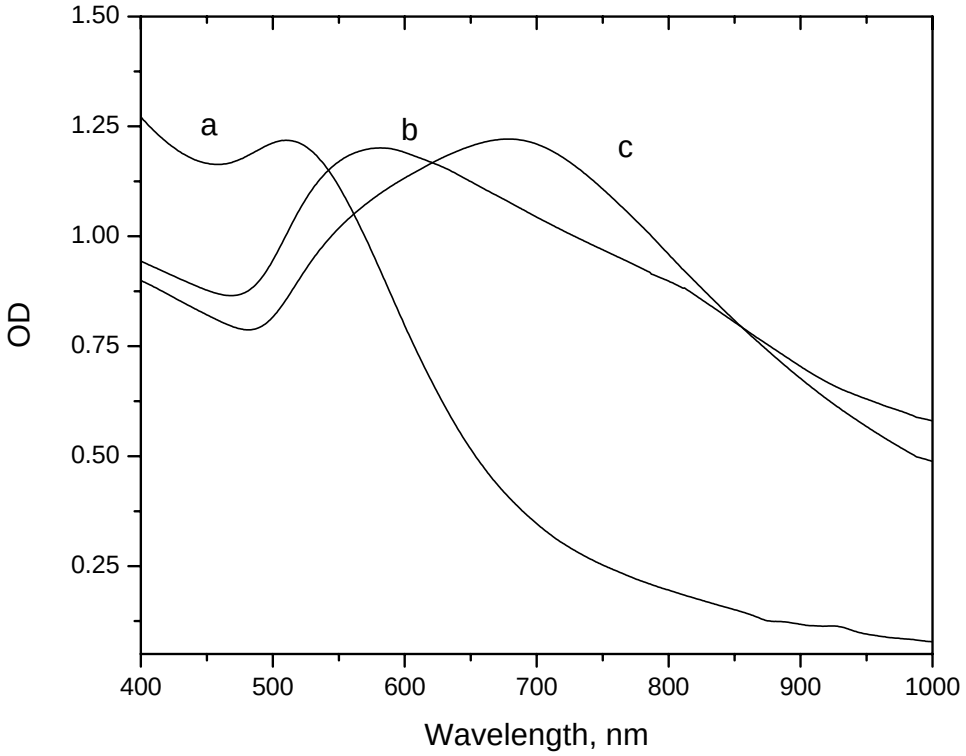

6.2.2.6 Faraday rotation characterization

Spectral dependence of Faraday rotation of Fe@Au core-shell nanoparticles were made in the visible range of the electromagnetic spectrum using standard normal-incidence geometry with the magnetic field parallel to the propagation of the light at room temperature. Nanoparticles were dispersed into neutral polymethylmethacrylate (PMMA) host and dried on a glass substrate. The resulting transparent magnetic film was used for the measurements. The contribution to Faraday rotation due to the nanoparticles was estimated by subtraction of the PMMA host on the glass substrate. Figure 6-7 shows two curves of Faraday rotation: one with a negative maximum (a) at around 460-470 nm and another one (b) at around 420-430 nm with a positive sign of rotation. The first spectrum corresponds to the rotation of plane polarized light due to Fe oxide nanoparticles (Fe_3O_4) [20] and the second one to our Fe@Au core-shell sample. The negative peak at 470 nm originates from localized states formed by interaction of 3d electrons of iron with p electrons of oxygen to give an InterValence Charge Transfer (IVCT) electron transition. Under optical excitation, electrons are transferred from Fe^{2+} to Fe^{3+} ions. This transition is mediated via oxygen; therefore, the presence of these oxidation states is required for this magneto-optical transition to occur. Moreover, the Faraday spectrum of another magnetic γ-Fe_2O_3 does not have any features in this spectral range. Therefore our Fe@Au core-shell nanoparticles exhibit

completely different behavior in Faraday rotation spectrum. The absence of iron oxide compound is manifested by the different sign of Faraday rotation and the peak position in our sample.

Figure 6-7. Faraday rotation of (a) Fe_3O_4; (b) Fe@Au core-shell nanoparticles.

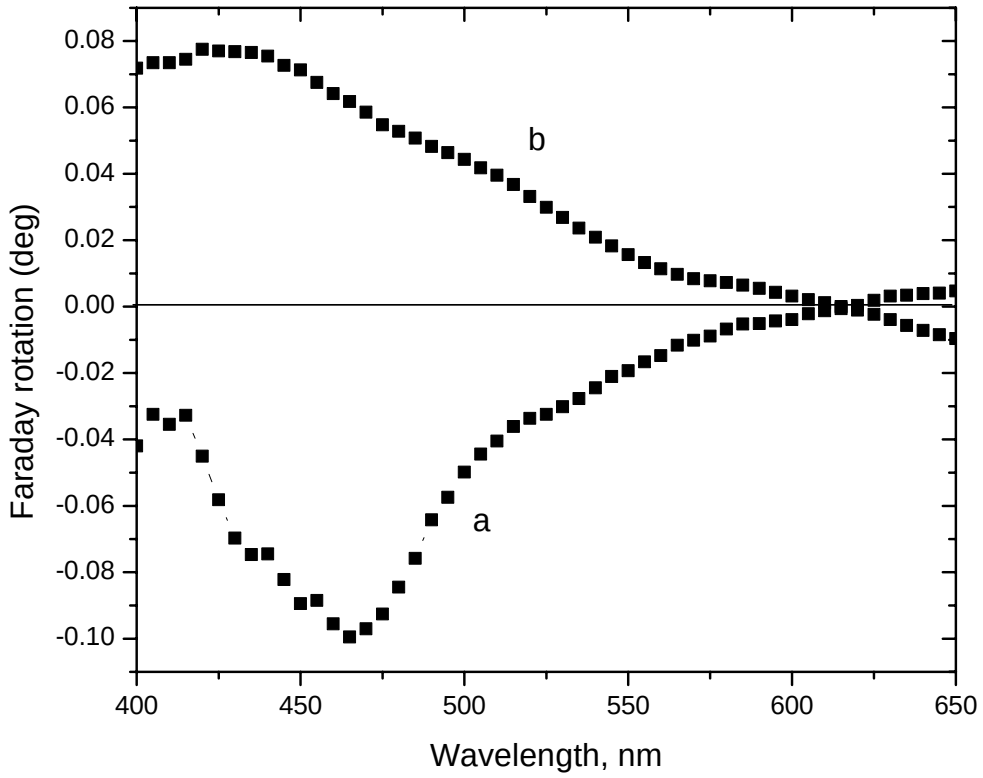

6.3 COBALT@GOLD CORE-SHELL STRUCTURE NANOCOMPOSITES

6.4.1 Synthesis

The reduction reactions were performed in solutions of polar aprotic solvents. 2 mmol of $CoCl_2$ were dissolved in NMPO (1-methyl-2-pyrrolidinone) to form blue solution (Designated as solution A). 4 mmols of Na were dissolved in NMPO with 4 mmols of naphthalene to form a dark green solution (Designated as solution B). 0.6 mmol of dehydrated $HAuCl_4$ was dissolved in NMPO (Designated as solution C). The solution A was added into solution B quickly with intensive stirring at room temperature. The color of reaction system changed to dark brown immediately. The mixture was further stirred for two hours and then centrifuged to remove the sodium chloride. A small amount of capping agent, 4-benzylpyridine, was then put into the solution. Heated and refluxed at 165 °C for 3 hours. After cooled down to 60 °C, the obtained black mixture was slowly added with solution C, then stirring and heat to 125 ^{o}C for 4 hours and get light blue solution. After that the reaction solution was centrifuged to get black paste. All the above operations are done in glove box. The sample was then washed with EtOH, 8% HCl solution, water and EtOH for three times, respectively. After dried in vacuum, the product was characterized with SQUID, XRD, and redispersed into hexane for TEM observation.

6.4.2 Characterization

6.4.2.1 TEM results

Figure 6-7 shows the morphology of gold coated cobalt nanoparticles. The magnification is 400K and the scale bar is 20 nm. The core-shell structure (Co@Au) can be observed in the image. Mean core size of the nanoparticles is ca. 6 nm (SD: 1 nm) with shells of ca. 2 nm (SD: 0.5 nm) thick. From the TEM results, we can see that the size distribution is not very well, some small size particles should be gold particles.

From the EDS result, we can see the atomic ratio between cobalt and gold is 85.4:14.6. And there is not oxygen in the sample. In the spectrum, the peak for Cu would due to the TEM grid and the peak for C would due to the organic solution. This sample was exposed to air. Since cobalt was not oxidized, we can announce that the cobalt was completely coated with gold.

Figure 6-7. TEM and EDS results for Co@Au sample, ~6 nm (SD: 1 nm) core and ~2 nm (SD: 0.5 nm) shell.

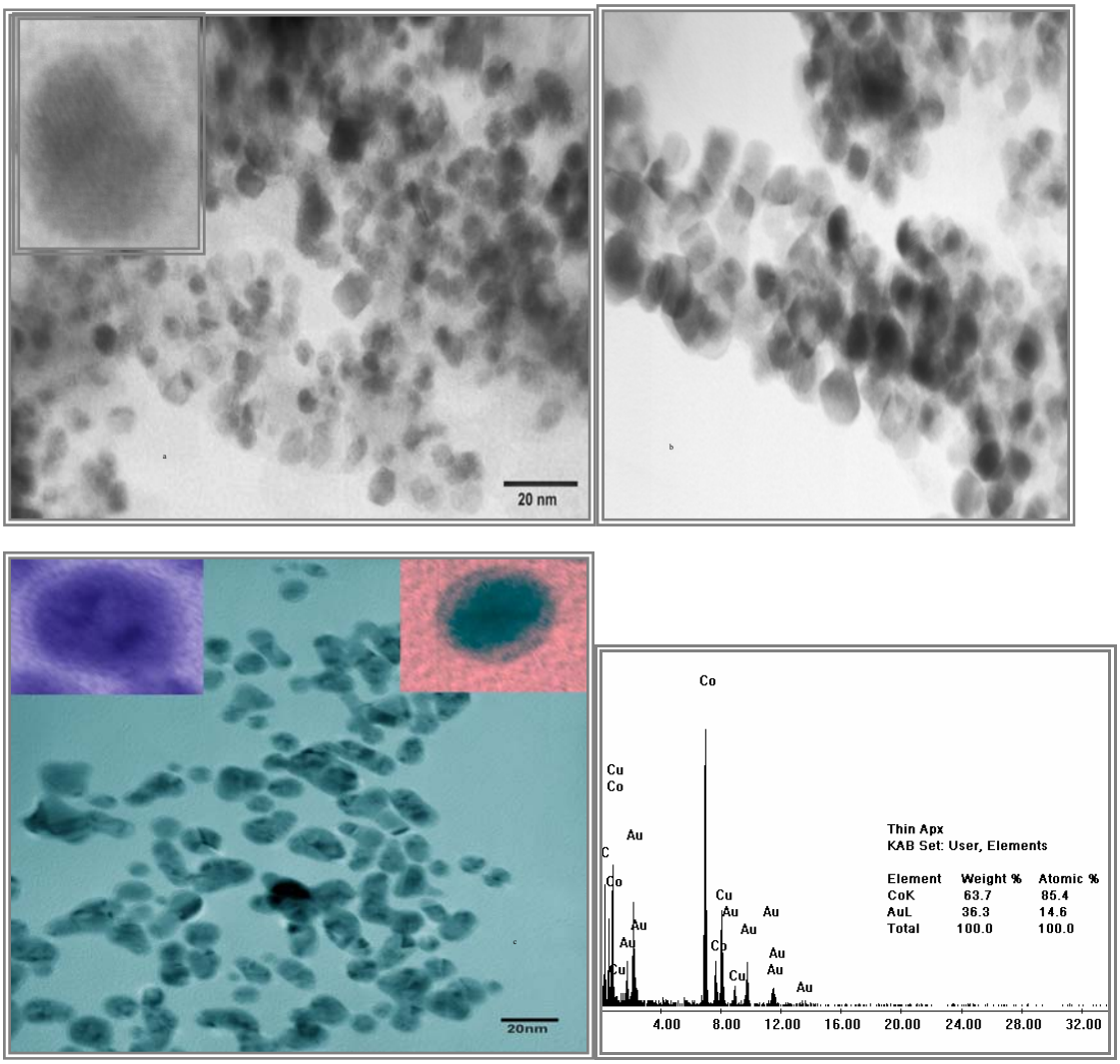

6.4.2.2 XRD results

The XRD pattern of Co@Au nanoparticles is shown in Figure 6-8. In the result, there are the diffraction peaks which correspond to PDF card of Au (4-784) (FCC metallic gold) and Co (5-727). For gold, all the peaks can be identified, 2θ=38.2, 44.4, 64.6, 77.5 and 81.7, for cobalt, the peaks at 2θ=53.2, 57.2, 60.9, 81.8 and 91.1 can be identified. No oxidation state of cobalt can be found from XRD, which can prove that the cobalt was completely coated with gold. The XRD result is identification with EDS result. Another evidence is the magnetic property of the product as shown in Figure 6-9, which shows the existence of cobalt.

Figure 6-8. XRD pattern for the Co@Au sample, all the reflections correspond to FCC Au and Co.

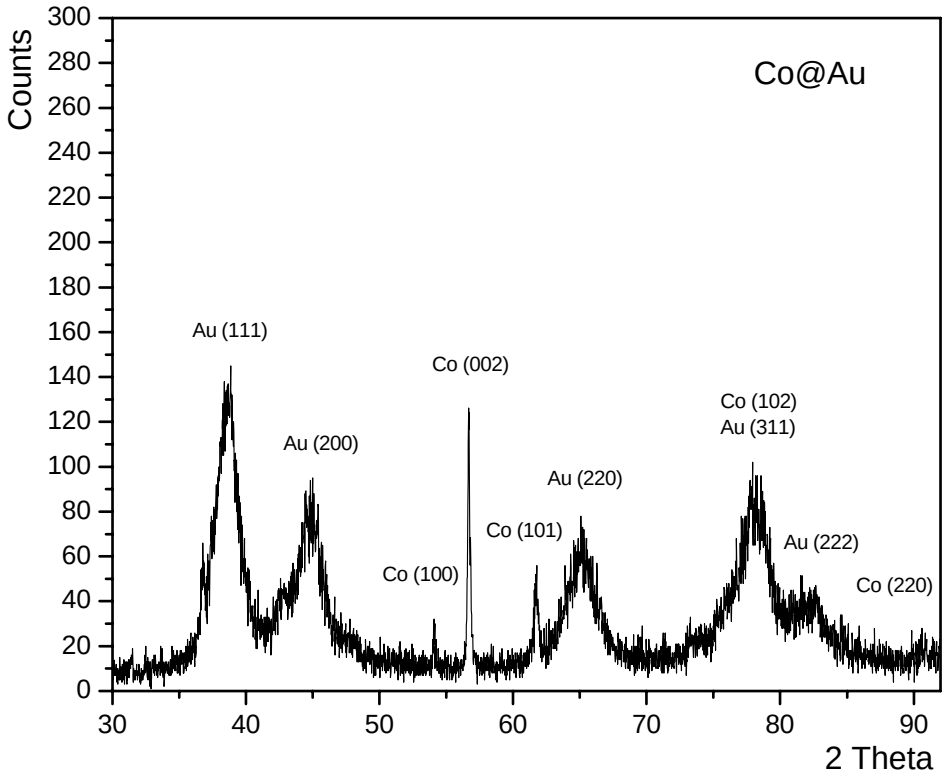

6.4.2.3 Magnetic properties

The SQUID measurement of the product shows that it is a ferromagnetic material with coercivity of 535 Oe at room temperature (as shown in Figure 6-9). The magnetic saturation is about 28.6 emu/g. The reduction of the magnetic saturation of the sample compared with pure cobalt would due to the containing of gold and organic materials. Since the sample exposed to air is still ferromagnetic, we can conclude that the nanoparticles of Co coated completely with gold shell had been synthesized successfully.

Figure 6-9. Magnetic hysterisis loop for Co@Au sample at 300 K. The saturation magnetization is 28.6 emu/g. Inset shows the coercivity is 535 Oe at room temperature.

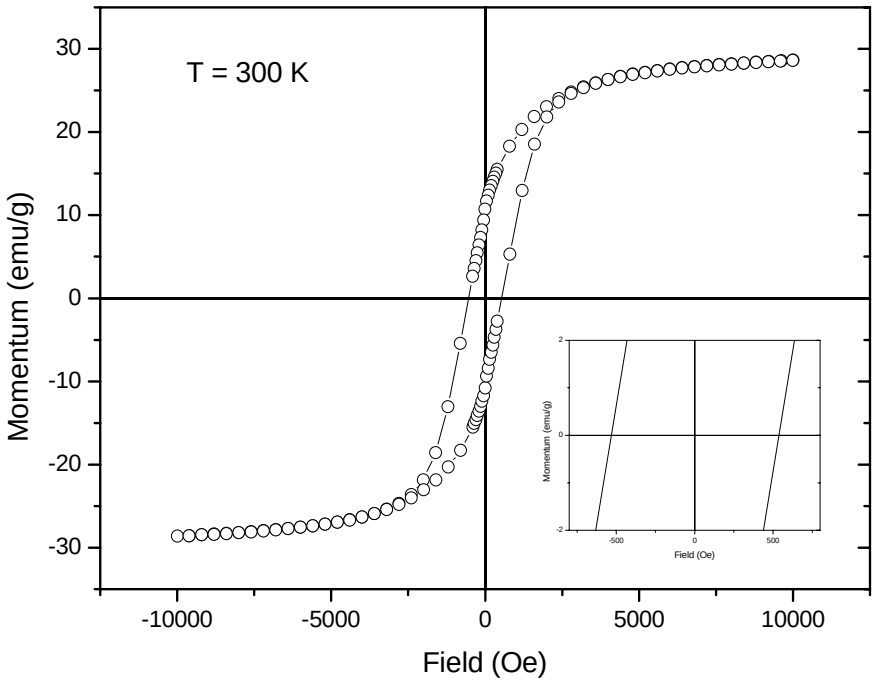

6.5 CONCLUSIONS

Gold-coated iron and cobalt nanoparticles (Fe@Au, Co@Au) were successfully synthesized in non-aqueous 1-methyl-2-pyrrolidinone. Several methods were used to characterize the product. The metal@Au nanoparticles are stable in neutral aqueous and acidic conditions, and potentially provide a wide range of opportunities for biosensor and biomedical applications. The reported method is currently being used and expanded for other systems, including the transition metals Ni, Mn as a core and Pt, Au as a shell.

6.6 LITERATURE

[1.] Bodker, F.; Morup, S.; Linderoth, S. *Phys. Rev. Lett.* **1994**, *72*, 282.

[2.] Pathmamnoharan, C.; Philipse, A. P. *J. Colloid Interface Sci.* **1998**, *205*, 340.

[3.] Szabo, D. V.; Vollath, D. *Adv. Mater.* **1999**, 11, 1313.

[4.] Carpenter, E. E.; Seip, C. T.; O'Connor, C. J. *J. Appl. Phys.* **1999**, 8, 5184.

[5.] Kinoshita, T.; Seino, S.; Okitsu, K.; Nakayama, T.; Nakagawa, T.; Yamamoto, T. A. *J. Alloys and Compounds* **2003**, *359(1-2)*, 46.

[6.] Carpenter, E. E.; Calvin, S.; Stroud, R. M.; Harris, V. G., *Chem of Mater* **2003**, *15(17)*, 3245.

[7.] Teng, X.; Black, D.; Watkins, N. J.; Gao, Y.; Yang, H. *Nano Letters* **2003**, *3(2)*, 261.

[8.] Sobal, N. S.; Hilgendorff, M.; Moehwald, H.; Girsig, M. *Nano Letters* **2002**, *2(6)*, 621.

[9.] Lyon, J. L.; Fleming, D. A.; Stone, M. B.; Schiffer P.; Williams, M. E., *Nano Letters* **2004**, *4(4)*, 719.

[10.] Brust, M.; Bethell, D.; Schirin, D. J.; Kiely, C. J. *Adv. Mater*. **1995**, *7*, 795.

[11.] Hainfeld, J. F.; Powell, R. D. *J. Histochemistry & Cytochemistry* **2000**, *48(4)*, 471.

[12.] O'Connor, C. J.; Carpenter, E. E.; Sims, J. A. U.S. Pat. 2002068187, **2004**.

[13.] Szabo, D. V.; Vollath, D. *Adv. Mater.* **1999,** *11*, 1313.

[14.] Kolesnichenko, V.; Ban, Z.; Goloverda, G.; O'Connor, C. J. Abstracts of Papers, 224th ACS National Meeting, Boston, MA, United States, August 18-22, **2002**.

[15.] Sun, Y.; Xia, Y. *J. Am. Chem. Soc.* **2004,** *126*, 3892.

[16.] Asada, S. *Nippon Kadaku Kaishi*, **1984**, *12*, 1372.

[17.] Lazarides, A. A.; Schatz, G. C. *J. Phys.Chem. B* **2000**, *104*, 460.

[18.] Averitt, R. D., Sarkar, D.; Halas, N. *J. Phys. Rev. Lett.* **1997**, *78*, 4217.

[19.] Averitt, R. D.; Westcott, S.; Halas, N. *J. Opt. Soc. Am. B*, **1999**, *16 (10)*, 1824.

[20.] Barnakov, Y. A.; Scott, L. B.; Golub, V.; Kelly, L.; Reddy, V.; Stokes, K. L. *J. Chem. Phys. Solids*, **2004**, 65, 1005.

CHAPTER 7 SYNTHESIS OF POLYMER COATED NANOPARTICLES[1]

7.1 INTRODUCTION

The synthesis and processing of nanoparticles consisting of metallic nanocrystal cores and organic monolayer shells promise interesting technological applications[2]. It is well known that magnetic nanoparticles have been used in various areas such as bearings, seals, lubricants, heat carriers, printing, recording, and polishing media[3, 4]. In recent years, investigations of magnetic nanoparticles in biological applications have proceeded at a rapid pace. Areas of interest include contrast agents for magnetic resonance imaging (MRI), drug delivery, rapid biological separation, and therapy[5, 6, 7]. In these applications, the fine control of particle sizes, size distributions, and surface properties are important. For nanoparticles prepared by precipitation from solutions, uncontrollable aggregation effects can be detrimental to many applications (e.g., electronics). Common stabilizers such as polymers, surfactants, and dendrimers have been used to increase nanoparticle stability. Polymeric shells have some unique advantages because of the flexibility in controlling the compositions and chemical functionality of the polymers. Several

methods have been developed for coating nanoparticles with polymers. Among the various surface-engineering approaches using polymers, layer-by-layer deposition through charge balance between positive and negative polyelectrolytes is a powerful method. This approach, however, has not been successfully developed into a method that can coat nanoparticles with diameters on the order of tens of nanometers. Another method is to coat nanoparticles by in situ polymerization reactions, which provides an alternative method to increasing nanoparticle stability. Wang et al. have reported the synthesis of Fe_2O_3 coated with polystyrene by solvent-free atom transfer radical polymerization[8]. Li et al. have reported the synthesis of cross-linked polymeric core/shell structure for iron oxide and polystyrene[9]. Here, we report a method involving the direct coating of nanoparticles by poly (vinylpyrrolidone) (PVP) to form metal@polymer in a core@shell arrangement. In previous work, PVP has been used as a coating material by ligand exchange[10], or as a protective polymer to avoid aggregation[11]; Here, PVP is used as a surface-coating or surface-capping agent. PVP offers the further benefit of biocompatibility. PVP has been validated for hybridoma cell growth and subsequent antibody production and found to be non-toxic. PVP in its pure form is safe to the extent that not only is it edible by humans, it is used as a blood plasma expander for trauma victims. Consequently, PVP-coated magnetic core-shell materials may have potential applications in biomedicine.

The structures of the synthesized iron@PVP core-shell nanoparticles have been carefully characterized and the method developed could be potentially used as a prototype reaction for various metal-based nanoparticles because of the similarity of surface structures among different types of metal. The process of forming such kind of core-shell structure is given by equation 7-1.

Equation 7-1. The reactions for the process of forming polymer coated core-shell structure nanoproducts.

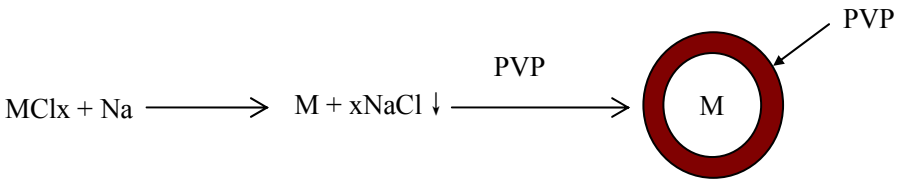

7.2 EXPERIMENTS

The reactions were conducted in polar aprotic solvents. For iron coated with PVP, in a typical synthesis as shown in Scheme 7-1, 2 mmol of $FeCl_3$ was dissolved in 4 mL NMPO (1-methyl-2-pyrrolidinone) to form a yellow solution ***A***. 6 mmol of metallic Na was dissolved in 6 mL NMPO with 6 mmol of naphthalene to form a dark green solution ***B***. 0.005 mmol of PVP (M.W. 55,000) was dissolved in 2 mL NMPO to from a colorless solution ***C***. The solution ***A*** was quickly added to solution ***B*** with rapid stirring at room temperature. The color of the resulting mixture immediately changed to dark brown. The mixture was further stirred for 2 h and then centrifuged to remove the NaCl by-product. Solution ***C*** was then added to the mixture followed by heating and refluxing at 130 °C for 1 h. A black mixture was obtained and cooled to room temperature. All operations were performed in an argon-filled glove box. The obtained product was removed from the glove box and separated in a strong magnetic field (H = 5 kOe) to yield a black paste. The paste was washed repeatedly with alcohol in the same magnetic field until a colorless suspension was obtained.

Scheme 7-1. The reaction route for synthesizing polymer coated metallic core-shell structure nanoparticles.

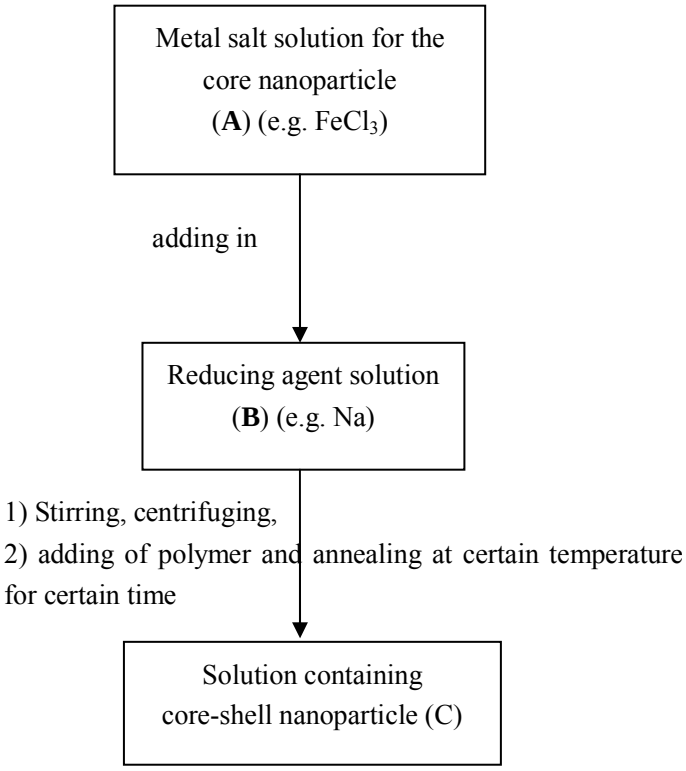

Transmission electron microscopy (TEM) images were recorded on a JEOL 2010 microscope at an accelerating voltage of 200 kV. The TEM specimens were prepared by placing a drop of alcohol-suspended nanoparticles on a carbon-coated copper grid (Ted Pella). A FT-IR spectrometer (Thermo Nicolet NEXUS 670 FT-IR) was used to measure the absorption of the core-shell nanoparticles dissolved in alcohol solution and compared with pure PVP dissolved in alcohol solution. X-ray powder diffraction (XRD) patterns were obtained on Philips X'pert-MPD diffractometer. Magnetic measurements were performed on Quantum Design MPMS-5S SQUID magnetometer.

7.3 CHARACTERIZATION

7.3.1 TEM and EDS.

Figure 7-1(a, b, c, d) shows four typical TEM images of Fe@PVP nanoparticles. The dark contrast near the centers of the particles shows cores with a diameter of about 9 nm. The light contrast on the periphery of the particles reveals the shells with a thickness of about 3 nm. The average diameter of the core-shell particles is 15 nm with ~9% size deviation. And from the TEM images, we can easily find the linear chains of nanoparticles, which formed in zero magnetic field. Philipse et al.[12] reported this kind of dipolar chain structure, and claimed that the

reason for forming this structure is the dipole-dipole interactions. They also mentioned for iron nanoparticles to exhibit the rich linear chain structure, the particle size should be > 8 nm. The size of our sample is in the region. And for magnetite, the particle size to exhibit the rich linear chain should be > 16 nm[13]. Figure 7-1e shows the selection area electron diffraction pattern (SAED) for the sample and demonstrates that the coated iron particles possess high crystallinity and are single phase. The lattice plane distances calculated from the diffraction rings are consistent with those of α-Fe as lattice planes {110}, {200}, {211}, {220}. However, in high resolution TEM (HRTEM), no lattice fringes can be observed; this is likely due to the polymer coating. The composition of the nanoparticles was estimated by EDS (Figure 8-1f), which shows the presence of copper, and iron. The copper is from the TEM grid, and the iron is from the sample.

Figure 7-1. (a) (b) (c) (d) TEM images of iron coated with PVP nanoparticles, 15 nm (15%) and the core is ~9 nm. (e) diffraction pattern for the Fe@PVP sample, which corresponds to iron. (f) EDS result of Fe@PVP particle.

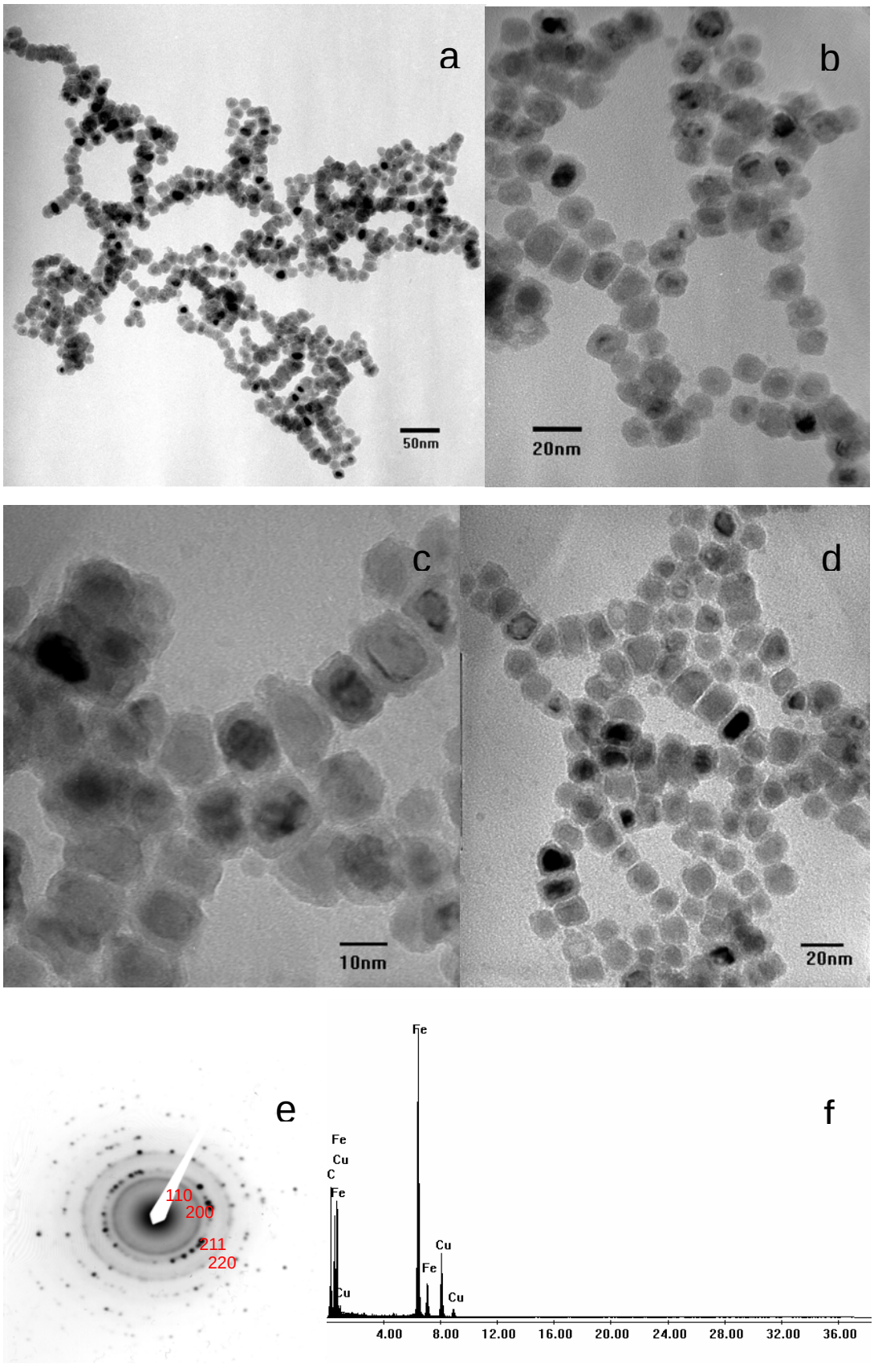
a
50nm
b
20nm
c
10nm
d
20nm
e
110
200
211
220
f
Fe
Cu
C
Fe
Cu
Fe
Cu
Cu
4.00
8.00
12.00
16.00
20.00
24.00
28.00
32.00
36.00

7.3.2 X-ray diffraction.

The presence and phase purity of iron in the Fe@PVP sample were confirmed by X-ray diffraction (XRD), as shown in Figure 7-2. All observed reflections correspond to the α-Fe (JCPDS 6-696). This result confirms that the iron nanoparticles are successfully coated and passivated by the polymer. According to the Scherrer method, the average diameter of the Fe cores is about 8 nm (±0.4 nm), in agreement with the observations from the TEM.

Figure 7-2. XRD pattern of Fe@PVP sample, all the reflections correspond to iron, and no iron oxides.

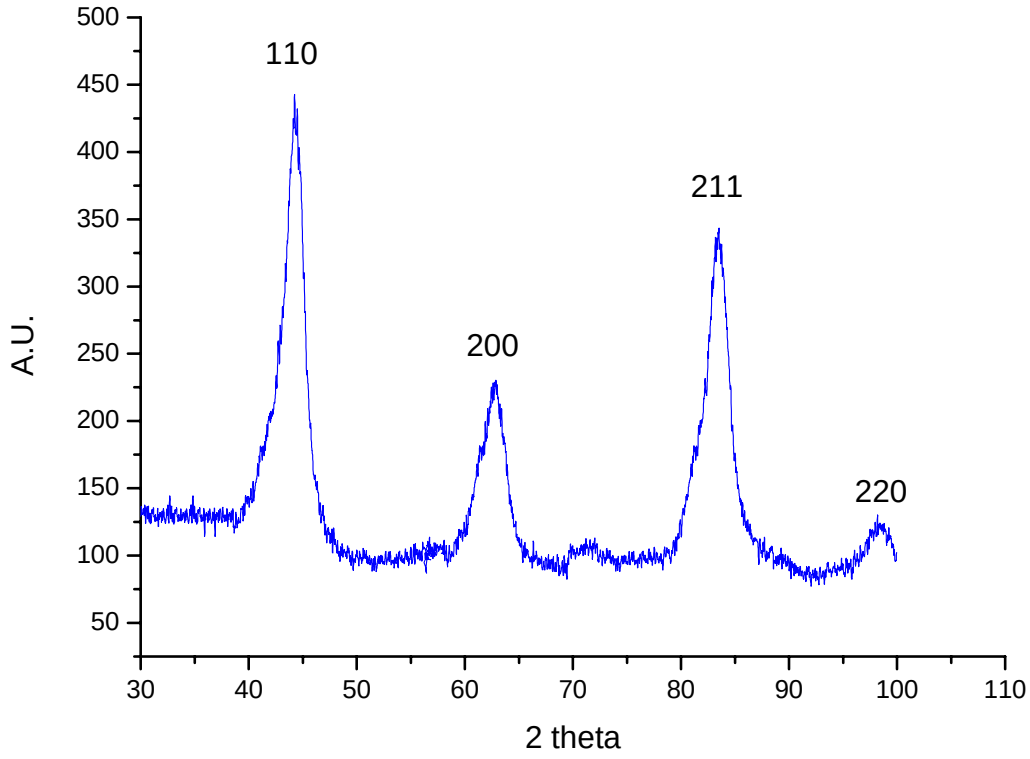

7.3.3 Magnetic properties

The Fe@PVP core-shell nanoparticles are ferromagnetic at room temperature. Figure 7-3 shows the hysteresis loop measured at room temperature. The saturation magnetization (MS) for the coated sample is 51 emu/g and the coercivity (HC) is about 24 Oe. Compensating for the mass of PVP from the initial reactants, the MS of the Fe cores is ~180 emu/g Fe. Bulk iron has a large MS of 216 emu/g. However, the M_S of iron powders is typically 60-70% of that of pure iron, or about 130-151 emu/g. The value that is obtained does match with the value reported for iron powder. It should be mentioned that iron oxides (Fe_3O_4, γ-Fe2O3) are superparamagnetic in this size range, and can have a maximum magnetic saturation about 100 emu/g.

Figure 7-3. Magnetic hysteresis loop at room temperature for Fe@PVP core-shell nanoparticles.

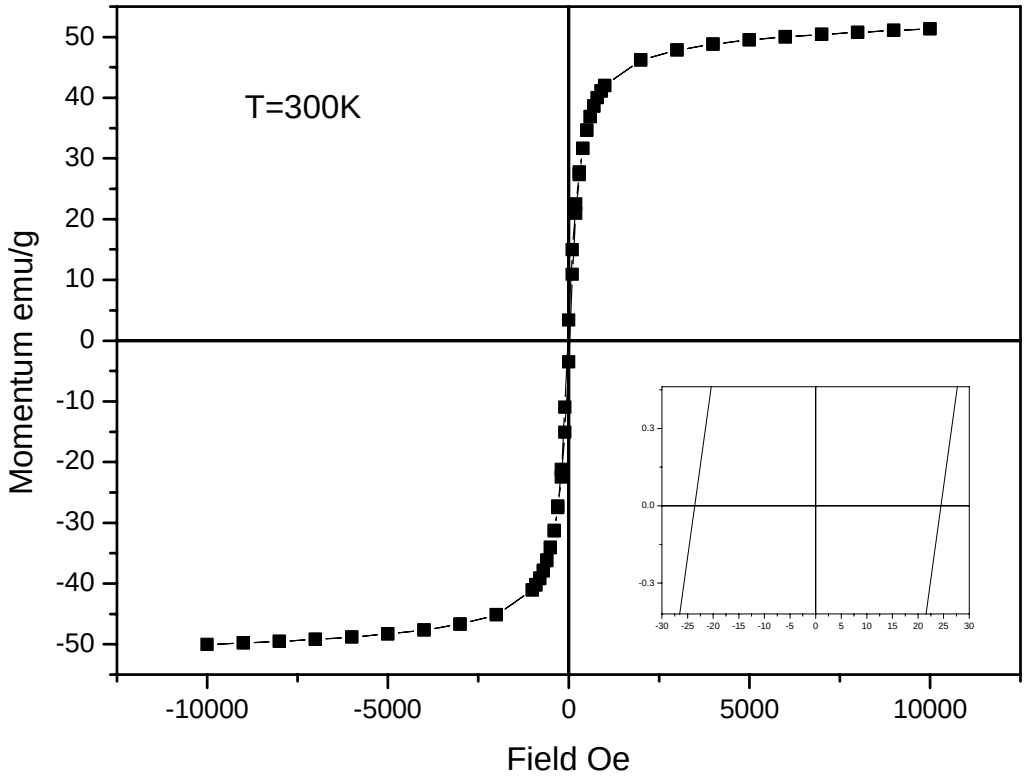

7.3.4 FT-IR analysis.

In Figure 7-4, the FTIR spectrum of Fe@PVP is compared with that of pure PVP in alcohol. The strong correlations between the spectra confirm the presence of PVP in the Fe@PVP nanocomposite. The symmetric (2850 cm^{-1}) and asymmetric (asym, 2921 cm^{-1}) stretches of CH_2, as well as the scissor deformation (1467 cm^{-1}) modes could be observed in both samples. PVP contains C-N and C=O bonds due to the functional groups in its individual unit. The C-N and C=O absorption peaks were observed at ν1019 cm^{-1} and ν1663 cm^{-1}, respectively, in both samples.

Figure 7-4. FT-IR spectra of Fe@PVP core-shell nanoparticles in alcohol (dot red line) and pure PVP in alcohol (solid line).

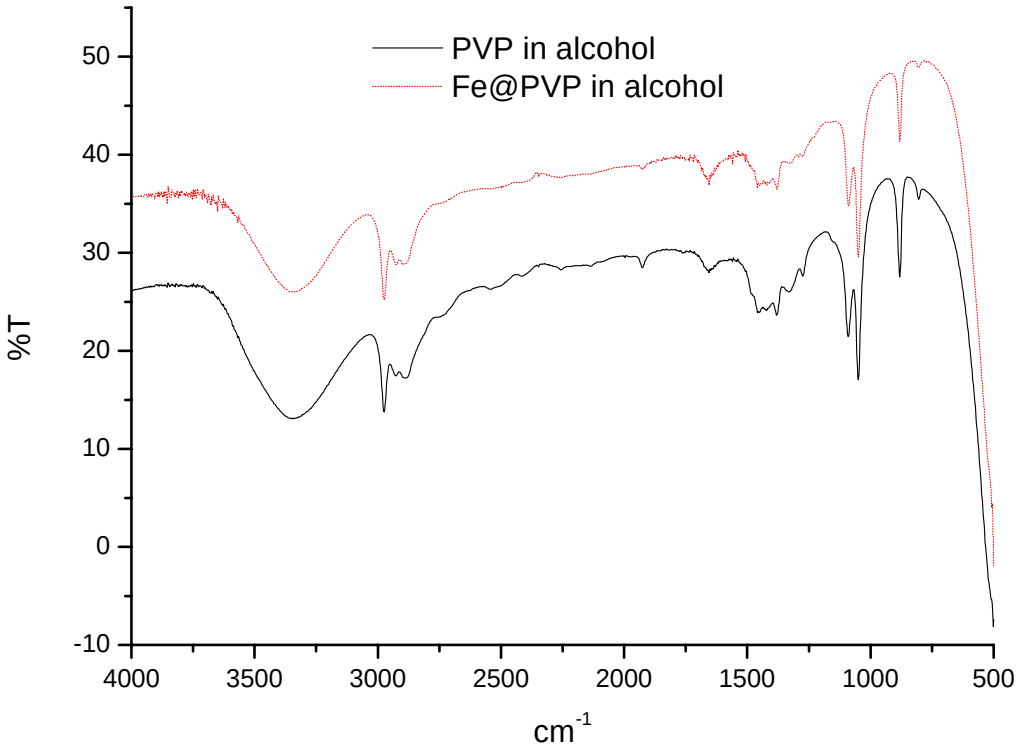

7.4 DISCUSSION

Mechanism for the core-shell structure.

PVP has a structure of a polyvinyl skeleton with polar groups. The donated lone pairs of both nitrogen and oxygen atoms in the polar groups of one PVP unit may occupy two sp orbital of the iron ions to form a complex compound. We hypothesize that this is the first step of the core-shell structure formation. The subsequent step is the PVP-accelerated formation of a large amount of iron nuclei. The third step is the formation of polymer-coated iron core-shell-structured particles. There is little doubt that PVP prevents the iron particles from aggregating according to previous works[14, 15]. Although the prohibiting effect of PVP has been seen in the present work, partial agglomeration also takes place as a result of the magnetic properties of iron and possibly the cross-linking of PVP shells. In addition, an aqueous solution of polymer coated iron nanoparticles stored for over 3 months at room temperature remained stable. The fine stability of the nanocomposite solution was due to PVP as protective agent for iron particles.

7.5 CONCLUSIONS

PVP-coated iron nanoparticles (Fe@PVP) were successfully synthesized in non-aqueous 1-methyl-2-pyrrolidinone. Several methods were used to characterize

the product. The Fe@PVP nanoparticles are stable in neutral aqueous solutions, and potentially provide a wide range of opportunities for biosensor and biomedical applications.

7.6 LITERATURE

[1] Ban, Z.; Cushing, B.; O'Connor, C. J. *Langmuir* submitted.

[2] Templeton, A. C.; Wuelfing, W. P.; Murray, R. W. *Acc. Chem. Res*. **2000**, *33*, 27.

[3] Moser, A.; Takano, K.; Margulies, D. T.; Albrecht, M.; Sonobe, Y.; Ikeda, Y.; Sun, S. H.; Fullerton, E. E. *J. Phys. D-Appl. Phys*, **2002,** *35*, 157.

[4] Zeng, H.; Li, J.; Liu, J. P.; Wang, Z. L.; Sun, S. H. *Nature* **2002**, *420,* 395.

[5] Brigger, L.; Dubernet, C.; Couvreur, P. *Adv. Drug Deliv. Rev.* **2002**, *54*, 631.

[6] Doyle, P. S.; Bibette, J.; Bancaud, A.; Viovy, J. L. *Science* **2002**, *295,* 2237.

[7] Portet, D.; Denizot, B.; Rump, E.; Lejeune, J. J.; Jallet, P. *J. Colloid Interface Sci.* **2001**, *238*, 37.

[8] Wang, Y.; Teng, X.; Wang, J.-S.; Yang, H. *Nano Letters* **2003**, *3*, 789.

[9] Li, G.; Fan, J.; Jiang, R.; Gao, Y. *Chem. Mater*. **2004**, *16*, 1835.

[10] Sun, S.; Anders, S.; Hamann, H. F.; Thiele, J.-U.; Baglin, J. E. E.; Thomson, T.; Fullerton, E. E.; Murray, C. B.; Terris, B. D. *J. Am. Chem. Soc*. **2002**, *124*(12), 2884.

[11] Shin, E. Y.; Fang, J.; O'Connor, C. J.; Golub, V.; Wang, C.; Jun, M.-J. *Key Eng. Mater*. **2005**, *277*, 956.

[12] Butter, K.; Bomans, P. H. H.; Ferderik, P. M.; Vroege, G. J.; Philipse, A. P. *Nature Materials* **2003** *2*, 88.

[13] Klokkenburg, M.;, Vonk C.; Claesson, E. M.; Meeldijk, J. D.; Erne, B. H.; Philipse, A. P. *J. Am. Chem. Soc*. **2004** *126(51)* 16707.

[14] Silver, P. Y.; Herrera-Urbina, R.; Duvauchelle, N.; Vijayakrishnan, Y.; Tekaia-Elhsissen, K. *J. Mater. Chem.* **1996**, *6*, 573.

[15] Sun, Y.; Xia, Y. *Science* **2002**, *298*, 2176.

CHAPTER 8 CONCLUSIONS

Several kinds of nanomaterials in different environments and structure, including spherical nanoparticles, nanowires and core-shell structure composites were successfully synthesized in same system.

For metallic nanomaterials, ~10 nm Fe nanoparticles, ~6 nm Au nanoparticles, and ~100 nm Bi nanoparicles were prepared and characterized.

For bimetallic nanomaterials, $Fe_{50}Co_{50}$ alloy and Bi doped with Mn were synthesized and characterized. For FeCo alloy, after annealing at 500 °C, a pure phase of Fe50Co50 was obtained. And we first synthesized the nanowires of bismuth doped with manganese. By studying intermediates at different temperatures during the growth process of nanowires, the evolution of the crystallization of metallic products and the mechanism of the formation of the nanowires are investigated.

For core-shell structure nanocomposites, including either gold as the shell or polymer as the shell were also synthesized and carefully characterized. Au-coated magnetic Fe nanoparticles have been successfully synthesized by partial replacement reaction in a polar aprotic solvent with about 11 nm core of Fe and about 2.5 nm shell of Au. HRTEM images show clear core-shell structure with

different crystal lattices from Fe and Au. SQUID magnetometry reveals that particle magnetic properties are not significantly affected by the overlayer of a moderately thick Au shell. The Au-coated particles exhibit a surface plasmon resonance peak that red-shifts from 520 to 680 nm. And poly (vinyl pyrrolidone) (PVP) coated iron nanoparticles also have been successfully synthesized in a polar aprotic solvent, which shows the well-defined core-shell structures. In this approach, poly (vinyl pyrrolidone) (PVP) was employed as the coating polymer directly coated on metallic core (iron) nanoparticles.

In summary, this study successfully and systematically synthesized several kinds of nanocomposites in a system. The synthetic procedure is simple, economic and easily scaled-up for further applications. And many techniques were employed to characterize the products.

VITA

Zhihui Ban was born on November 5, 1972 in Yingkou, Liaoning Province, P. R. China. He earned his Bachelor of Science Degree in Chemical Engineering from Zhejiang University, which is one of the top three universities in China, in July of 1996. Then he earned his Ph.D. in Environmental Chemical Engineering from Dalian Institute of Chemical Physics, Chinese Academy of Sciences, in June of 2001. And in September of 2001, he entered the Ph.D. program at the University of New Orleans and joined Dr. O'Connor's group in Advanced Materials Research Institute to perform his research in nano-materials sciences. Throughout most of his academic career in University of New Orleans, he worked in a laboratory at AMRI as a research assistant. In the spring of 2004, Zhihui received his Master of Science degree.